



HAL
open science

Synaptic changes upon removal of extracellular perineuronal nets in adult mouse visual cortex

Giulia Faini

► **To cite this version:**

Giulia Faini. Synaptic changes upon removal of extracellular perineuronal nets in adult mouse visual cortex. *Neurons and Cognition [q-bio.NC]*. Université Pierre et Marie Curie - Paris VI, 2017. English. NNT : 2017PA066363 . tel-01737978

HAL Id: tel-01737978

<https://theses.hal.science/tel-01737978>

Submitted on 20 Mar 2018

HAL is a multi-disciplinary open access archive for the deposit and dissemination of scientific research documents, whether they are published or not. The documents may come from teaching and research institutions in France or abroad, or from public or private research centers.

L'archive ouverte pluridisciplinaire **HAL**, est destinée au dépôt et à la diffusion de documents scientifiques de niveau recherche, publiés ou non, émanant des établissements d'enseignement et de recherche français ou étrangers, des laboratoires publics ou privés.

Université Pierre et Marie Curie
Ecole doctorale Cerveau-Cognition-Comportement
Institut du Cerveau et de la Moelle Epinière

THESE DE DOCTORAT EN NEUROSCIENCES

SYNAPTIC CHANGES UPON REMOVAL OF EXTRACELLULAR
PERINEURONAL NETS IN ADULT MOUSE VISUAL CORTEX

Soutenue le 19 Septembre 2017

par **Giulia Faini**

Composition du jury:

Dr Bertrand Lambolez
Dr Valérie Crépel
Dr Renato Frischknecht
Dr Ariel Di Nardo
Dr Tommaso Pizzorusso
Dr Jean Christophe Poncer

Président
Rapportrice
Rapporteur
Examineur
Examineur
Membre invité

Dr Alberto Bacci

Directeur de thèse

"I think it's a romantic notion that you can replicate the critical period later in life. Some things just don't unhappen"

Michael Stryker

ACKNOWLEDGEMENTS

First of all, I would like to thank Valérie Crépel, Renato Frischknecht, Bertrand Lambomez, Ariel Di Nardo, Tommaso Pizzorusso and Jean Christophe Poncer for being part of my thesis jury. In particular, many thanks to Tommaso Pizzorusso and Jean Christophe Poncer for their suggestions and feedback during the two thesis committees.

Grazie mille a Gianmichele Ratto e Silvia Landi per aver collaborato a questo progetto con grande interesse ed aver prodotto i dati *in vivo*.

Alberto, ti ringrazio di cuore per avermi dato la possibilità di cominciare la mia vita scientifica nel tuo labbbbboratorio e con questo bel progetto. Sei sempre stato di buon consiglio, d'ascolto, di supporto. Grazie per l'educazione scientifica che mi hai trasmesso, per i tuoi incoraggiamenti quasi paterni quanto per il tuo ampio repertorio di battute ed espressioni.

Charlotte, merci pour tout ce que tu m'as appris, tes précieux conseils et ton implication dans le projet. Je t'en remercie profondément.

Un grand merci aux Bacci-ettes, pour la bonne ambiance et les rigolades. Cristina, grazie per gli Arcade Fire, U2 e le Doc Martens. Joana, obrigada pela tua bondade e osteus conselhos. Andrea, gracias por tu ayuda preciosa. Angela, grazie per farmi senti Roma un po più vicina. Javier alias pedorro, gracias por el maté-que-no-me-gusta. Martin, tak til at værdsætte mig (nogle gange) elektro (et merci à google translate). Camille et Sofia, votre bonne humeur me manque. Sans oublier la Ménagerie et ces Happy Hour.

Merci aux collègues et amis de la team Miles: Farah, pour ta douceur et ta gentillesse. Giampa, non montarti troppo la testa, ma un piccolo ringraziamento te lo meriti vâ. Mérie, nos pauses et délires m'ont bien manqué cette dernière année, mais heureusement que l'on se rattrape en dehors du labo.

Merci aussi à tous les potos présents depuis de si nombreuses années avec qui j'aime décompresser, profiter des concerts, des sorties en tout genre, de cinéma et de discussions autour d'un bon verre.

Enfin, grazie a mamma, papa ed Ale per aver sempre creduto in me. A tutta la famiglia in Italia che non vedo quanto vorrei ma alla quale penso spesso. Ed un applauso a Dimitrii che mi ha motivato, su(o)pportato e dato un bell'esempio da seguire.

TABLE OF CONTENTS

LIST OF ABBREVIATIONS	11
Chapter 1: INTRODUCTION	13
1.1 The mouse visual system	15
1.1.1 Some considerations on sensory system and vision	15
1.1.2 Architecture and properties of the mouse visual system	16
1.1.2.1 The retina: first element of the chain	20
1.1.2.2 The dorso lateral geniculate nucleus: relay between the eye and the cortex	21
1.1.2.3 The primary visual cortex: first cortical level of visual processing	24
1.2 Cortical plasticity – Experience-dependent visual plasticity	36
1.2.1 Critical period of plasticity	36
1.2.2 Ocular dominance plasticity as a model to study experience-dependent plasticity.....	38
1.2.3 Cellular, molecular and structural mechanisms of critical period	39
1.2.3.1 Role of inhibition	39
1.2.3.2 Mechanisms of ocular dominance plasticity at the circuit level	42
1.2.4 Adult plasticity and the reopening of windows of plasticity.....	43
1.3 Extracellular matrix and Perineuronal Nets	46
1.3.1 Extracellular matrix in the central nervous system	46
1.3.2 Perineuronal Nets	46
1.3.2.1 Overview	46
1.3.2.2 Molecular and structural organization of PNNs.....	49
1.3.2.3 Formation and development of PNNs.....	51
1.3.3 Roles of perineuronal nets	52
1.4 Why looking at layer 4 of primary visual cortex?	56

1.5 Aim of the study.....	57
Chapter II: MATERIALS AND METHODS	61
2.1 Animals	63
2.2 <i>In vivo</i> enzymatic degradation of PNNs in V1	63
2.3 <i>In vivo</i> expression of the light-sensitive channel ChR2 in the dLGN	64
2.4 Sensory deprivation in adult mice by monocular deprivation.....	65
2.5 Preparation of acute slices for electrophysiology.....	65
2.6 Electrophysiology and optogenetic stimulation.....	66
2.7 <i>In vivo</i> recordings	69
2.8 Immunohistochemistry.....	70
2.9 Data analysis	71
2.10 Statistical tests	72
Chapter III: RESULTS	73
3.1 <i>In vivo</i> enzymatic removal of PNN in V1 of adult mice	75
3.2 PNN removal alters the visual gain adaptation curve <i>in vivo</i> , and increases the power of visually-evoked oscillations	76
3.3 Developmental changes of firing dynamics and passive properties of PV cells and PNs. No apparent effect induced by disruption of PNNs	78
3.3.1 Developmental changes.....	78
3.3.2 Firing dynamics and passive properties are not altered by PNN removal.....	81
3.4 Developmental changes of action potential waveform of both cell types. No apparent effect induced by disruption of PNNs	81

3.5 Developmental maturation of synaptic transmission onto PV cells and PNs, and alterations induced by PNN digestion.....	85
3.5.1 Development of glutamatergic transmission onto L4 neurons and effects of PNN removal... 85	85
3.5.2 Development of GABAergic transmission onto L4 neurons and effects of PNN removal	87
3.5.3 Effects of PNN removal on quantal synaptic transmission onto PV cells	89
3.6 Does monocular deprivation alter the E/I balance after PNN removal?.....	91
3.6.1 Firing dynamics, passive properties and action potential shape are not altered.....	91
3.6.2 Effects of monocular deprivation on synaptic transmission onto PV cells and PNs following enzymatic PNN removal in adult mice	94
3.7 PNN removal does not alter unitary GABAergic connections in L4.....	96
3.8 <i>In vivo</i> expression of the light-sensitive channel ChR2 in the dLGN. Double injections .	99
3.9 PNN disruption increases thalamocortical glutamatergic synapses specifically onto PV cells	101
3.10 PNN disruption increases thalamocortical feed-forward inhibition onto PV cells	103
Chapter IV: DISCUSSION	107
REFERENCES.....	117

LIST OF ABBREVIATIONS

AMPA	α -amino-3-hydroxy-5-methyl-4-isoxazole propionic acid
AP	action potential
aCSF	artificial cerebrospinal fluid
BC	basket cell
BDNF	brain-derived neurotrophic factor
Br12	Brain-derived link protein 2
C4-6ST	4-6 sulfation
CrtI-1	cartilage-link protein 1
CB1	cannabinoid receptor type 1
CCK	cholecystokinin
Ca ²⁺	calcium
CamKII	calcium/calmodulin dependent protein kinase II
ChABC	chondroitinase ABC
ChR2	channelrodopsin-2
CP	critical period
CSPG	chondroitine sulfate proteoglycan
dLGN	dorsolateral geniculate nucleus
GalNAc	N-acetylgalactosamin
E/I	excitation/inhibition
E _{Cl}	equilibrium potential for chloride
ECM	extracellular matrix
EPSC	excitatory postsynaptic current
FFI	feed-forward inhibition
FS	fast-spiking
GABA	γ -aminobutyric acid
GAG	glycosaminoglycan
GC	ganglion cell
HA	hyaluronic acid
H-ase	hyaluronidase
IN	interneuron

IPSC	inhibitory postsynaptic current
K ⁺	potassium
L 1 - 6	layer 1 - 6
LFP	local field potential
LTD	long-term depression
LTP	long-term potentiation
MD	monocular deprivation
NMDA	N-methyl-D-aspartic acid
Na ⁺	sodium
OD	ocular dominance
ODP	ocular dominance plasticity
Otx2	orthodenticle homeobox 2
PBS	phosphate-buffered saline
PN	principal neuron
PNN	perineuronal net
PV	parvalbumin
PX	X day post-natal
PYR	pyramidal
RF	receptive field
Rm	membrane resistance
RS	regular spiking
RTN	reticular thalamic nucleus
SS	spiny stellate
SST	somatostatin
Tn-R	tenascins-R
TTX	tetrodotoxin
V1	primary visual cortex
V1b	binocular region of the primary visual cortex
V1m	monocular region of the primary visual cortex
VEP	visual evoked potential
VIP	vasoactive intestinal polypeptide
Vrest	resting membrane potential
WFA	wisteria floribunda agglutinin

Chapter 1: INTRODUCTION

1.1 The mouse visual system

1.1.1 Some considerations on sensory system and vision



Figure 1.1. Through the eyes of a mouse. From (Baker, 2013).

One fundamental principle of sensory systems is that they are highly organized but plastic and sensitive to experience. For decades, the visual system has been used as the ideal model to study neuronal microcircuits organization and hierarchy, functional topographic maps and activity-dependent mechanisms of neuronal plasticity (Fig. 1.1).

In the 1960's Hubel and Wiesel were pioneers in the investigation of the visual system and its capability to transform simple visual inputs from the two eyes, into a 3D complex perception of the external world (Hubel, 1982; Wiesel, 1982). In 1981, they received the Nobel Prize in Physiology or Medicine for their revolutionary and fundamental discoveries. Hubel and Wiesel performed their studies in cats, which have a more accurate vision than mice, being the latter nocturnal animals that perceive their environment by mostly using their whiskers. Nevertheless, rodents (and especially mice) offer the possibility to manipulate and monitor neurons with high precision, allowing the investigation at the cellular and synaptic level, using *in vitro* and *in vivo* circuit analysis, optogenetics, electrophysiology and calcium imaging. This can be accomplished thanks to the ability of identifying and manipulating specific cell types and pathways (Huberman and Niell, 2011). Indeed, in the last decades, a large amount of studies have shown the importance of using mice as a model in vision research (Sirotnin and Das, 2010; Huberman and Niell, 2011; Baker, 2013).

Presently, the anatomic and functional properties of sensory systems are well studied. In particular, the sensory pathways and circuit interplays of the mouse visual system is well understood.

As a gross (and admittedly oversimplified) representation of the sensory flow within the central nervous system (Fig. 1.2), the information coming from the external world is detected by sensory organs (in our case the retina), then integrated in the thalamus (dorsolateral geniculate nucleus or dLGN) which is the first relay of visual information in the brain, and subsequently decoded and processed in the neocortex (primary visual cortex, referred to V1).

Layer 4 (L4) of V1 is the major input layer of the cortex. From L4, the visual information is then propagated and integrated in layer 2/3 (L2/3) and relayed to other cortical associative areas, which are responsible for feedback modulations (Alitto and Usrey, 2003). The integration of sensory information from and to different sensory cortical areas is believed to provide a coherent representation of the external world. Here I will focus on the primary visual cortical area of mice, V1.

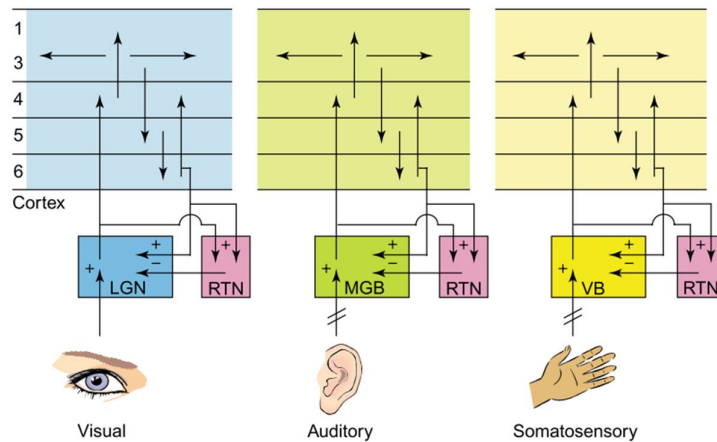


Figure 1.2. Corticothalamic circuitry for the visual (blue), auditory (green) and somatosensory (yellow) systems. All three systems share a similar basic organization. Thalamocortical interactions begin with excitatory projections from thalamic relay neurons – located in the LGN, MGB (medial geniculate body), and VB (ventrobasal nucleus) —to neurons in L4 of primary visual, auditory, and somatosensory cortex. Neurons in cortical L6 in turn give rise to excitatory feedback to the thalamus. Corticothalamic feedback axons terminate directly onto relay neurons and interneurons in thalamic relay nuclei. Corticothalamic axons also extend collateral projections into the reticular nucleus (RTN). RTN neurons then give rise to inhibitory projections that terminate on thalamic relay neurons. Modified from (Alitto and Usrey, 2003)

1.1.2 Architecture and properties of the mouse visual system

General organization:

The generation of a single image originating from the two eyes (binocular vision) requires a complex brain circuitry. In the mouse and others mammals, the visual system is composed of a multitude of levels (or units) organized in a highly hierarchical way. Each unit receives both feedforward information from the lower levels, and feedback connections from higher,

associative levels. In addition, synaptic connectivity within single units adds a significant level of modulation of sensory information.

As in other sensory and motor systems, each hemisphere of V1 processes the information originating from the contralateral visual field (Fig. 1.3). In order to obtain such structured pathway, most of the retinal cells (projections shown in blue in Fig. 1.3) cross the midline through the optic chiasm and project to the dorsal part of the dLGN of the contralateral side (for review, see (Casagrande et al., 2002; Hübener, 2003). A minority of axons (5-10%) from the ipsilateral retina (red in Fig. 1.3) does not decussate but instead project to the ipsilateral dLGN. Therefore, inputs from both eyes remain fully segregated already in the thalamus. This segregation is maintained in the next station of the visual path, L4 of V1, which represents the major first input of visual information within the neocortex. This architecture gives rise to visual maps and *retinotopy* (discussed below).

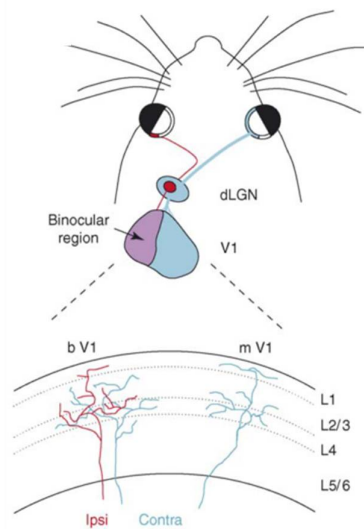


Figure 1.3. Organization of pathways from retina to visual cortex. The biggest part of the primary visual cortex (V1) receives input only from the contralateral retina (blue). The lateral third of V1 is innervated by ipsilateral projections (red). Despite the fact that neurons in the binocular region (bV1) are dominated by contralateral eye input, most neurons respond to both eyes. Thalamocortical axons from the dLGN arborize mainly in L4 but also in superficial layers (L1-3). From (Hofer et al., 2006b).

According to the scheme described above, the majority of neurons in rodents V1 receive input mostly from the contralateral retina (monocular region of V1 or V1m). Yet, a smaller proportion of V1 also receives ipsilateral projections, processing visual information from the

ipsilateral eye. In this binocular region of V1 (V1b), most neurons respond to visual stimuli presented to both eye, although the input from the contralateral eye is overall stronger. V1 is therefore governed by an *Ocular dominance (OD)* bias, meaning that neurons respond preferentially to the stimulation of one eye (I will better discuss this concept in the context of visual plasticity). It is important to note that visual information is driven by parallel paths both in the retina and dLGN, whereas V1 is the first site where inputs from both eyes converge and can compete at the synaptic level. In contrast to cats, mice lack clear segregated OD columns, but most neurons in mouse V1b receive input from both eyes and differ distinctly in their OD.

In sum, one hallmark of the visual system is its remarkable hierarchy, the so-called retinotopic maps (giving rise to ocular dominance bias) and the notion of receptive field.

Retinotopy and Receptive Field:

Retinal cells are activated within tiny and precise spots located all around the retina. The small region of the retina that generates a spike in response to a light stimulus is named the *receptive field (RF)* (Niell and Stryker, 2008). Classically, a receptive field is defined as the area of the sensory space in which stimulus presentation leads to a response from a particular sensory neuron. As shown in figure 1.4, visual cells can be classified as “on-center–off-surround” and “off-center- on-surround” cells: on-center cells fire action potentials when the center of their receptive field is illuminated, while off-center cells behave the opposite, as they are activated by the stimulation of the surround region. These RFs overlap, and fill the entire retinal surface. Many of these visual cells converge onto the same postsynaptic neuron in the dLGN, which further converge onto the same neuron in V1. In this way, this *retinotopic* organization of the visual pathways is maintained from the retina all the way to V1 and results in a complete and continuous map of the visual field. Therefore, the analysis of the different retinal receptive fields allows reconstructing the retinal map of the retina in neocortical visual area V1.

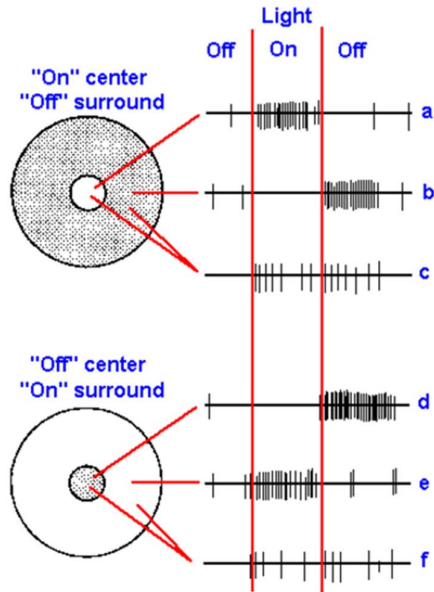


Figure 1.4. Receptive fields of two retinal ganglion cells. Fields are circular areas of the retina surrounded by an annulus of different properties. The cell in the upper part of the figure responds when the center is illuminated (on-center, a) and when the surround is darkened (off surround, b). The cell in the lower part of the figure responds when the center is darkened (off-center, d) and when the surround is illuminated (on-surround, e). Both cells give on- and off- responses when both center and surround are illuminated (c and f), but neither response is as strong as when only center or surround is illuminated. Adapted from (Hubel, 1963).

Neuronal tuning:

The notable hierarchy and configuration of the visual system that I discussed above, together with the high degree of convergence between the three main actors of the visual processing (retina – dLGN – V1), make neurons of the primary visual cortex extremely selective for specific sensory features. In other words, neocortical principal neurons are “tuned” to specific stimuli. Indeed, some cells (defined as simple cells) detect edges or bars oriented with a certain angle, while others respond most strongly to stimuli that have a direction of motion or speed (complex cells). This notion of *stimulus selectivity* and simple-complex cells has been first described by Hubel and Wiesel (HUBEL and WIESEL, 1959).

It turns out that neurons in the cortical area V1 are tuned and selective for a variety of sensory features, including spatial frequency, speed, direction, orientation, as well as contrast gain control and contrast-invariant tuning. A large number of studies investigated these selective responses, aimed to define the circuit and cognitive aspects of feature selectivity (Zariwala et al., 2011; Priebe and Ferster, 2012; Stevens, 2015; Priebe, 2016; Ringach et al., 2016). Interestingly, it was shown that in L2/3, excitatory pyramidal neurons that are tuned to the same feature are also more strongly connected between themselves (Ko et al., 2013). Also, it is worthy to mention here that whereas principal glutamatergic neurons are strongly tuned to

sensory features, inhibitory interneurons are broadly tuned, *i.e.* they respond similarly to stimuli possessing different characteristics (Chen et al., 2013).

The visual system structure, connectivity, retinotopic maps and RF properties have been extensively characterized by electrophysiological experiments performed both *in vitro* and *in vivo*. Moreover, in the last decade, the studies of visual cortical activity, and the role played by specific cortical neurons, have reached a unprecedented precision, thanks to the implementation of new cutting-edge imaging and optogenetic techniques, and novel optical tools (Schuett et al., 2002; Boyden et al., 2005; Heimel et al., 2007; Ko et al., 2013; Zhuang et al., 2017).

In order to understand how all this circuitry gives rise to visual processing, I will present the different cellular components of this hierarchical architecture, from the eye to the brain, to see how their properties can serve vision and plasticity, from both anatomical and physiological aspect.

1.1.2.1 The retina: first element of the chain

As shown in figure 1.5, this sensory peripheral organ has a structure organized over multiple layers: three layers of cell bodies (stained in blue) and two layers of neurites (in green), formed by five classes of neurons: photoreceptors, horizontal cells, bipolar cells, amacrine cells, and finally ganglion cells (GC) (Hoon et al., 2014; Masland, 2012).

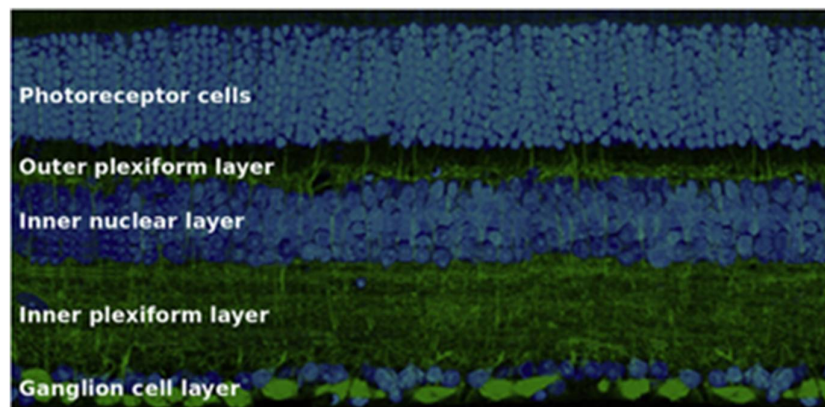


Figure 1.5. The retina is composed of three nuclear layers (containing cell bodies – in blue), and two plexiform layers (neurites – in green). Adapted from (Masland, 2012).

The role of the retina is to convert an optical image into a neuronal signal. This transformation involves 3 stages: *i*) the retina detects photons via millions of photoreceptor cells - cones and rods (Fu and Yau, 2007). They are distributed all across the retina, and each cell can only detect light coming from a specific and tiny point in the retinal space *ii*) the retina transmits these signals to bipolar neurons via excitatory chemical synapses, and *iii*) further integrates visual information at the level of GC, the output elements of the retina, as they project to the brain through the optic nerve. At each of these stages, there are lateral connections from horizontal and amacrine cells that provide feedback inhibition. Figure 1.6 illustrates the wiring between the different cell types of the retina (Gollisch and Meister, 2010).

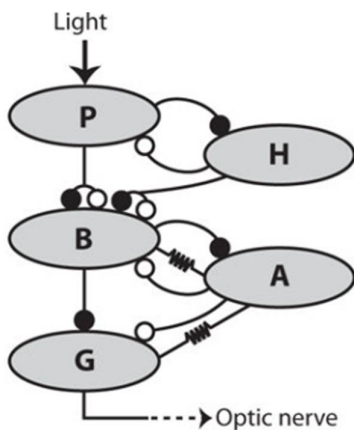


Figure 1.6. Circuitry in the retina, where P = photoreceptors, H = horizontal cells, B = bipolar cells, A = amacrine cells, and G = ganglion cells. The neurons in the retina are connected through chemical synapses that are either excitatory (closed circles) or inhibitory (open circles). Moreover, Gap junctions led to electrical coupling (marked by resistor symbols). From (Gollisch and Meister, 2010).

Retinal cells are excited in a more efficient way by shining light on small circular spots. This is the *Receptive Field* (RF) of retinal cells (Carcieri, 2003; Huberman et al., 2009; Rivlin-Etzion et al., 2011; Chen et al., 2014).

When leaving the retina via ganglion cell axons, visual sensory information is relayed to the thalamus.

1.1.2.2 The dorso lateral geniculate nucleus: relay between the eye and the cortex

The thalamus is the major afferent path to the neocortex. Indeed, all information directed to the neocortex has to pass through this intermediate structure. The thalamus is composed of several nuclei, each of them generating specific pathways targeting different cortical areas. Visual information coming from the retina reaches the dLGN and is then relayed to the visual

cortex. Interestingly, however, only 5–10% of the input to geniculate relay cells originates from the retina. The other 90% of the synapses are modulatory inputs from local inhibitory neurons (Sherman and Guillery, 2004; Yang and Cox, 2007), descending inputs from the visual cortex (cortico-geniculate), and ascending inputs from the brainstem. The circuitry is illustrated in figure 1.7.

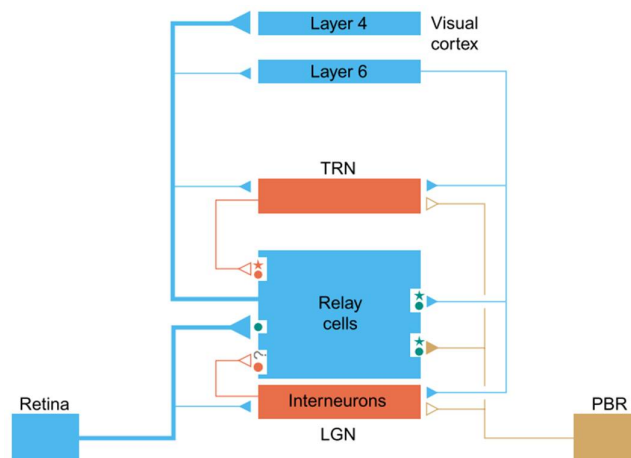


Figure 1.7. Schematic view of the main connections of the dLGN. Inhibitory (opened triangles) or excitatory (filled triangles) synapses are shown together with the post-synaptic receptors activated by each input on relay cells, and the neurotransmitters involved. Abbreviations: LGN lateral geniculate nucleus; PBR parabrachial region; TRN thalamic reticular nucleus. From (Murray Sherman, 2001).

The thalamus has been extensively investigated in terms of its anatomical organization, connectivity, basic neural response properties, and synaptic, biochemical, and molecular features. Here I will specifically focus on its anatomy and circuitry that will be of interest for the rest of my thesis work.

dLGN anatomy:

The mammalian dLGN is organized in multiple layers. In particular, in higher mammals, such as cats and primates each layer receives input from one eye only (monocular input): layers 2, 3 and 5 receive information from the ipsilateral eye whereas layers 1, 4 and 6 process inputs from the contralateral retina (Preston and Evans, 2011). In rodents, this laminar segregation of dLGN is less clear-cut and more difficult to investigate (Torborg and Feller, 2004). However, in contrast to the classical monocular structure of cats, some neurons in rodent dLGN respond to

stimulation from either eye, indicating that dLGN can integrate visual information in a more binocular fashion than higher mammals (Grieve, 2005; Zhao et al., 2013; Howarth et al., 2014).

dLGN circuitry:

Relay glutamatergic neurons of dLGN receive strong inhibitory inputs from the reticular thalamic nucleus (RTN), which is a shell-like structure of parvalbumin-positive (PV) GABAergic inhibitory neurons, which are highly interconnected and send inhibitory collaterals to dLGN neurons (Tanahira et al., 2009). This loop of recurrent connections between dLGN glutamatergic and RTN GABAergic neurons (Fig. 1.7), together with the endowment of specific Ca^{2+} channels in both structures, is responsible for the generation of rhythmic activity (Huguenard and McCormick, 2007).

The major target of the dLGN is essentially L4 of V1, and, less extensively, a small portion of L6. dLGN input to the neocortex provides powerful feedforward excitation onto both excitatory and inhibitory cortical neurons (Latawiec et al., 2000; Amitai, 2001; Bagnall et al., 2011; Kloc and Maffei, 2014). In addition to the prominent innervation of visual cortical L4, a previous study indicated that a portion of the dLGN projects to superficial L1 and L2 of V1 (Wickersham et al., 2007).

Importantly, the excitatory feedback from the neocortex onto dLGN originates almost exclusively from L6 (Bourassa and Deschenes, 1995). Several studies have demonstrated that this top-down signal can modulate the responses and receptive field of dLGN cells to visual stimuli and thus influence the firing pattern, synchronization, sensory responses and plasticity mode of thalamic cells (Sillito and Jones, 2002; Worgotter et al., 2002; Briggs and Usrey, 2008; Usrey and Alitto, 2015).

Moreover, thalamic activity is modulated by local interneurons that provide feedforward inhibition (FFI) following GC activation (Guillery and Sherman, 2002). Within dLGN, inhibition is mediated by $GABA_c$ receptors (Schlicker et al., 2004) as well as tonic $GABA_A$ conductances (Bright et al., 2007). Interneurons have the property to dynamically release GABA from dendrites and axons (Acuna-Goycolea et al., 2008). This local mediated inhibition refines RF of thalamic cells by enhancing surround inhibition (Norton et al., 1989) and it also controls the number of visually evoked responses of thalamic neurons as well as the precision of their timing (Blitz and Regehr, 2005).

In conclusion, although the thalamus is classically considered as a passive relay from the eyes to the cortex, dLGN is actually able to filter and introduce more complexity in the visual information flow before it reaches V1. The dLGN can therefore determine what, when and how information is delivered to V1 (Saalmann and Kastner, 2011), according to the behavioral demand of neurons.

1.1.2.3 The primary visual cortex: first cortical level of visual processing

As mentioned above, the thalamus relays visual information mostly to L4 of visual neocortical area V1. In this section, I will present the general organization of the neocortex from its anatomy to the cellular elements, which is common to all sensory systems including the visual one.

In all mammals, the neocortex is divided into six layers (Fig. 1.8) from the pial surface to the white matter. The neocortex is about 2 mm-thick, and contains ~ 50.000 neurons/mm³. The study of its laminar organization, the so-called *cytoarchitectonics* is the field of research of many groups since the 20th

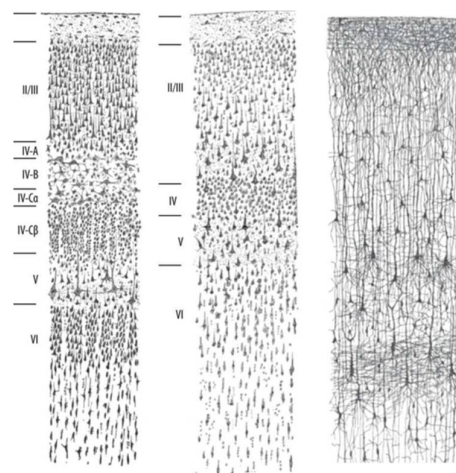


Figure 1.8. Drawing of neocortical layers from Ramon y Cajal 1911. Left: Nissl staining of the adult visual cortex of human. Middle: Nissl staining of the adult motor cortex of human. Right: Golgi staining of the infant human neocortex.

Century. Since then, the anatomy (Douglas and Martin, 2004) and physiology of this structure has been very well described. Moreover, in recent years the development of novel optical and optogenetic tools allowed the dissection of specific circuits involved in visual processing (Nagel et al., 2003; Stosiek et al., 2003; Boyden et al., 2005; Carandini et al., 2015). Yet, an ongoing debate on the operating principals of the cerebral cortex still persists (Wallace and Kerr, 2010).

What is certain is that the elaborate and fundamental functions performed by the neocortex (such as sensory perception and motor behavior) are possible because of the tight interplay of heterogeneous but stereotypic organized networks, composed of multiple cell types arranged in micro-to-large scale neuronal circuits (Silberberg et al., 2002). As a general motif of

neocortical circuits (shared by all sensory areas), two main types of neurons compose these neuronal networks: excitatory glutamatergic neurons, which form about 70-80% of cortical neurons and inhibitory interneurons that use γ -aminobutyric acid (GABA) as neurotransmitter and make up to ~20% of the entire cortical neuronal population (Fig. 1.9). Glutamatergic neurons, are mainly characterized by the pyramidal shape of their cell bodies, presence of dendritic spines and long-range axonal projections (Spruston, 2008). In contrast, GABAergic inhibitory neurons encompass many subtypes. They exhibit non-pyramidal morphologies, smooth aspiny dendrites, and local axonal projections (Ascoli and Alonso-Nanclares, 2008; DeFelipe et al., 2013). The density, the morphological (soma and dendritic arborization) and electrophysiological properties of both cell types are layer-dependent. These two main actors are reciprocally interconnected so that cortical functions depend on the correct arrangement of neural circuits between them (for review see (Isaacson and Scanziani, 2011b; Harris and Shepherd, 2015). A detailed description of cortical cell types is provided below.

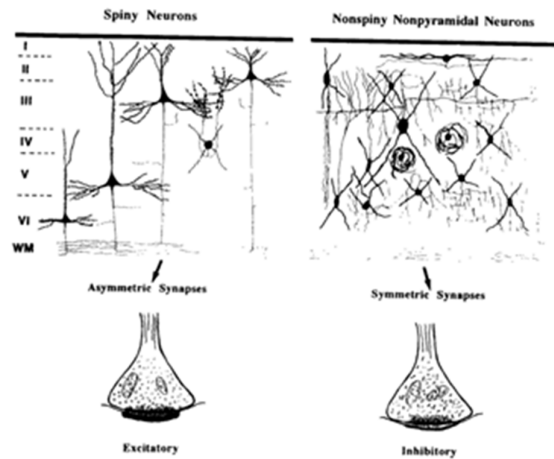


Figure 1.9. Schematic diagram showing the classes of neurons and synapses in the cerebral cortex. From (DeFelipe and Fariñas, 1992).

Cortical processing:

The cortex works via a combination of feedforward drive (bottom-up from the previous sensory order), feedback drive (top-down context from the next stage), and prior drive (expectation), as illustrated in figure 1.10. Each stage is under control of modulators and oscillatory activity (Heeger, 2017). In this scenario, the feedforward stream is driven by

external information influencing the sensory machinery, whereas the feedback pathway is conveyed by an internal context built from previous experiences (Larkum, 2013).

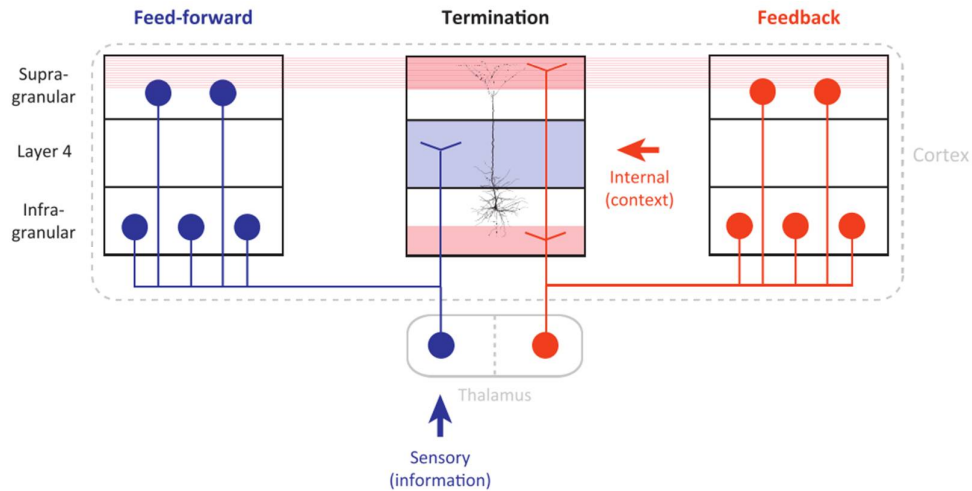


Figure 1.10. General scheme for feed-forward and feedback connectivity between cortical areas. In the middle panel, a L5 pyramidal neuron (black) has been superimposed to coloured rectangles to highlight the location of the dendrites relative to the large-scale wiring of the cortex. From (Larkum, 2013).

Circuitry within a cortical column:

As a general scheme of the sensory cortical microcircuits (Fig. 1.11), the input layer is L4, and, less extensively, L6 (as mentioned above), whereas superficial L1 and L5a are mostly targeted by associative thalamus (Larkum, 2013). Then, sensory information is relayed within vertically oriented functional units named '*cortical column*' (for review see (Rockland, 1998)). L4 projects massively to supra-granular L2/3, which is considered an integrative layer, as it receives feedforward information from L4 as well as feedback input from other cortical areas. L2/3 project to L5 whose pyramidal neurons project back to subcortical regions. To conclude this scheme, L6 provides a direct powerful feedback excitatory modulation to thalamic nucleus as well as an indirect feedback via a monosynaptic intracortical connection from L4 (Feldmeyer, 2012) (Qi and Feldmeyer, 2016). For review on the cortical organization described above see (Bence and Levelt, 2005; Allene et al., 2015).

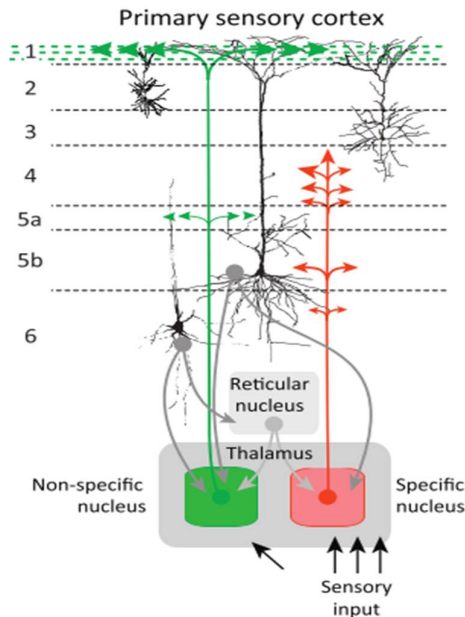


Figure 1.11. Excitatory neocortical microcircuits. Example for the somatosensory system but the architecture is identical for all sensory systems. From (Larkum, 2013). In each layer, local interneurons modulate the responses of excitatory neurons (not shown).

Although the thalamus is the main source of input to the neocortex, more than 20 different subcortical structures projecting to neocortex have been identified (Tigges, J., and Tigges, 1985). Moreover, cortical neurons receive excitation from different cortical areas. Thus, thalamus and neocortex work together to shape sensory responses (Reinhold et al., 2015). In the visual system, it was recently shown the crucial role of cortical circuits as amplifiers of tuned thalamic excitation during visual stimuli (Lien and Scanziani, 2013).

Excitatory cortical neurons:

The major type of cortical neurons (80-90%), usually referred to as Principal Neurons (PN), share similarities in their morphological and electrophysiological properties (Fig. 1.12) and form a quite homogenous group at first glance (Peters A, 1984; Connors and Gutnick, 1990) (Peters A, 1984). These cells use the excitatory amino acid glutamate as their primary neurotransmitter. Glutamatergic neurons receive local inhibitory GABAergic inputs onto both soma and axons depending on the type of interneurons. In contrast, most of the excitatory synaptic drive arrives through the dendrites from multiple sources. Generally, proximal dendrites receive inputs from local sources whereas the distal apical tuft is contacted by inputs from more distant cortical and thalamic pathways. Dendrites, by their passive and active biophysical properties, determine neurons input-output functions by influencing the integration of synaptic signals through temporal and spatial summation (Major et al., 2013). For a review on dendritic integration see (Stuart and Spruston, 2015). The postsynaptic sites where most of these dendritic excitatory inputs take place were first discovered by Santiago Ramón y Cajal (Yuste, 2015) and are referred to as 'spines'. These structures, covered by thousands of excitatory neurons, are highly plastic and play an important role in activity-dependent changes of synaptic efficacy such as long-term potentiation (LTP) or long-term depression (LTD) (Rocheffort and Konnerth, 2012).

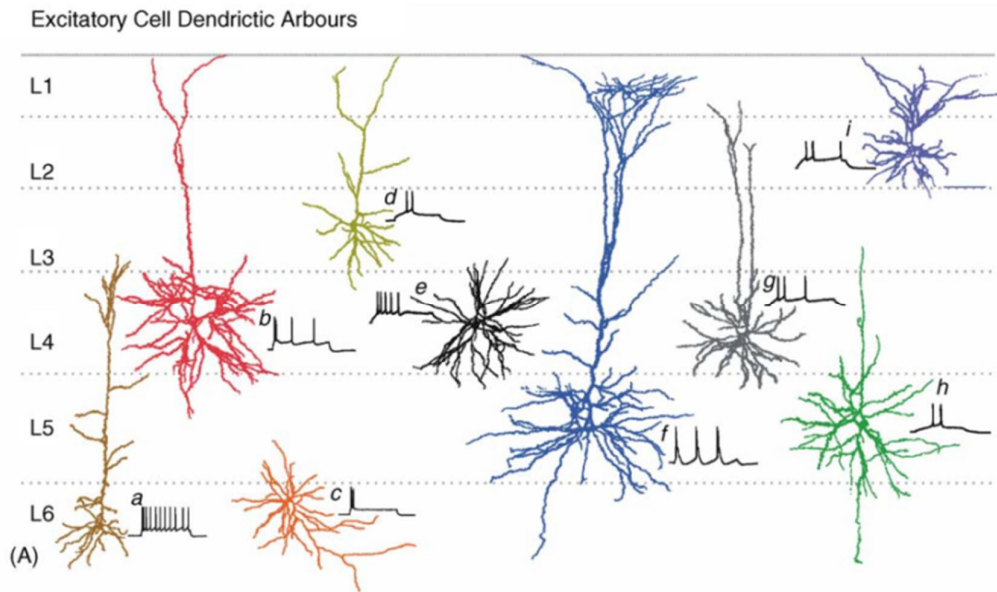


Figure 1.12. Diversity of excitatory neurons across cortical layers. Several examples of reconstruction of dendritic tree of excitatory neurons of layers 2–6 shown together with the corresponding firing pattern. From (Bannister, 2005).

Electrophysiologically (Fig. 1.13), most neocortical excitatory neurons typically fire in a regular spiking (RS) manner, meaning that they show adapting action potentials (AP), followed by a steady-state regular firing in response to depolarizing current pulses (McCormick et al., 1985). However, some deep L5 pyramidal neurons fire repetitive bursts, and they are thus classified as intrinsically bursting neurons (Agmon and Connors, 1989).

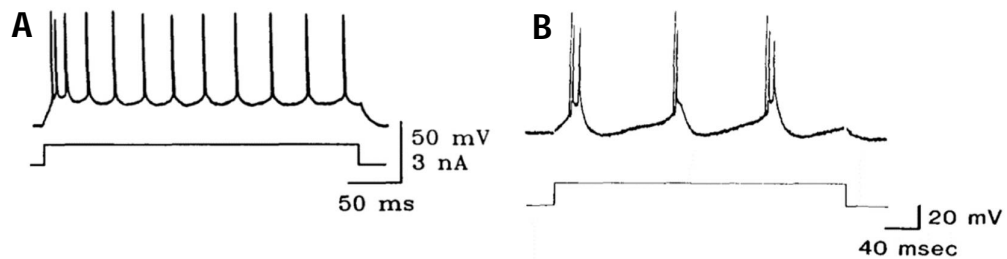


Figure 1.13. Example firing pattern of two types of excitatory neurons. (A) Representative regular spiking discharge of excitatory neocortical neurons in response to depolarizing current injection. From (Connors and Gutnick, 1990) (B) Representative intrinsically bursting neuron of L5, in response to current injection. From (Agmon and Connors, 1989).

Based on morphological features, we can typically distinguish two main groups of principal neurons: the pyramidal (PYR) cells, and the spiny stellates (SS) cells (Feldman, 1984), which essentially differ from each other across and within layers by the size and shape of their cell body, the extent of their dendritic arborization and the density of the spines (DeFelipe and Fariñas, 1992; Spruston, 2008). Pyramidal somata are situated in L2–6 whereas spiny stellate are within L4 of primary sensory areas. What essentially differentiates a PYR neuron with a SS cell is that the first one presents an apical dendrite that extend through the layers above the soma. This lead to the fact that PYR, contrary to SS, can receive, via their long distal apical tuft, top-down projections from higher order areas of the cortex, situated in the most superficial layers. In addition, cortical excitatory principal neurons can be classified according to their projection patterns (*e.g.* cortico-cortical vs. cortico-striatal vs. cortico-tectal) (Brown and Hestrin, 2009) or their functional connectivity in response to sensory stimulation (Ko et al., 2013). The specific connectivity blueprint of different pyramidal neurons is reviewed in Allene *et al.*, 2015 (Allene et al., 2015).

Inhibitory cortical neurons:

Sensory relevant information is carried by long-range glutamatergic excitatory neurons. However, the activity of excitatory neurons is strongly modulated by a rich diversity of local inhibitory GABAergic interneurons. Although encompassing the minority of cortical neurons (10-20%) GABAergic neurons play a critical role in controlling, modulating and shaping the activity of principal neurons. Within brain networks, excitation works in "balance" with inhibition (E/I balance) in order to perform correct circuit computations underlying sensory processing (Isaacson and Scanziani, 2011a). Indeed, an imbalance between the E/I ratio leads to neurological and psychiatric disorders such as epilepsy, autism and schizophrenia (Marín, 2012; Gao and Penzes, 2015; Nelson and Valakh, 2015). Similarly to excitatory neurons, also inhibitory cells share some common characteristics. First, they all use the γ -aminobutyric acid (GABA) as neurotransmitter (Klausberger and Somogyi, 2008). Second, according to Ramón y Cajal's definition, they are 'short axon cells' (Ramon y Cajal, 1899), and indeed they almost exclusively modulate the local neuronal network, due to their restricted axonal and dendritic arborizations. For this reason they are called interneuron (IN). Importantly, however, several studies indicate the existence of long-range GABAergic neurons (Tamamaki and Tomioka, 2010; Lee et al., 2014; Yuan et al., 2017). Another common feature of inhibitory interneurons is the lack or sparse expression of dendritic spines (Kubota et al., 2011). Finally, their soma,

contrary to PNs, can be contacted by both glutamatergic and GABAergic synapses (R. Douglas, H. Markram, 2004).

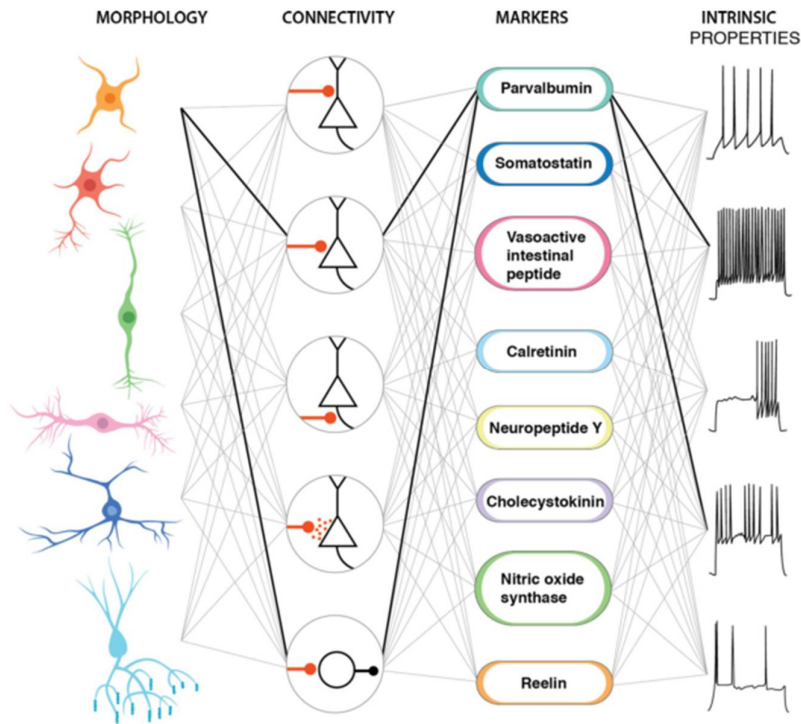


Figure 1.14. Multiple dimensions of interneuron diversity. Interneuron cell types are usually defined using a combination of criteria based on morphology, connectivity pattern, synaptic properties, marker expression and intrinsic firing properties. The highlighted connections define fast-spiking cortical basket cells, from (Kepecs and Fishell, 2014).

Despite these common morpho-functional characteristics, INs form a spectacularly heterogeneous neuronal population. Indeed, INs' remarkable diversity is based on their morphological, electrophysiological and connectivity properties, as well as the expression of molecular markers, such as Ca^{2+} -binding proteins and neuropeptides (Gupta, 2000; Ascoli and Alonso-Nanclares, 2008; DeFelipe et al., 2013). Figure 1.14 resumes the rich diversity of the GABAergic cortical neurons. Due to the overlap of the different morphological and functional features attempting to define different IN subclasses, to date a clear classification of the many cortical IN subtypes is far from being established. Even though the classification of cortical GABAergic interneurons is problematic, perhaps one relevant functional classification relies on their specialized connectivity with different domains of PNs (Fig. 1.15) that generates an efficient division of labor of different forms of inhibition during cortical activity. Indeed, we can typically distinguish the perisomatic-targeting basket cells (BC) and the axo-axonic chandeliers

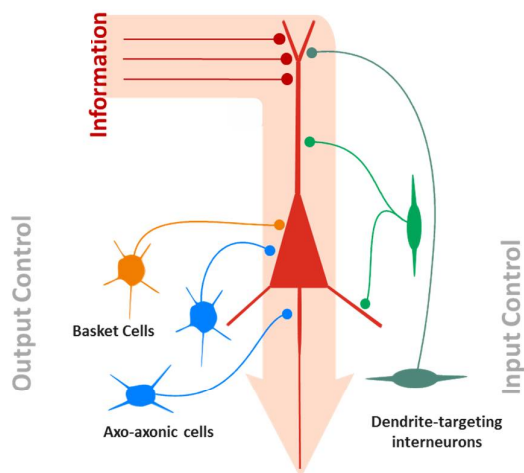


Figure 1.15. Oversimplified scheme of cortical GABAergic circuits controlling principal pyramidal neurons directly and indirectly. The information coming onto principal cells can be specifically and directly filtered by different interneuron types, which can be specialized in output (left) or input (right) control. From (Méndez and Bacci, 2011).

cells. The precise targeting of BCs and chandelier cells on the output region of PNs allows a precise control of PN output spiking activity. Basket cells, which represent the largest population of INs (about 50%) can be divided into two large subclasses: the PV-expressing and the cholecystokinin (CCK)-expressing basket cells that express cannabinoid receptor type 1 (CB1R) (Freund and Katona, 2007). PV⁺ basket cells sustain high-frequency firing, receive strong excitation, release GABA very reliably, and are considered the clockwork of cortical networks, as they synchronize a large population of

principal cells (Buzsáki and Draguhn, 2004; Freund and Katona, 2007; Klausberger and Somogyi, 2008). Conversely, basket cells expressing CB1Rs (and CCK) receive less excitation, cannot sustain high-frequency firing, release GABA more asynchronously and unreliably (Hefft and Jonas, 2005), and are negatively modulated by endocannabinoids (Kano et al., 2009). Notably, CCK⁺ cells are the specific target of subcortical neuromodulators, such as acetylcholine and serotonin, and this, together with their more 'capricious' GABAergic transmission led to the hypothesis that CCK⁺ cells exert a fine-tuning of cortical activities and might play a key role in the control of mood (Freund and Katona, 2007; Varga et al., 2009). This functional classification of PV and CCK BCs derive mostly from studies in the hippocampus (Freund, 2003; Szabadics J, Varga C, Molnar G, Olah S, Barzo P, 2006; Freund and Katona, 2007). Indeed, a deep knowledge of the different distribution of CCK and PV cells in different neocortical layers and areas is missing. Yet, we know that CCK/CB1 BCs are mostly located in superficial cortical layers (L1 and L2/3), where they share the perisomatic control of PN excitability with PV BCs. In contrast, L5 PNs are almost exclusively modulated by PV BCs (Allene et al., 2015). Importantly, both PV and CCK cells include several subtypes that can be classified by their specific connectivity patterns.

Another major subclass of cortical inhibitory cells is represented by dendrite-targeting interneurons such as Martinotti cells (which express the neuropeptide somatostatin or SST) and neurogliaform cells (which express high levels of neuronal nitric oxide synthase). Dendrite-targeting interneurons filter glutamatergic synaptic input, which, in PNs, mostly occurs at dendritic spines. Therefore, dendritic inhibition plays a crucial role in modulating dendritic non-linearity and input-output transformations, as well as plasticity of glutamatergic synapses (Palmer et al., 2012). Also SST cells are not a uniform cell type, and a clear picture of their different subtypes is only now beginning to emerge (Scheyltjens and Arckens, 2016). For a review on the different subtypes of INs see (Markram et al., 2004; Druga, 2009).

In addition to the connectivity logic of interneurons onto PNs, cortical inhibitory neurons can be recruited by distinct excitatory circuits (Isaacson and Scanziani, 2011b; Roux and Buzsáki, 2015). Excitatory inputs arising from cortical and subcortical regions can diverge onto both principal cells and interneurons, giving rise to *feed-forward inhibition* (Fig. 1.16A). This form of inhibition is ubiquitous, is triggered by long-range connections, and plays an important role in shaping and controlling the precise time window of PN spiking activity. This type of inhibition is exceptionally strong in L4 in which PV interneurons are potently recruited by thalamic fibers (Pouille, 2001; Gabernet et al., 2005; Cruikshank et al., 2007). *Feedback inhibition* is divided in recurrent inhibition (Fig. 1.16B) or lateral inhibition (Fig. 1.16C). In both cases a PN fires first and recruits a postsynaptic inhibitory neuron, which in turn suppresses the activity of the same (recurrent) or a neighboring PN (lateral) (Silberberg and Markram, 2007). Lateral inhibition is important for example in the visual cortex where it drives surround inhibition (Adesnik et al., 2012), which is a basic mechanism for setting and modulating the receptive fields. Furthermore, a form of *direct inhibition* arises when long-range GABAergic inputs from distant regions drive local inhibition in the circuit (Fig. 1.16D). Another important circuit, in which inhibitory neurons are involved, is *disinhibition*, which takes place when GABAergic neurons target other GABAergic neurons (Fig. 1.16E). This can mediate network synchrony or disinhibition of principal neurons (Sohn et al., 2016).

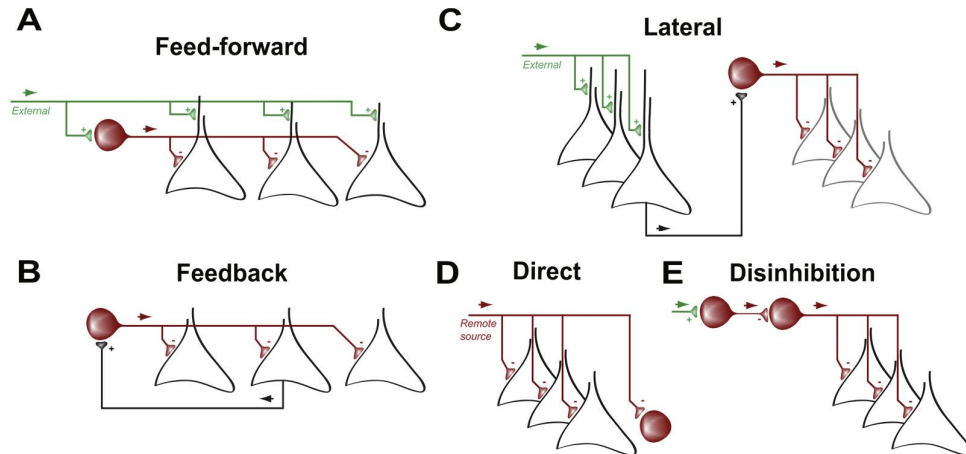


Figure 1.16. Main forms of inhibitory microcircuits. (A) Feed-forward inhibition (B) Feed-back inhibition. (C) Lateral inhibition. (D) Direct inhibition. (E) Disinhibition. Interneurons are in red, afferent excitatory inputs from an external source in green and local principal neurons in black. Modified from (Roux and Buzsáki, 2015).

Inhibition of inhibition is a common feature in cortical circuits. In particular, visual cortex activity relies on distinct inhibitory connectivity patterns (Pfeffer et al., 2013). For example, we know that PV INs inhibit strongly themselves via autaptic transmission and mutual inhibition between PV cells (see paragraph below dedicated to PV cells). Moreover, SST INs have a preference for other types of INs, and tend to avoid other SST cells. An important disinhibitory cortical circuit involves interneurons expressing the vasoactive intestinal polypeptide (VIP). These interneurons are specialized in contacting other GABAergic neurons selectively, and they have a particular preference for SST cells, although they also inhibit PV cells with a lower extent (Pfeffer et al., 2013; Kepecs and Fishell, 2014). VIP IN-dependent disinhibition has been recently described to underlie several cognitive functions, including auditory discrimination (Pi et al., 2013), sensory-motor integration (Lee et al., 2013) and working memory (Kamigaki and Dan, 2017).

The parvalbumin-positive fast-spiking interneurons:

In this section, I will expand on one subtype of neocortical INs, which is of particular interest for my thesis work: the fast-spiking (FS), PV-positive basket cell, which contacts the perisomatic region of principal neuron with a basket-like axonal structure (Fig. 1.17A). These cells have a multipolar morphology and extended dendritic arborization that often spans

several cortical layers, allowing them to be recruited by different excitatory afferent pathways, such as feedforward and feedback circuits (Pouille, 2001; Gabernet et al., 2005; Cruikshank et al., 2007). They express the Ca²⁺-binding protein parvalbumin, defining them as belonging to the PV cell classes (Kawaguchi et al., 1987). PV is an endogenous Ca²⁺-binding protein that controls both synchronous and asynchronous GABA release (Manseau et al., 2010). PV expression starts in the second week of postnatal age in mice, and, in the hippocampus, PV levels are inversely correlated with the degree of plasticity of the network: PV expression diminishes when the network is plastic and increases with reduced plasticity (Donato et al., 2013, 2015). The specific expression of PV is generally used as a marker to recognize these cells in anatomical studies, and allowed the generation of transgenic mice in which PV cells can be identified and/or manipulated (Taniguchi et al., 2011).

Fast-spiking cells owe their name to their firing pattern in response to depolarizing current steps, as they can display abrupt high firing frequency (several hundred Hz). Importantly, FS cells can fire up to 600-800 Hz *in vivo* during seizure activity (Timofeev et al., 2002). *In vitro*, spike trains are typically non-adapting, and action potentials exhibit a large and fast afterhyperpolarization, as shown in figure 1.17B (McCormick et al., 1985). These INs are endowed with everything is needed to make them “fast machines”: *i*) on their dendrites, they express a high density of voltage-gated potassium channels of the Kv3 subtype (Chow et al., 1999) which have high activation threshold, fast activation, and fast deactivation properties, thus allowing fast repetitive firing (Rudy and McBain, 2001) *ii*) they express high levels of sodium channels allowing fast AP propagation along the entire axonal length (Hu and Jonas, 2014) *iii*) they possess short membrane time constants and low input resistance (Nörenberg et al., 2010) *iv*) they express ultra-fast AMPA receptor conductance (and no or little NMDA conductance) *v*) they release rapidly and reliably GABA at their terminals. Furthermore, by targeting the soma and proximal dendrites of principal neurons, they provide powerful perisomatic inhibition (Freund and Katona, 2007) controlling and synchronizing the firing of a large number of PNs during gamma activity (Cardin et al., 2009; Sohal et al., 2009) as well as in gain control of sensory processes (Atallah et al., 2012).

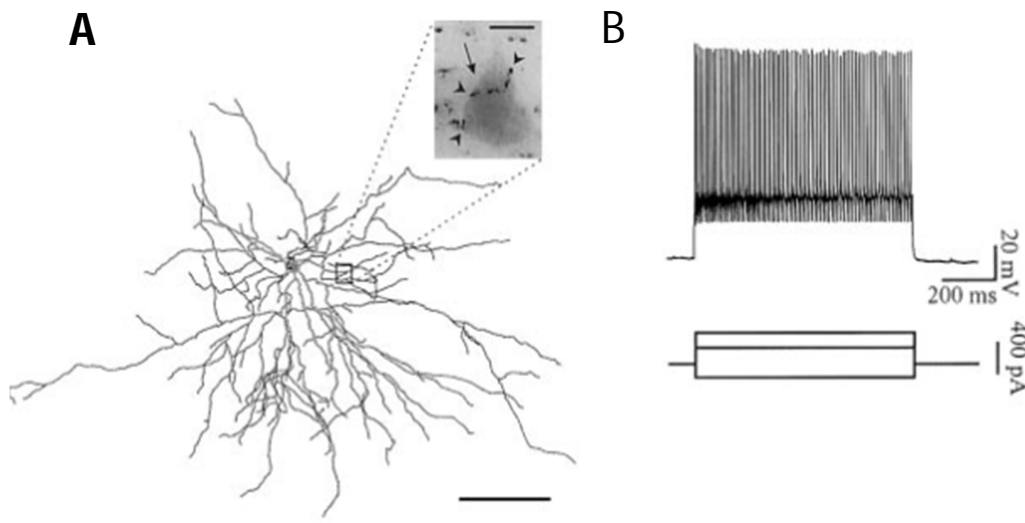


Figure 1.17. Firing properties and morphology of a PV-positive neuron. (A) Reconstruction of a small multipolar interneuron. The inset shows boutons (arrowheads) in close apposition to a slightly background-stained pyramidal cell soma (arrow), indicating a basket-like structure. Bar: 10 μm . **(B)** Firing pattern (in current clamp) after injection of current pulses. From (Angulo, 2002).

A recent study (Hioki, 2015) analyzed the compartmentalization of inputs onto PV cells: in neocortical L4, they receive more cortical inhibitory synapses onto proximal dendrites, whereas excitatory inputs from cortical PNs are located on the most distal dendritic portions. In contrast, excitatory thalamic axons have no preferences in the targeting PV cells (Bagnall et al., 2011). Importantly, PV cells are strongly coupled to other PV cells via chemical synapses and gap junctions (Galarreta and Hestrin, 2002) and show a high degree of self-inhibition via functional autaptic GABAergic synapses (Tamás et al., 1997; Bacci et al., 2003; Bacci and Huguenard, 2006) that drive a particular type of disinhibition in the circuits. For review see (Deleuze et al., 2014). Figure 1.18 illustrates anatomical (A and B) and functional (C) evidence of autapses in neocortical PV interneurons.

Finally, PV cells have implication in several neurologic disorders including epilepsy and schizophrenia (Marín, 2012) and are therefore important therapeutic targets. They are also essential in mediating experience-dependent plasticity (Hensch, 2005a). The next chapter of the manuscript is dedicated to cortical plasticity and the fundamental role of PV cells.

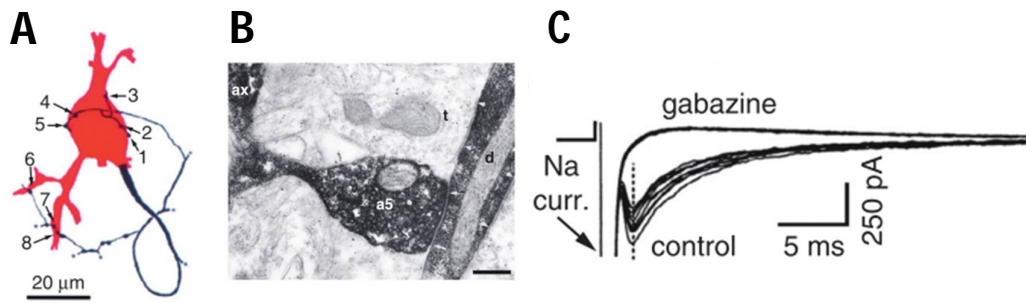


Figure 1.18. Massive self-inhibition of PV cells. (A) Subcellular distribution of autaptic contacts on a FS cell (1-8). Soma and dendrites are in red, axon in black. (B) Electron microscope image illustrating a self-innervating bouton ($\alpha 5$) targeting its own dendrite. Scale bar: 0.3 μm . (C) Representative traces illustrating synchronous GABAergic (gabazine-sensitive) autaptic release on a FS interneuron from rat neocortex. Autaptic transmission is induced by voltage steps eliciting fast inward Na currents (truncated). The dotted line indicates the peak of the response, showing fixed latency and peak-amplitude fluctuation. From (Deleuze et al., 2014).

1.2 Cortical plasticity – Experience-dependent visual plasticity

1.2.1 Critical period of plasticity

Why is it much easier for a child to learn a foreign language as well as a music instrument for instance? Why can young individuals learn something new so easily? Why are certain pathological conditions reversible in kids, but not in adults, like for instance recovering from visual deficits?

A hallmark of sensory systems is their sensitivity to experience which shapes and influence their maturation and affects their structures. Indeed, any perturbation of sensory experience has profound long lasting modifications in the organization and functioning of the system. This sensitivity and increased susceptibility to certain stimuli is present only during a specific time window where the brain and circuits are highly plastic and sensitive to the external world. This is the so called *critical period* (CP) of plasticity (Fig. 1.19), typical of juvenile's brain and very limited in adulthood. This window of heightened plasticity, during which neuronal circuits are sculpted and reorganized, requires environmental inputs for the proper maturation of brain connectivity, function and behavior. CPs are present across a variety of species, from humans

to drosophila and their duration (from weeks to years) is proportional to the lifespan of the species (Berardi et al., 2000). As indicated in figure 1.19, there are different CPs, depending on specific brain functions and circuits.

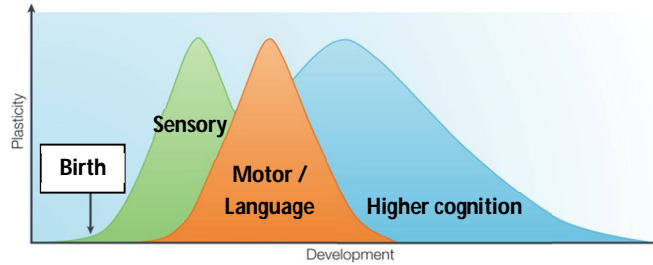


Figure 1.19. Windows of heightened plasticity in the developing brain. Adapted from (Takao K Hensch, 2005b)

As illustrated in figure 1.20, in the mouse visual system, retinotopic maps form well before eye opening which occurs around the second postnatal week (P14). Orientation-selective and contralateral-eye-driven neurons are already present at eye opening. During the subsequent days, neurons become more sensitive to visual stimulation, more selective for orientation tuning and their responses to inputs from the ipsilateral eye increase. During the CP (between P22 and P35 in rodents, with a peak typically around P28), the orientation preference of cortical neurons goes from mismatched eye-specific preferred orientations to binocular matching (Smith and Trachtenberg, 2007; Bhaumik and Shah, 2014). Importantly, an abnormal visual experience early in life leads to amblyopia (a condition known as *lazy eye*), a severe and permanent visual deficit resulting in a number of defects in spatial vision, such as decreased visual acuity and depth perception (McKee 2003).

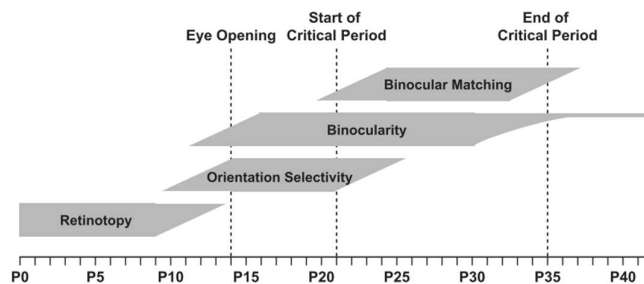


Figure 1.20. Developmental time course of the rodent visual system. From (Espinosa and Stryker, 2013).

In summary, the pre-CP is guided by molecular and neuronal signals that are genetically determined and mostly independent from external stimuli, while the maintenance and refinement of the neuronal microcircuits for binocular vision are driven by experience and environmental inputs during the CP.

1.2.2 Ocular dominance plasticity as a model to study experience-dependent plasticity

For a long time, the visual system has been the gold-standard model to study experience-dependent plasticity (Priebe and McGee, 2014). As mentioned at the beginning of the manuscript, pioneering experiments by Hubel and Wiesel showed that neurons in the visual cortex respond preferentially to the stimulation of the contralateral eye, providing an OD bias of neuronal responses. Their seminal work on kitten showed that the occlusion of one eye (by means of lid suture) during the CP induces a shift in the responses of cortical neurons: cells that in normal conditions would have been activated by the closed eye respond to the input coming from the non-deprived, opened eye (Wiesel and Hubel, 1963). This phenomenon, typical of young animals, is limited in adults. The shift in spiking toward the non-deprived eye is usually detected by single-unit electrophysiological recordings in V1 and quantified with an OD score (contralateral bias index), as represented in figure 1.21.

Sensory deprivation is widely used as a paradigm to study plasticity in the visual system and is very well documented. Indeed, only two or three days of a monocular deprivation (MD) in young mice are sufficient to produce a pronounced shift in OD, by creating a discordant binocular integration of inputs from the two eyes (Gordon and Stryker, 1996; Wang et al., 2010). This produces a loss of the responses throughout the deprived eye followed by an increase in the input from the open eye. The rapid functional effects of MD are underlined by anatomical rewiring of cortical circuits (Trachtenberg and Stryker, 2001; Maffei et al., 2004; Nahmani and Turrigiano, 2014) and thalamic afferents (Antonini and Stryker, 1996; Coleman et al., 2010). This paradigm will be better discussed later in section 1.2.3.2, in relation with the experiments we performed. For review on experience-dependent plasticity see (Hensch, 2005a; Hensch and Fagiolini, 2005; Levelt and Hübener, 2012).

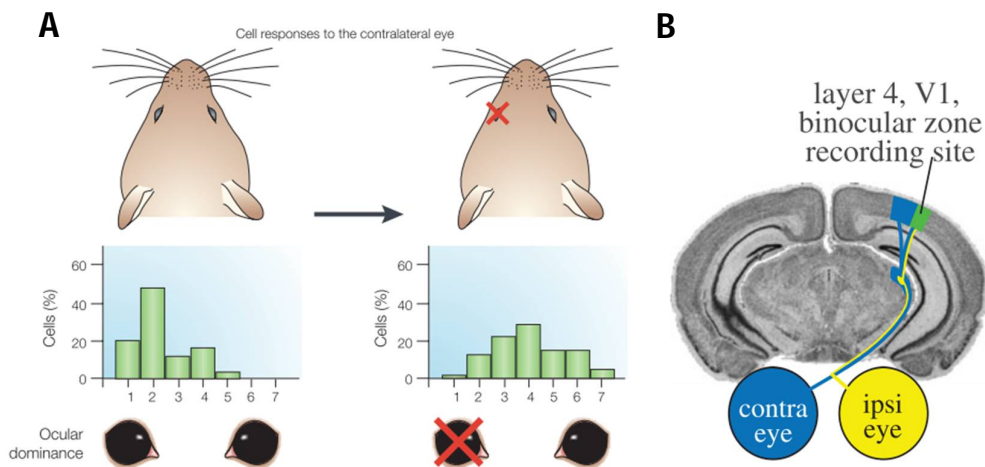


Figure 1.21. Ocular dominance (OD) plasticity in the visual cortex of juvenile mice. (A) Monocular deprivation (MD) produces a loss of response to the deprived eye and a gain of open-eye input, as measured by the neuronal discharge of single units from the mouse visual cortex. The OD of cells, rated on a seven-point scale of neuronal responsiveness, indicates a typical bias toward the contralateral eye (1–3) in the rodent. After 3 or more days of MD, the distribution shifts toward the open, ipsilateral eye (4–7). From (Takao K Hensch, 2005b). **(B)** Recordings are made from electrodes implanted in L4 of the binocular zone of V1 (green), receiving independent input from the contralateral (blue) and ipsilateral (yellow) eyes. From (Cooke and Bear, 2013).

Although many efforts have been dedicated to the investigation of plasticity in visual system, the cellular, synaptic and circuit mechanisms underlying critical period's plasticity are still elusive, and are of great interest in today's Neuroscience, because of the important implications for both normal and pathological conditions (Bardin, 2012).

1.2.3 Cellular, molecular and structural mechanisms of critical period

1.2.3.1 Role of inhibition

Fast synaptic inhibition shapes all forms of cortical activity (Isaacson and Scanziani, 2011a) and the modulation of experience-dependent structural plasticity is not an exception, as an optimal E/I balance is required for plasticity. It is now known that the onset of the CP is determined by the maturation of local inhibitory GABAergic circuits (Fagiolini and Hensch, 2000; Hensch, 2005b; Levelt et al., 2011). Accordingly, it is possible to shift the timing of the CP

for ODP by acting on such circuits *i.e* by manipulating inhibitory transmission (Fig. 1.22). Indeed, if inhibitory neurons in the cerebral cortex do not mature properly, the opening of CP does not occur. Conversely, if the level of inhibition is enhanced early in development, CP will open prematurely. The consensus is that two thresholds for inhibition are required to trigger and terminate the CP of plasticity. Experimentally, a series of studies demonstrated the crucial role of sensory stimuli and inhibition in the onset and offset of the CP. If mice are reared in complete darkness (dark rearing) from birth, CP is delayed, highlighting the essential role of visual inputs (Fagiolini et al., 1994). Visual stimuli provide the synthesis and the secretion of the specific growth factor brain-derived neurotrophic factor (BDNF). BDNF is produced by excitatory neurons and triggers the maturation of inhibitory neurons. Accordingly, overexpression of BDNF accelerates the onset of the CP (Huang et al., 1999), whereas blocking its signaling prevents the development of ODP (Cabelli et al., 1997). Interestingly, it is possible to accelerate the onset of CP by directly administrating the benzodiazepine diazepam, which is a GABA_AR positive allosteric modulator (Hensch et al., 1998). Another example of the crucial modulatory role of cortical inhibition is given by experiments using knock-out mice for an important isoform of the GABA synthesizing enzyme *Gad65*. *Gad65* KO mice show no CP for ODP following brief MD (Hensch et al., 1998), and plasticity is restored only after administration of benzodiazepines (Hensch et al., 1998; Fagiolini and Hensch, 2000; Iwai et al., 2003).

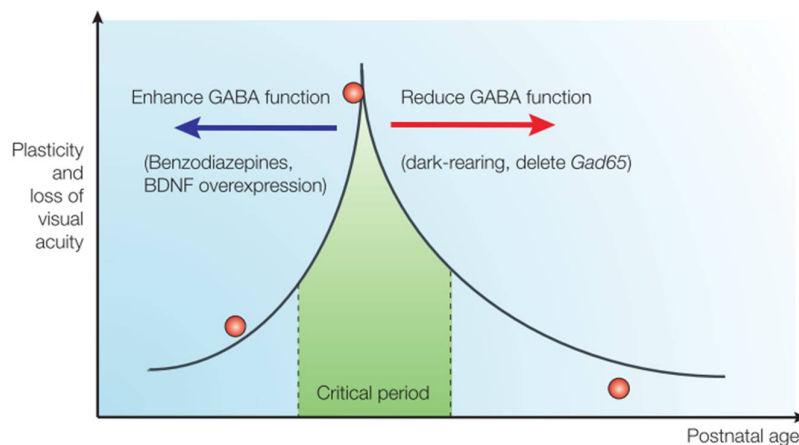


Figure 1.22. GABA-mediated control of the critical period. Sensitivity to MD is restricted to a critical period. The onset of plasticity can be delayed by directly preventing the maturation of GABA-mediated transmission by gene-targeted deletion of *Gad65*, which encodes a GABA-synthetic enzyme, or by dark-rearing from birth (red arrow). Conversely, the critical period can be anticipated by enhancing GABA transmission directly with benzodiazepines just after eye-opening or by promoting the rapid maturation of interneurons through BDNF expression (blue arrow). From (Takao K Hensch, 2005b).

In particular, PV-positive interneurons, which mature in parallel with the onset of the CP, have been indicated as key modulators of experience-dependent plasticity. Indeed, the specific blockade of the potassium channel Kv3.1, highly expressed in PV cells, leads to impaired ODP (Takao K Hensch, 2005b). In addition, in mice where the α -1 subunit of the GABA_AR is insensitive to benzodiazepines, CP cannot be induced (Fagiolini, 2004), suggesting again that PV interneurons are involved, as this subunit is enriched in inhibitory synapses formed by PV basket cells on the soma and proximal dendrites of PNs (Klausberger et al., 2002).

Another intriguing major actor in PV cell maturation and visual plasticity is the transcription factor Otx2. Interestingly, this function is accomplished through a non-cell autonomous mechanism. Otx2 is a homeoprotein, and the Otx2 gene locus is silent in juvenile and adult cortex. The Otx2 protein reaches cortical structures from extra-cortical sources: Otx2 is globally synthesized in the choroid plexus (Spatazza et al., 2013), which secretes the protein in the cerebrospinal fluid. Otx2 is then internalized preferentially in cortical PV cells, triggering their maturation and subsequently initiating the CP (Sugiyama et al., 2009; Prochiantz et al., 2014). Otx2 can be detected in PV cells of V1 before P20, increases during the CP, and plateaus thereafter. In mice, cortical infusion of recombinant Otx2 protein before CP onset accelerates CP timing, while the extracellular blocking of Otx2 protein delays CP onset (Sugiyama et al., 2008).

Others factors, related to PV cells' correct maturation and functioning, are important for the regulation of the CP in the visual cortex. Among them, we can cite: the circadian clock genes (Kobayashi et al., 2015), the immediate early gene NARP (Gu et al., 2013), the polysialic acid (Di Cristo et al., 2007), the Neuregulin-1/ErbB4 signaling (Sun et al., 2016) as well as the CREB-mediated gene transcription. In particular, recent evidence indicates that CREB regulated microRNAs, such as miR-132, are involved in visual plasticity (Tognini et al., 2011; Tognini and Pizzorusso, 2012).

To conclude, inhibition, which is mediated essentially by PV interneurons, is crucial to shape the CP of visual plasticity by initiating and terminating this window of increased plasticity. In the next paragraph, I will summarize how inhibition acts to regulate plasticity, at the network and circuit level.

1.2.3.2 Mechanisms of ocular dominance plasticity at the circuit level

Although it is clear that PV interneurons are central actors in the control of CP shaping and timing, how these cells regulate plasticity is not completely understood. Recent studies have proposed that a transient suppression of PV cell firing may gate cortical plasticity (Kuhlman et al., 2013). Monocular deprivation results in a biphasic profile of neuronal responses: first, within 3 days of MD, neurons in the binocular region of V1 initially decrease their responses to the contralateral closed eye. Then, after 7 days, neuronal responses to both the open and deprived eyes are enhanced (Mrsic-Flogel et al., 2007). These findings were confirmed, *in vivo*, by two recent papers that provide evidence that CP is triggered by a disinhibitory microcircuit (Hengen et al., 2013; Kuhlman et al., 2013). In both cases, excitatory neurons' responses after MD decrease and then gradually return to baseline level. This restoration of binocular-like firing rates is due to a rapid and transient inhibition of PV cells (which decrease their activity) which results into disinhibition of pyramidal neurons. Thus, deprivation-induced CP is defined by a rapid drop in PV cell inhibition, a subsequent loss of deprived eye responses, followed by potentiation of responses to both eyes.

It is now widely accepted that the loss of cortical responsiveness to deprived eye stimulation after MD involves some form of Hebbian-like LTD (Yoon et al., 2009; Cooke and Bear, 2013; Hengen et al., 2013) involving NMDAR-mediated endocytosis of postsynaptic AMPA and mGluR5 receptors (Sidorov et al., 2015), as well as a strengthening of PV to PYR synapses (Maffei et al., 2006, 2010; Lefort et al., 2013; Nahmani and Turrigiano, 2014). This enhancement of inhibition after MD can be detected across different cortical layers, including layer 2/3 (Kannan et al., 2016). In contrast, the delayed synaptic potentiation is due to homeostatic scaling and requires the GluA2 subunit of AMPARs.

To summarize, MD-mediated plasticity during the CP is accompanied by Hebbian LTD mechanisms and a gain in PV to pyramidal cell inhibition that, together, will depress principal cell firing. This elicits a homeostatic process that restores V1 cortical firing.

ODP during the CP is also accompanied by anatomical and structural changes. 3 days of MD during the CP are sufficient to induce ODP and anatomical alterations of thalamocortical (TC) synapses, such as reduction of TC bouton density in V1b (Coleman et al., 2010), accompanied by synaptic depression at TC synapses (Khibnik et al., 2010). Similarly, plasticity can be seen at

the level of dendrites: spine motility from L5 pyramidal neurons is increased after short MD in V1b (Majewska and Sur, 2003; Oray et al., 2004).

Finally, a theory has been recently proposed to explain the role of inhibition in opening the CP (Toyoizumi et al., 2013). The transition from pre-CP to CP plasticity is possible, because the maturation of inhibition selectively suppresses spontaneous neuronal activity, but not visual environmentally-evoked inputs, switching learning cues from internal (spontaneous activity) to external (visual inputs) sources.

1.2.4 Adult plasticity and the reopening of windows of plasticity

Even though neuronal plasticity is a key feature of the CP, it is not exclusively restricted to this time window of development. Indeed, mature brains also present plasticity, to some extent. In the visual system, ODP during adulthood has been reported by several studies. Indeed, *in vivo* long term formation and turnover of dendritic spines in adult visual cortex after sensory experience has been reported (Trachtenberg et al., 2002). Moreover, a mature brain is more susceptible to plasticity if it has already been subject to a MD earlier in life (Hofer et al., 2006a, 2009). Importantly, adult visual plasticity depends on NMDA receptors, which strengthen the inputs originating from the open eye (Sawtell et al., 2003). Finally, adult plasticity is correlated with the developmental decline of the transcriptional factor CREB (Pham et al., 2004).

What mostly differentiates juvenile versus adult ODP is that, in mature brain, longer periods of MD are required to obtain the shift of the responses (> 4-7 days in adult versus 2-3 days in young mice) (Pham et al., 2004; Hofer et al., 2006a; Sato and Stryker, 2008). Furthermore, the magnitude of the OD shift is smaller in adults, as compared to juvenile subjects (Pham et al., 2004; Hofer et al., 2006a; Sato and Stryker, 2008). Mechanistically, MD-induced plasticity shows also other disparities between adult and young mice. In young animals, the effect is biphasic with a rapid loss in deprived-eye responses followed by a delayed increase of open-eye response strength (Frenkel and Bear, 2004; Mrsic-Flogel et al., 2007; Sato and Stryker, 2008). Conversely, in adult mice, the dominant change is a reversible potentiation of responses from the open eye (Sawtell et al., 2003; Pham et al., 2004; Hofer et al., 2006a; Sato and Stryker, 2008). At the level of neuronal morphology, MD in adults leads to a decrease in spine motility and either an increase (Mataga et al., 2004; Oray et al., 2004) in spine density or no

change (Hofer et al., 2009), depending on the cell type; the effects are opposite during the CP. Moreover, no changes in TC bouton density were reported in adults. Finally, adult visual plasticity is more sensitive to anesthesia affecting GABAergic neurotransmission and therefore experiments in adult anesthetized mice can influence the detectability of adult plasticity. For reviews on adult visual plasticity see (Fischer et al., 2007; Morishita and Hensch, 2008; Hübener and Bonhoeffer, 2014).

Nevertheless, adult brain capacity for plasticity remains relatively limited. Once cortical circuits are mature, molecular brakes appear gradually and are responsible for the restriction of plasticity and the closure of the CP. Such brakes can be both structural (PNNs, myelin factors) and functional (Lynx protein for instance), by providing physical impairment to neurotransmission between previously formed connections and by acting on neuro-modulatory systems respectively (see below). Manipulating these brakes allows reopening of windows of plasticity in adult brains (Bavelier et al., 2010; Takesian and Hensch, 2013) and this field of research is of great interest for nervous system damage recovery as well as the development of therapeutic strategies for several brain disorders (Fig. 1.23).

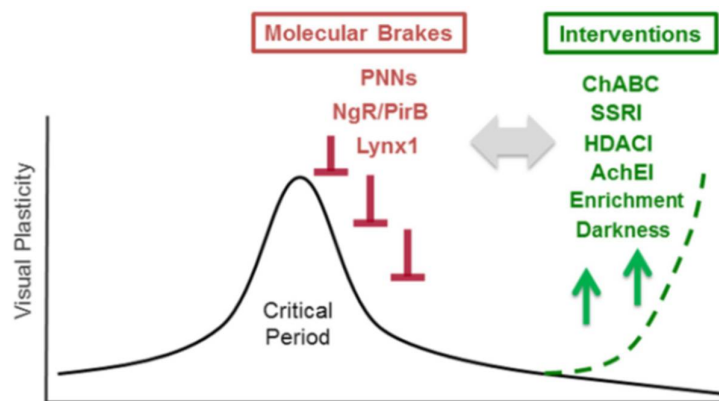


Figure 1.23. Critical period of visual cortex plasticity. Several endogenous “molecular brakes” (red) that close the critical period have been identified. These include perineuronal nets (PNNs), myelin-related Nogo receptor (NgR) and PirB, and a nicotinic brake Lynx1. From (Nabel and Morishita, 2013).

First, plasticity can be reopened in the adults by resetting the immature lower level of inhibition: exposure of adult animals to darkness (He et al., 2007) as well as administration of an antagonist of GABA_AR (Berardi et al., 2003) enhance ODP. Accordingly, transplanting embryonic inhibitory neurons in the postnatal visual cortex was shown to restore plasticity (Southwell et al., 2010; Tang et al., 2014; Davis et al., 2015). Furthermore, several studies

highlighted the benefits of raising adult animals in an enriched environment (EE): exposure to EE reactivates juvenile-like plasticity in aged rats (Scali et al., 2012). Moreover, adult rats, which have been monocularly deprived during the CP (amblyopia) recover normal visual acuity and OD if raised in EE (Sale et al., 2007). A similar effect is obtained when animals are treated with the anti-depressant fluoxetine, a selective inhibitor of the serotonin uptake (Vetencourt et al., 2008). Both treatments (EE and fluoxetine) reduce GABAergic inhibition in the visual cortex (Vetencourt et al., 2008) and hippocampus (Mendez et al., 2012), and increase the expression of BDNF growth factor, a critical factor for experience-dependent plasticity (Huang et al., 1999). Similarly, visual plasticity in adults is limited by the structural brake myelin-related Nogo receptor signaling. Indeed, intracortical myelin matures at the end of the visual CP (McGee, 2005) and contains inhibitory proteins such as Nogo, which binds to its neuronal Nogo receptor. Knock-out mice for the Nogo receptor exhibit ODP well beyond the normal CP (McGee, 2005) as well as mice lacking functional paired immunoglobulin-like receptorB (PirB), a receptor with high affinity for Nogo (Bochner et al., 2014).

Interestingly also epigenetic mechanisms, such as a downregulation of acetylation and phosphorylation, play a role in the closure of the CP for OD. Stimulating histone acetylation can reactivate ODP in adult mice (Putignano et al., 2007).

Finally, a class of proteins, the Lynx family, has been recently identified as a functional brake: removal of Lynx 1 (an acetylcholine receptor antagonist) during adulthood re-induces a juvenile-like plasticity by enhancing nicotinic acetylcholine receptor and resetting the local excitatory-inhibitory balance (Morishita et al., 2010).

Among all the key players involved in restricting plasticity in adulthood described above, the most prominent and best studied plasticity brake is a specific molecular family of the extracellular matrix: the perineuronal nets (PNN), which accumulate specifically around PV interneurons at the end of the CP of plasticity. Enzymatic digestion of PNNs after the closure of the CP reactivates ocular dominance plasticity in the visual cortex (Pizzorusso, 2002), and makes fear memory in the amygdala susceptible from erasure (Gogolla et al., 2009). Given the role of inhibition in experience-dependent plasticity and the specific wrapping of PV cells by PNNs, it is crucial to understand how PNNs act in modulating experience-dependent plasticity at the cellular and network level.

1.3 Extracellular matrix and Perineuronal Nets

1.3.1 Extracellular matrix in the central nervous system

The extracellular space of the central nervous system (CNS) is organized into a loose scaffold called extracellular matrix (ECM) that represents 10-20% of the brain volume. This ECM provides an essential microenvironment for neurons and is a highly dynamic structure that is constantly being remodeled, either enzymatically or non-enzymatically (Mikami and Kitagawa, 2013). ECM molecules are synthesized by both neurons and glial cells and are then secreted in the extracellular space where they accumulate to protect, compartmentalize, and regulate the physiology of specific cell types. (Dityatev and Schachner, 2003, 2006; Dityatev et al., 2010; Frischknecht and Happel, 2016). However, PNN-like structures appear also in the absence of glial cells (Miyata et al., 2005) and dissociated hippocampal neurons in culture can form net-like ECM (John et al., 2006; Dityatev et al., 2007; Frischknecht et al., 2009). Neuronal ECM exists in two different configurations: a diffuse ECM which is present throughout the brain and a densely packed matrix, also known as perineuronal nets (Gundelfinger et al., 2010). While the diffuse ECM form is permissive for synaptic restructuration and axonal growth and is present in embryonic and juvenile brains, PNNs, which appear later in development, limit major plastic phenomena of the adult CNS (discussed in details in the next section).

1.3.2 Perineuronal Nets

1.3.2.1 Overview

PNNs were first described by Camillo Golgi in the late 19th century as a “kind of corset of neurokeratin (neural protein fibers) which impeded the spread of current from cell to cell”. PNN is a specialized form of ECM of the central nervous system that surrounds the cell body of many neurons, and extends along their proximal dendrites in a mesh-like structure (Fig. 1.24) with open “holes” at the sites of synaptic contacts (Celio and Blumcke, 1994; Celio et al., 1998; Wang and Fawcett, 2012).

In recent years, the neuroscientific community devoted a remarkable interest on PNN research. The reason is certainly due to the fact that the maturation and accumulation of PNNs is a feature of the mature brain, whereas plasticity is restricted to the young immature brain

(Pizzorusso, 2002; Gogolla et al., 2009; Bardin, 2012). A selective turnover of PNNs is essential for maintaining the brain homeostasis and is tightly regulated by the specific cleavage operated by several extracellular proteases, including a family composed of a disintegrin and metalloproteinase domain with thrombospondin motifs (hence their name ADAMTs) and matrix metalloproteinases (MMPs) (Zimmermann and Dours-Zimmermann, 2008).

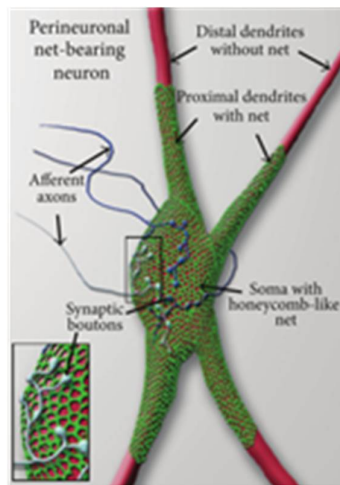


Figure 1.24. Schematic view of a perineuronal net-bearing neuron. A neuronal cell body with its proximal dendrites (red) covered by the net (green). Presynaptic boutons occupy the holes (blue) From (De Winter et al., 2016).

PNNs are widely distributed in various brain regions and are mainly present in the cortex, hippocampus, thalamus, brainstem, and the spinal cord. Importantly, dysfunctions of PNN formation are implicated in several neuronal disorders such as schizophrenia, epilepsy, autism and Alzheimer's Disease (Pantazopoulos and Berretta, 2016). In the neocortex (essentially in primary sensory areas), PNNs are strongly enriched preferentially around PV cells (Seeger et al., 1994; Miao et al., 2014) as illustrated in figure 1.25, and are thought to be responsible for maintaining the E/I balance in the adult brain (Hensch and Fagiolini, 2005; Galtrey and Fawcett, 2007; Kwok et al., 2011). I will discuss more in detail the role of PNN associated to PV cells in regulating brain plasticity section 1.3.3.

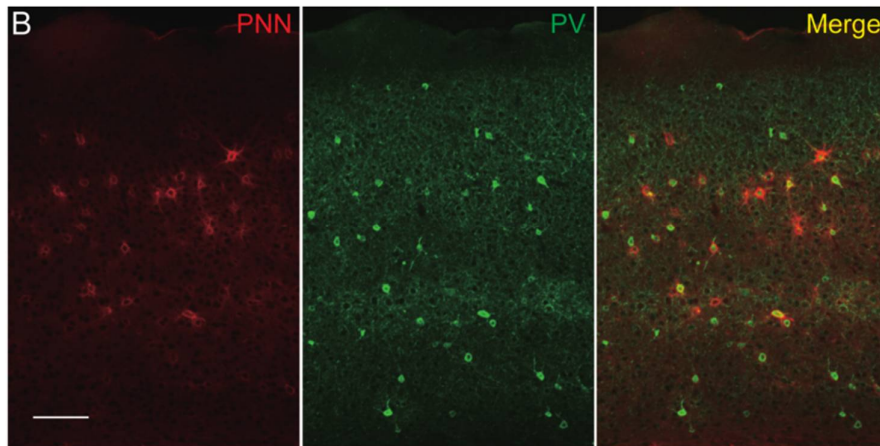


Figure 1.25. Confocal image of PNN (red) enwrapping parvalbumin (PV)-containing interneurons (green) in the mouse visual cortex. The nets are stained with *Wisteria floribunda agglutinin* (WFA). Scale bar, 100 μ m. From (Miao et al., 2014).

In cortical structures PNN are mainly associated with inhibitory neurons, as PNN expression around pyramidal neurons is rare (Alpár et al., 2006). Yet, recent studies reported that PNN also co-localize with glutamatergic neurons (Fig. 1.26) in other brain regions such as the CA2 region of the hippocampus (Carstens et al., 2016) and the amygdala (Morikawa et al., 2017).

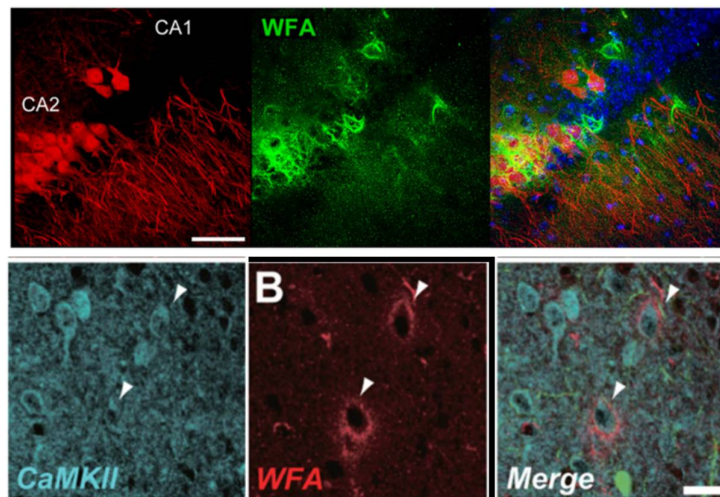


Figure 1.26. Confocal image of PNN enwrapping glutamatergic neurons. Top: PNN (green) around glutamatergic cells (red) in the hippocampus. From (Carstens et al., 2016). Bottom: glutamatergic cells (blue) are surrounded by PNN (red) in the lateral amygdala. From (Morikawa et al., 2017). The nets are stained with *Wisteria floribunda agglutinin* (WFA).

1.3.2.2 Molecular and structural organization of PNNs

Since the discovery of PNNs by Golgi and colleagues, neuroscientists have been more and more intrigued by this lattice-like structure that tightly enwraps neurons and has been recognized to play important functional roles, such as neuronal plasticity. The investigation and the study of their molecular composition and fine structure benefit from several tools and various staining techniques to visualize their fine anatomical organization. The most frequently used tools to reveal PNNs are compounds that have high affinity to the N-acetylgalactosamine residues of the nets, such as the plant lectin *Wisteria floribunda agglutinin* (WFA) as illustrated in figure. 1.27 (Brückner et al., 1998;

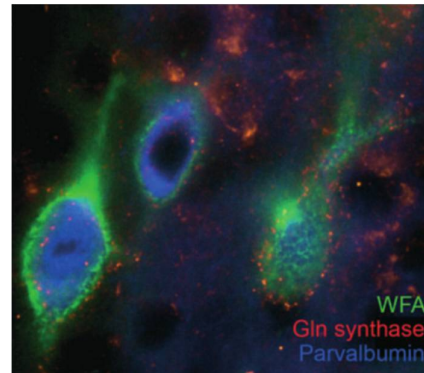


Figure 1.27. Example of PV cells enwrapped by PNN which are stained with WFA. Extracellular PNN (green) surround PV cells (blue). Glial processes (red) are in close contact with neurons *in vivo*. From (Gundelfinger et al., 2010).

Yamada et al., 2015; Fader et al., 2016), the *Vicia villosa agglutinin* or the *Soy bean agglutinin*. In addition, anionic or cationic iron colloid allow the detection of negatively or positively charged components of PNNs (Seeger et al., 1994). Finally, it is also possible to use antibodies against PNN components such as CAT 315 which stains the chondroitin sulfate proteoglycans, (Dino et al., 2006; Ueno et al., 2017).

From *in vitro* studies – acute slices and cultures - it appears that the density and molecular composition of PNNs are heterogeneous and differ between brain areas and the types of neurons enwrapped by PNNs (Lander et al., 1997; Matthews et al., 2002; Dauth et al., 2016; Fader et al., 2016; Lensjø et al., 2017a).

As shown in figure 1.28, PNNs are majorly composed of different macromolecules (proteins and sugars), including: chondroitine sulfate proteoglycans (CSPGs), hyaluronic acid (HA), link proteins and tenascins-R (Tn-R), which form a complex structure anchored to the cell membrane surface. In this architecture, the backbone is the HA (synthesized by a member of transmembrane enzyme, the hyaluronan synthases) where CSPGs (aggrecan, versican, brevican and neurocan –from the lectican family) bind via their N-terminal domain. This interaction is maintained and consolidated by Link proteins (cartilage-link protein 1 or brain link protein 2) through the C-terminal domain. This molecular interaction is further stabilized

by the trimeric Tn-R which can bind up to three CSPGs (Fig. 1.29) (Yamaguchi, 2000; Deepa et al., 2006; Galtrey and Fawcett, 2007; Kwok et al., 2010, 2011; Djerbal et al., 2017). CSPGs consist of a single-core protein covalently bound by serine residues to varying numbers of polysaccharide glycosaminoglycan (GAG) chains. GAG chains are unbranched polymers composed of repeated disaccharides. Each disaccharide consists of a glucuronic acid and an amino sugar, the N-acetylgalactosamine (GalNAc, also known as chondroitin sulphate E). GalNAc residues of the GAG chains can be mainly sulfated in position 4 or 6, generating 4-sulfation (C4ST) or 6-sulfation (C6ST), respectively (Mikami and Kitagawa, 2013). During development, there is a dynamic shift in the sulfation arrangement: C6ST is abundant in the juvenile brain, whereas C4ST is dominant in the mature brain (Kitagawa et al., 1997; Miyata et al., 2012). Four members of CSPG belonging to the Lectican family have been identified by molecular cloning: aggrecan, versican, neurocan and brevican. The first three are mostly found in the ECM, whereas brevican can be found both in the ECM and linked to the cell membrane via a glycosylphosphatidylinositol anchor (Seidenbecher et al., 1998). In addition, while aggrecan is present on almost all PNN-positive neurons, the other lecticans are only found in subpopulations of PNN-positive neurons (Galtrey et al., 2008). Further, the negative charges carried by the sulfate groups give the GAGs a strong negative charge allowing the attraction of several cationic elements, important for their maturation and regulation of plasticity.

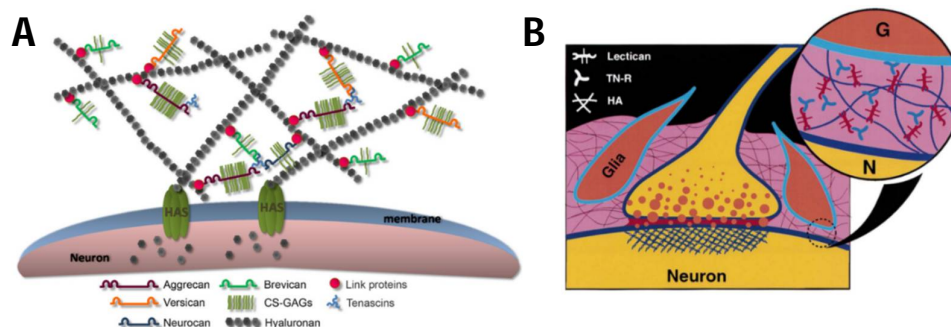


Figure 1.28. Schematic structure of PNNs. (A) the major components are CSPGs from the lectican family (aggrecan, versican, brevican and neurocan), hyaluronan (HA) which is synthesized by the hyaluronan synthase (HAS), link proteins and tenascin-R (Tn-R) which form a complex architecture anchored to the cell membrane by hyaluron. From (Kwok et al., 2011) (B) PNN allow the tight coupling between neuronal and glial cells. From (Yamaguchi, 2000).

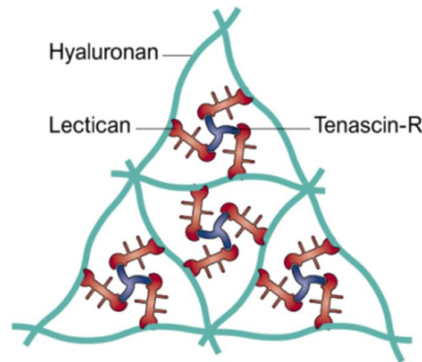


Figure 1.29. Ternary complex formed by CSPGs (red), hyaluronan (light blu) and tenascin-R (dark blu). From (Dityatev and Schachner, 2003).

1.3.2.3 Formation and development of PNNs

PNNs mature relatively late in post-natal development and, importantly, their accumulation around PV cells coincides with the end of CP of plasticity (Pizzorusso, 2002; Nowicka et al., 2009; Ye and Miao, 2013). Figure 1.30A,B indicates the developmental profile of PNNs in mouse V1 and the timing of their accumulation around cortical neurons: during the CP (post-natal day 22 to 35), very few PNNs enwrap neurons, as revealed by WFA staining. The density of PNNs is strongly enhanced at P35 and reaches adult levels after 3 months, in all cortical layers.

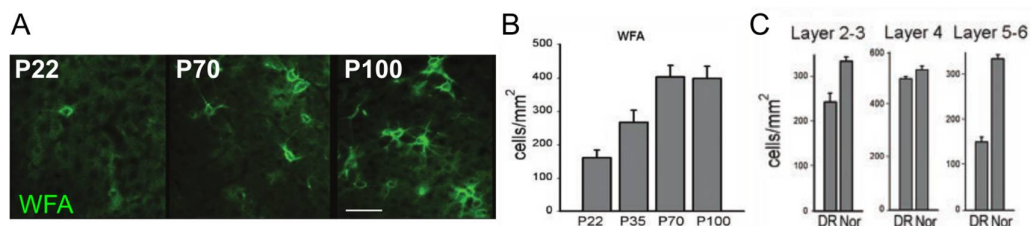


Figure 1.30. Developmental profile of PNNs in V1 at different post-natal ages and effect of dark rearing. (A) WFA staining in mice V1 at P22, P70 and P100. (B) density of cells positive for WFA (C) density of WFA-positive cells in normal condition (NOR) and after dark rearing (DR). Scale bar, 50 μ m. Modified from (Pizzorusso, 2002).

Following *in vivo* enzymatic disruption of PNNs in adult rodents several months are required for the complete recovery of the nets (Brückner et al., 1998; Lensjø et al., 2017b). Several lines of evidence have demonstrated that PNN development is an activity-dependent process that requires normal levels of neuronal activity. Indeed, neuronal depolarization by elevating

extracellular potassium enhances the formation of PNNs (Brückner and Grosche, 2001). Accordingly, blocking spiking activity with tetrodotoxin (TTX) diminishes the formation of PNNs in mouse visual cortical slices (Reimers et al., 2007) as well as in dissociated cell cultures (Dityatev et al., 2007). This last study also showed that activities of Ca²⁺-permeable AMPA receptors and L-type Ca²⁺ channels are necessary for PNN development.

Sensory experience is another factor that influences the establishment of PNNs. Indeed, PNN formation is reduced by early and prolonged dark rearing in the visual cortex (Fig. 1.30C) as well as early whisker trimming in the barrel cortex, both delaying PV cell maturation (see section 1.2.3.1) (McRae et al., 2007; Ye and Miao, 2013). Interestingly, MD, accompanied by environmental enrichment, reduces WFA staining, and thus PNN expression. This decrease is coincident with a reduction in GABAergic signaling (Sale et al., 2007).

It has been reported from *in vitro* modeling that aggrecan, hyaluronan synthase and cartilage-link protein (Crtl1) are sufficient and necessary for PNN formation and integrity (Carulli et al., 2010; Giamanco et al., 2010). Recent data also suggest that the brain-derived link protein Bral2 is essential for PNN formation. In fact, mice lacking this link protein have attenuated PNNs (Bekku et al., 2012).

Finally, the pattern of sulfation of the GAG chains is also a critical step for the formation of PNNs. Indeed, transgenic mice overexpressing C6ST-1, a sulfotransferase enzyme that catalyzes the 6-sulfation of chondroitin sulfate chains, retain juvenile-like pattern of sulfation and present alteration in PNN development (Miyata et al., 2012; Miyata and Kitagawa, 2016).

1.3.3 Roles of perineuronal nets

Many studies assessed the roles of PNNs in the adult CNS (Frischknecht and Happel, 2016). One of the most common and effective experimental approach (which I also used in my experiments) to study the functional roles of PNNs consists in removing the nets in the regions of interest by locally injecting the bacterial enzyme Chondroitinase ABC (ChABC) which cleaves the glycosaminoglycan chains from CSPGs (Brückner et al., 1998; Deepa et al., 2006). 48h are enough to disrupt PNNs (Pizzorusso, 2002), and an acute incubation of hippocampal cultures for 2h with ChABC is also sufficient to disrupt the net (Dityatev et al., 2007). It is important to note that this enzyme preserves some CSPG components. One can also use hyaluronidase (H-

ase), which selectively digests HA and removes the entire PNN components (Deepa et al., 2006). Application of this enzyme on mature hippocampal cultures has been shown to increase the excitability of network (Bikbaev et al., 2015). In addition, several genetic tools were developed to allow the investigation of specific components of PNNs, such as, for example, mice lacking link proteins (Carulli et al., 2010), Tenascin-R (Haunsø et al., 2000) or CSPG (Giamanco et al., 2010; Favuzzi et al., 2017). Finally, it is possible to act indirectly on PNN by targeting molecules that are responsible for PNN accumulation such as Otx2 (Beurdeley et al., 2012; Lee et al., 2017).

What are the functional roles of PNNs? An important clue to answer this question is provided by their maturation process. Indeed, as mentioned above, during postnatal maturation of neuronal networks and synaptic microcircuits, PNNs become more complex and start to tightly enwrap neurons, mainly PV cells. This process is paralleled by the closure of the CP of plasticity. Today we know that PNNs are a key factor in regulating plasticity in adult animals and in stabilizing synaptic contacts. Accordingly, many studies have indicated that synaptic plasticity is limited by the formation of these functional brakes around PV cell. Indeed, it has been shown that enzymatic digestion of PNNs by ChABC restores plasticity in adult visual cortex (Pizzorusso, 2002). In addition, the same manipulation allows the full structural and functional recovery of amblyopia in adult animals that have been monocular deprived since youth, *i.e* the restoration of ocular dominance, visual acuity as well as dendritic spine density (Pizzorusso et al., 2006). In line with this, adult transgenic mice deficient for CrtI-1 that have attenuated PNNs retain juvenile levels of ODP (Carulli et al., 2010).

Furthermore, PNN enrichment around PV cells is strongly regulated by Otx2, which plays a critical role in PV cell maturation, and the closure of the CP. This homeoprotein recognizes a sequence onto PNNs which allows its specific capture and transfer into PV cells. It has been shown that reducing Otx2 levels in PV cells by ChABC treatment or infusing a peptide that specifically blocks the transfer of Otx2 inside PV, reopens plasticity in adult mice (Beurdeley et al., 2012). For a review on the regulation of cortical plasticity by the interaction of PNN and PV neurons see (Bernard and Prochiantz, 2016).

Another important function of CSPGs at the subcellular level is inhibition of axonal sprouting and control of dendritic spines stability (for a review see (Levy et al., 2014)). Enzymatic removal of PNNs in the visual cortex of adult mice show an enhancement of spine mobility accompanied by a structural and functional plasticity (de Vivo et al., 2013). Accordingly, the

presence of PNNs influences synaptic plasticity by limiting dendritic spine motility in hippocampal slices (Orlando et al., 2012). Interestingly, PNNs were shown to restrict lateral mobility of AMPA receptors on principal neurons, supporting again their involvement in synaptic plasticity (Frischknecht et al., 2009), whereas, in aspiny neurons, the exchange of AMPARs was due to intracellular Ca^{2+} and independent of ECM (Klueva et al., 2014).

Although the role of PNNs in restricting plasticity has been mostly studied in the visual cortex, the effects on structural plasticity in other brain regions have also been reported. In the spinal cord, ChABC treatment promotes functional recovery after spinal cord injury (Bradbury et al., 2002; Massey, 2006). In the amygdala, PNNs are essential for making fear memories erasure-resistant in adult animals (Gogolla et al., 2009). In fact, an extinction protocol during the CP in juvenile rodents can suppress fear memory, whereas in adult animals, fear memory is preserved. However, this study showed that ChABC treatment in adults rendered fear memory susceptible from erasure, as in juveniles.

Additional evidence regarding the effect of PNN removal on synaptic plasticity is provided by several experiments in acute slices of different brain regions, which, however, are not in full agreement. Analysis of excitatory transmission and plasticity in hippocampal slices after incubation of ChABC as well as in mice lacking Tn-R revealed alterations of LTP and LTD (Bukalo et al., 2001). Similarly, mice deficient for brevican also exhibit impaired hippocampal LTP (Brakebusch et al., 2002). However, a recent study reported a contrasting effect with increased magnitude of LTP in hippocampal-treated animals (Carstens et al., 2016). In addition, PNN depletion in the perirhinal cortex was shown to increase recognition memory as well as LTD (Romberg et al., 2013). Very few studies attempted to investigate how ECM altered neuronal activity. It was shown that ChABC incubation in hippocampal cultures increases the excitability of interneurons (Dityatev et al., 2007) but a recent study performed on acute cortical slices reported a decrease in the firing rate of PV cells after incubation of ChABC (Balmer, 2016). Moreover, disruption of the ECM in mature neuronal cultures was shown to transiently enhance neuronal activity (Bikbaev et al., 2015) and a PNN digestion also alters synaptic transmission by decreasing evoked inhibitory transmission onto excitatory neurons in the visual cortex (Liu et al., 2013). Finally, a recent study performed *in vivo* suggests that PNN removal restores a juvenile-like phenotype by decreasing inhibitory activity as well as a potentiation of gamma oscillations, although direct analysis of inhibitory transmission in the presence and absence of PNNs was not performed (Lensjø et al., 2017b).

Additionally, PNNs could affect PV cell activity by acting as a buffer for extracellular cations via their negative charges (Morawski et al., 2015). PNNs can also attract and accumulate on the neuronal surface several growth factors and axon guidance molecules such as Semaphorin 3A whose chemorepulsive function may play a role in restricting axonal outgrowth (De Winter et al., 2016). Therefore, PNN around PV cells can form a compartmentalized microenvironment that regulates their basic synaptic physiology. Lastly, another important role of PNN is neuronal protection from oxidative stress (Cabungcal et al., 2013).

Figure 1.31 resumes three possible ways in which PNN can act on limiting plasticity: by forming a physical barrier to the formation of synapses, by forming a scaffold that attracts molecules inhibitory for axonal growth and by restricting lateral mobility of membrane receptors involved in synaptic plasticity.

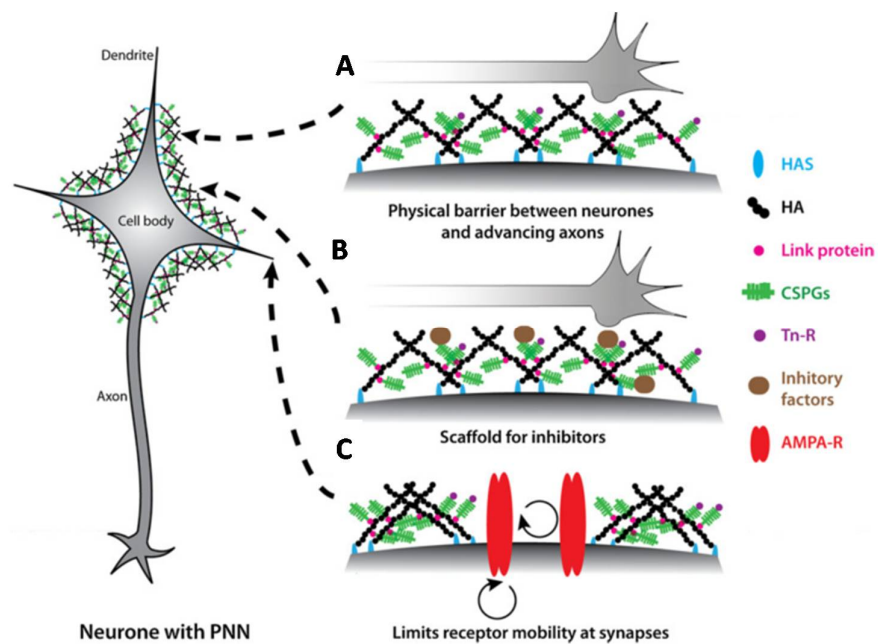


Figure 1.31. Three possible ways in which PNNs may act to restrict plasticity. (A) Formation of a physical barrier against the establishment of new synaptic contacts. Indeed, PNNs around dendrites and neuronal cell bodies can form a barrier against advancing axons. **(B)** Acting as a scaffold for the binding of molecules, which may then inhibit synaptic formation. **(C)** Restriction of receptor mobility at the synapses, influencing receptor exchange (AMPA receptor for instance). HAS: hyaluronan synthase; HA: hyaluronan; CSPGs: chondroitin sulfate proteoglycans; Tn-R: tenascin-R; AMPA-R: AMPA receptor. From (Wang and Fawcett, 2012).

In conclusion, while the involvement of PNNs in restricting plasticity has been widely documented, the cellular and synaptic mechanisms underlying PNN-dependent cortical plasticity are still unknown. Understanding these mechanisms is fundamental for advancing our knowledge on the ability of cortical circuits to learn and form memories. My Ph.D. project aimed to decipher these processes, using the mouse visual cortex as a relevant model.

1.4 Why looking at layer 4 of primary visual cortex?

The majority of studies of the visual cortex and experience dependent plasticity are interested in L2/3, but very few target L4. In the present work, we wanted to understand the role of PNNs in modulating cellular and synaptic effects on neocortical PV interneurons. We decided to focus on L4 for the following reasons:

1) PV cells enwrapped by PNNs are mainly located in L4 as we can see in figure 1.32. A removal of PNN by intracerebral injection of the degrading enzyme ChABC should bear relevant effects in this region.

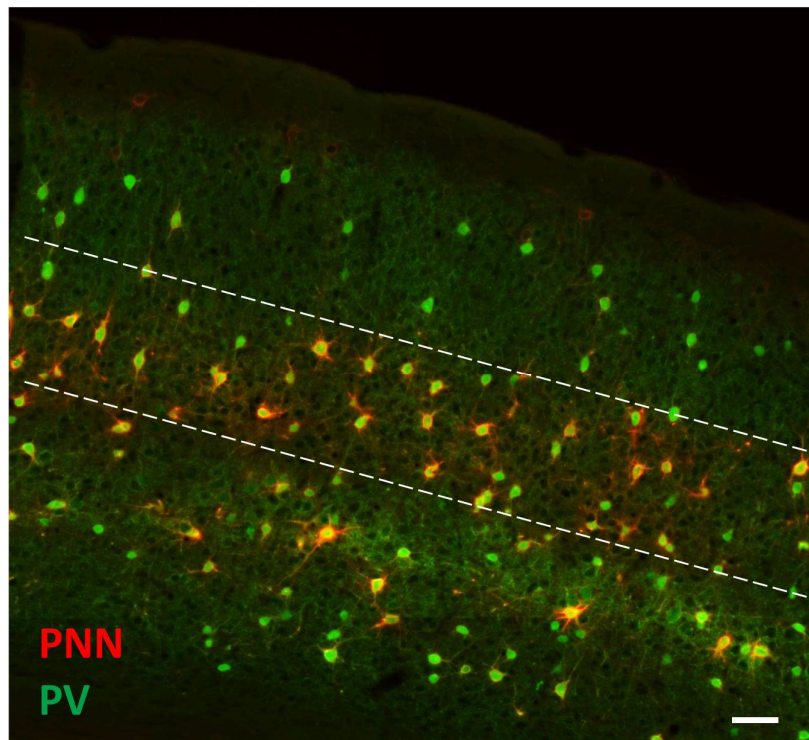


Figure 1.32. PNN surrounding PV cells are abundant in L4 of V1. PNNs are in red and PV in green. Cortical coronal slice from an adult mouse. Dotted lines delimitate layer 4. Scale bar: 60 μ m. Unpublished data.

2) L4 is the major input layer of the neocortex, and, as such, it receives sensory information from the retina (via the thalamus). PV cells represent one of the most prominent GABAergic interneuron subtypes of L4 and spiny stellate cells are the major excitatory principal neurons (PN) of this layer. As mentioned previously, these two type of neurons receive monosynaptic feedforward excitation from the thalamus (Gabernet et al., 2005; Cruikshank et al., 2007). Despite the fact that the proportion of the thalamic contacts is low, with respect to the overall synapses made in L4 onto both cell types - 13% for PV and 6% for PN - (Ahmed et al., 1994, 1997), this thalamic excitation is potent. In particular, PV cells are much more strongly recruited by TC afferents than glutamatergic PN (Gabernet et al., 2005; Sun, 2006; Hull et al., 2009) The powerful, reliable and efficient recruitment of PV cells by thalamic fibers occurs via clusters (hotspots) of thalamic boutons contacting PV interneurons (Bagnall et al., 2011). Therefore, in response to a sensory stimulation, the thalamus first recruits PV cells with high probability, eliciting a large disynaptic, feed-forward inhibition onto PN. This disynaptic inhibition limits the time window for PN cells to integrate incoming glutamatergic inputs into output spikes, thus increasing PN temporal fidelity to sensory stimuli (Pouille, 2001). Interestingly, however, a recent *in vivo* study (performed in cats) reported that thalamic inputs onto PV cells and PN are similar in strength (Sedigh-Sarvestani et al., 2017). This discrepancy can be either related to differences between slice and whole-animal studies, or due to variations in calcium concentrations between *in vivo* and *in vitro* preparations.

1.5 Aim of the study

Although the mechanisms underlying CP (and associated plasticity) have been extensively studied, the functional aspects linking PNNs to activity-dependent plasticity remain obscure (Bardin, 2012). The degradation of this extracellular proteoglycan network in adult animals was shown to re-open structural plasticity (Pizzorusso, 2002), a typical feature of the CP. However, the cellular and synaptic mechanisms underlying the unlocking of cortical plasticity are still unknown. Given the involvement of specific GABA circuits in experience-dependent plasticity and the specific accumulation of the PNN around PV cells (Hensch, 2005b), it will be crucial to understand the role played by this cortical cell subtype in the cellular and circuit mechanisms underlying PNN-dependent sensory plasticity. This will push forward our knowledge of cortical

circuit maturation and plasticity with important consequences for brain diseases. Indeed, accumulating evidence indicates that defects of PV basket cell-mediated circuits are involved in the development of several neuropsychiatric disorders, including schizophrenia and autism (Marín, 2012).

My PhD work has been focused on the properties of PV cells in L4 of V1 in the presence and absence of PNNs. I compared PV neurons with their glutamatergic counterparts, the spiny stellate cells (referred as PN). Both cells types are involved in layer 4 intracortical and thalamocortical microcircuits (Fig. 1.33).

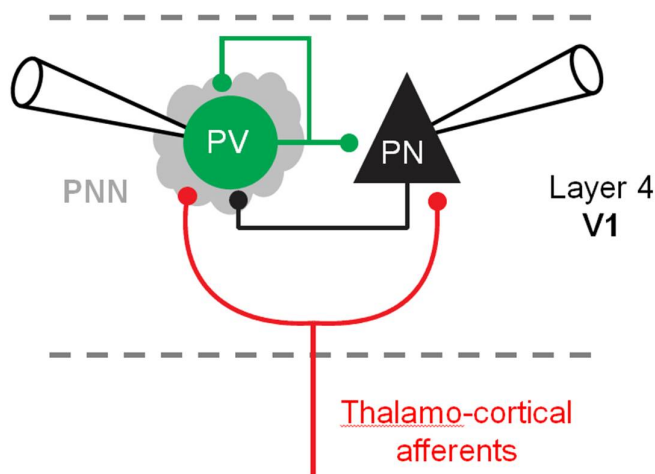


Figure 1.33. Experimental approach, involving intracortical local circuits and thalamocortical inputs onto PV cells and PNs. PV: PV-positive cell. PN: principal neuron. PNN: Perineuronal nets. Whole cell patch clamp recordings are performed in L4 of V1.

In order to understand the functional aspects linking PNNs to activity-dependent plasticity, I investigated the intrinsic and synaptic properties of both cell types at different ages, recapitulating the CP and the accumulation of PNNs around PV cells (Fig. 1.34) and in adult mice in the presence and absence of PNNs (after ChABC injection *in vivo*), as well as after triggering plasticity by a monocular deprivation. Moreover, I studied thalamocortical circuits in control conditions and without PNNs, in the presence and absence of monocular deprivation. The re-opening of cortical plasticity in adult animals induced by PNN removal can be in principle due to alterations of *i*) the intrinsic excitability and the passive properties of the neurons and/or *ii*) synaptic connectivity either local, within L4, or originating from the thalamocortical (TC) pathway. We therefore performed a thorough cellular and circuit

physiological characterization of L4 cortical neurons to determine whether removal of PNNs in adult animals would recapitulate juvenile features, typical of the CP.

I used a multidisciplinary approach: *in vivo* stereotaxic injection of viral vectors and ChABC, single and multiple patch-clamp recordings in acute cortical slices in young and adult (>P70) mice, optogenetics and immunohistochemistry. I have performed all *in vivo* stereotaxic injections and electrophysiological recordings in acute cortical slices. In addition, the laboratory established a collaboration with Dr. Gianmichele Ratto (Scuola Normale Superiore, Pisa, Italy) to investigate the functional role of PNN removal in visual processing *in vivo*. The results reported in this thesis are in the process of being included in a manuscript that will be shortly submitted for publication.

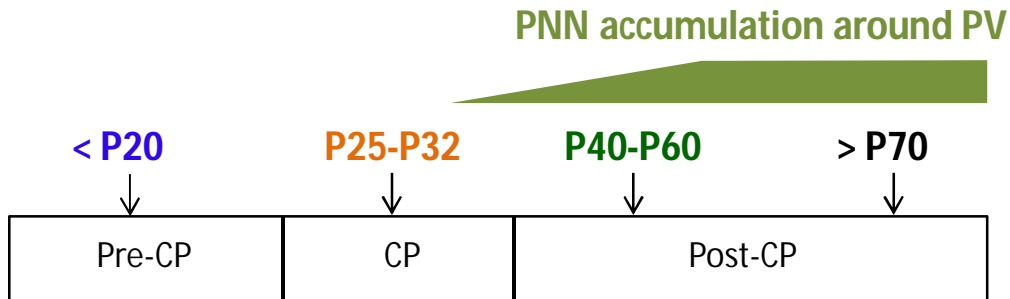


Figure 1.34. Range of post-natal ages investigated, recapitulating the critical period and the specific enwrap of PV neurons by the extracellular PNNs.

Chapter II: MATERIALS AND METHODS

2.1 Animals

Experimental procedures followed National and European guidelines, and have been approved by the authors' institutional review boards. In order to identify GABAergic transmission from PV interneurons we used PV-Cre mice (Jackson Laboratory Stock Number 008069). To selectively express EGFP in PV-positive cells, we bred PV:Cre with RCE:loxP (kindly provided by Gordon Fishell, New York University), obtaining PV-Cre::RCE mice. Male mice of different postnatal age groups were used, recapitulating developmental stages and accumulation of PNNs around PV cells: < P20 (before the CP), P25-P32 (CP), P40-P60 (maturation of PNNs) and >P70 (adult).

2.2 *In vivo* enzymatic degradation of PNNs in V1

To disrupt PNNs locally in V1, adult mice underwent a stereotaxic injection of the bacterial enzyme ChABC or phosphate-buffered saline solution (PBS - control). ChABC from *Proteus vulgaris* (from Sigma) was prepared beforehand: the powder was reconstituted in 0.01% bovine serum albumin aqueous solution for a final concentration of 100 mU/mL. Before each injection, reconstituted ChABC was diluted in a second buffer containing 50 mM Tris, 60 mM sodium acetate and 0.02% bovine serum albumin (pH = 8.0) in order to obtain a final concentration of 40 mU/mL (Pizzorusso, 2002; de Vivo et al., 2013). PBS (from Sigma) was used as control of the surgery (sham). Adult mice were placed in an anesthesia induction cage (3% isoflurane Iso-Vet®; 250 ml air) until they become completely insensitive to nociceptive stimuli (tail pinch) and then fixed on a stereotaxic apparatus with a mouth mask constantly delivering isoflurane (2-2.5% isoflurane; 200 ml air). The analgesic buprenorphine (0.1 mg/kg - Buprecare®) was intraperitoneally injected and an ophthalmic ointment was applied on the eyes. Body temperature was constantly controlled and maintained to 37.5° using a heating pad. After fixing the animal's head onto the ear bars, the head was carefully aligned in the X, Y and Z axis, and an incision was done in the skin (the local anesthetic bupivacaine was applied before incision; 0.25% in NaCl 0.9%) and a small hole was drilled in the right hemisphere at 2.7 mm lateral from Lambda. Small glass capillaries (external diameter of 40 µm; internal diameter of 60 µm), beveled in order to ensure a better penetration into the tissue and therefore produce less damages, were filled with filtered milliQ H₂O and carefully placed into the

injection syringe (Hamilton®, 1700-series, 10 µL) to avoid air bubbles. After withdrawing 200 nL of mineral oil, 1 µL of ChABC (or PBS) was aspirated inside the tip of the beveled pipette. A drop of Monastral blue was added to the solution to check the correct injection site and identify the slices with the injection site when cutting the brain for recordings. After controlling that the capillary was not clogged, two injections of 350 nL each (with a rate of 100 nL/min) were realized at a depth of 800 µm and then 400 µm, with 5 min of interval. Before removing the capillary from the brain, we waited 5 min in order to allow solution diffusion and to avoid backflow in the punctured channel. Lastly, the skin was sutured with a non-absorbable 3/0 filament (Ethicon®), an antiseptic (betadine) was applied on the skin and the mouse gently removed from the frame and kept at 37°C in a heated chamber until full recovery. Brain slices for electrophysiology were done 48 to 72 hours post-surgery.

2.3 *In vivo* expression of the light-sensitive channel ChR2 in the dLGN

Investigation of the TC pathway was done using an optogenetic approach, based on the genetic expression of the light-sensitive opsin channelrodopsin-2 (ChR2) on the membrane of targeted neurons of the visual (dLGN) thalamus. ChR2 is selective for monovalent and divalent cations, and its illumination with blue light results in a depolarization of the cell and therefore induction of spiking activity in a millisecond time-scale (Boyden et al., 2005). Nowadays, optogenetic activation is a commonly used tool to control neuronal activity in an optical, non-invasive way, both *in vitro* and *in vivo*.

To selectively express the light-sensitive ion channel ChR2 in glutamatergic neurons of adult mice dLGN, we performed stereotaxic injections of the adeno-associated (AAV) virus, in which expression of ChR2 was driven by the promoter of the calcium/calmodulin dependent protein kinase II (CaMKII) (AAV9.CaMKIIa.hChR2(H134R)-mCherry.WPRE.hGH; Addgene#: 20297, obtained from Penn Vector Core -University of Pennsylvania). We expressed the light-sensitive channel in the hemisphere where PNNs were degraded. The procedure was the same as for ChABC/PBS injections (see section 2.2) except for the following points: *i*) we used a rigid needle (Hamilton®, 33-gauge, 13mm, pst4-20°) more appropriate to target deep structures such as the dLGN *ii*) the coordinates of injection site were 2.06 mm posterior to Bregma – 2 mm lateral to midline – 3.2 mm depth from the surface of the skull *iii*) one injection of 50 nL

was realized at a rate of 50 nL/min (viral titer: 2.5×10^{13} particles/mL, diluted at a factor 5 in fresh PBS). After 10-12 days, sufficient for an adequate expression of the virus, mice were subject to ChABC or PBS injections and, in some cases, a monocular deprivation.

2.4 Sensory deprivation in adult mice by monocular deprivation

For experiments requiring sensory deprivation, at the time of injection of ChABC/PBS, just before removing the mouse from the stereotaxic apparatus, a lid suture of the left eye (contralateral to the injected hemisphere) was performed under a stereo microscope. The anti-inflammatory Diprosone (0.05% ointment) was applied on the eye and the superior and inferior eyelids were gently removed with fine scissors. Four stitches were realized with non-absorbable 6/0 filament (Ethicon®). 1-2 drops of the anti-inflammatory Tobradex were put in the sutured-eye and the mouse was removed from the frame and kept at 37°C in a heated chamber until full recovery. Mice were killed when signs of infection were observed or if the sutured eye re-opened. Brain slices for electrophysiology were done 48 to 72 hours post-surgery.

2.5 Preparation of acute slices for electrophysiology

In order to record intrinsic and synaptic properties of L4 neurons of V1, we prepared acute cortical slices from mice at different postnatal (P) ages (<P20; P25-P32; P40-P60 and >P70), and adult (>P70) mice previously injected with either PBS (sham) or ChABC. For these experiments, we used slices cut in the sagittal plane (350 μ m thick). In experiments from deprived-animals as well as in which TC neurons expressed ChR2, we cut slices in the coronal plane (300-350 μ m thick), to localize the binocular zone (V1b). Animals older than 25 days were subject to intracardial perfusion of ice-cold cutting solution (see below) before extracting the brain. This procedure improved the quality of slices and preserved the integrity of the tissue significantly. Animals were deeply anesthetized with pentobarbital (50mg/kg - Euthasol® Vet) and 100 μ L of Choay heparine was injected in the left ventricle of the heart before perfusion. Animals were then perfused through the heart (with a pump) with a choline-based cutting solution containing the following (in mM): 126 choline chloride, 16 glucose, 26 NaHCO₃, 2.5 KCl, 1.25 NaH₂PO₄, 7 MgSO₄, 0.5 CaCl₂, cooled to 4°C and equilibrated with 95% O₂ / 5%

CO₂. The brain was then quickly removed (for groups of mice aged <P20, the procedure started at this point, after deep anesthesia) and immersed in the same cutting choline-based solution (4°C, equilibrated with 95% O₂ / 5% CO₂). Slices were cut with a vibratome (Leica VT1200S) in cutting solution and then incubated in oxygenated artificial cerebrospinal fluid (aSCF) composed of (in mM): 126 NaCl, 20 glucose, 26 NaHCO₃, 2.5 KCl, 1.25 NaH₂PO₄, 1 MgSO₄, 2 CaCl₂ (pH 7.35, 310-320mOsm/L), initially at 34°C for 30 min, and subsequently at room temperature, before being transferred to the recording chamber where recordings were obtained at 30-32°C.

2.6 Electrophysiology and optogenetic stimulation

Whole cell patch clamp recordings were performed in L4 of the primary visual cortex neurons V1. In MD-deprived animals, cells were patched in the binocular portion V1b. Inhibitory PV-expressing interneurons, labeled with GFP, were identified using LED illumination (OptoLED, blue, $\lambda=470\text{nm}$, Cairn Research, Faversham, UK) and thanks to their typical fast-spiking firing behavior in response to depolarizing DC current steps. Excitatory principal neurons (PNs) were visually identified using infrared video microscopy by their relatively small size round cell body and no apical dendrites. Accordingly, when depolarized with DC current pulses PNs exhibited a typical firing pattern of regular-spiking cells. We used different intracellular solutions depending on the type of experiment and the nature of the responses we wanted to assess. To study intrinsic excitability, AP waveform and glutamatergic spontaneous transmission, electrodes were filled with an intracellular solution containing (in mM): 127 K-gluconate, 6 KCl, 10 Hepes, 1 EGTA, 2 MgCl₂, 4 Mg-ATP, 0.3 Na-GTP; pH adjusted to 7.3 with KOH; 290-300 mOsm. The estimated reversal potential for chloride (E_{Cl}) was approximately -69 mV based on the Nernst equation. To measure GABAergic currents (both sIPSCs and uIPSCs in paired recordings), neurons were recorded using an intracellular solution containing (in mM): 65 K-gluconate, 70 KCl, 10 Hepes, 1 EGTA, 2 MgCl₂, 4 Mg-ATP, 0.3 Na-GTP; pH adjusted to 7.3 with KOH; 290-300 mOsm. The estimated E_{Cl} was approximately -16 mV based on the Nernst equation. Under these recording conditions, activation of GABA_A receptors resulted in inward currents at a holding potential (V_h) of -70 mV . Experiments using optical stimulation of ChR2-positive TC fibers were done with a cesium-based intracellular solution containing (in mM): 125 CsMeSO₃, 3 CsCl, 10 Hepes, 5 EGTA, 2 MgCl₂, 4 Mg-ATP, 0.3 Na-GTP, 5 QX314-Cl; pH adjusted to 7.3 with CsOH; 290-300 mOsm. This solution allowed voltage-clamping neurons at

any desired membrane potentials. E_{Cl^-} was approximately -63 mV based on the Nernst equation. Voltage values were not corrected for liquid junction potential. Patch electrodes were pulled from borosilicate glass capillaries and had a typical tip resistance of 2-3 M Ω . Signals were amplified with a Multiclamp 700B patch-clamp amplifier (Molecular Devices), sampled at 20-50 KHz and filtered at 4 KHz (for voltage-clamp experiments) and 10 KHz (for current-clamp experiments). Signals were digitized with a Digidata 1440A and acquired using the pClamp 10 software package (Molecular Devices).

For intrinsic excitability experiments neurons were recorded in current-clamp mode. In order to avoid any contribution of developmental differences and variations in the membrane resistance (R_m) on the frequency-current curves, in each cell, the injected current was adjusted as a function of R_m . This value was determined by the Ohm law ($I = \Delta V/R_m$): we injected an amount of current (I) to obtain a ΔV of ~ 10 mV, depending on the actual R_m of each cell, and increasing the amount of depolarizing current to obtain a ΔV of 5 mV, for a total of 15 current steps.

Single AP were obtained by injecting brief (2 ms) current steps of increasing amplitude from a V_m of ~ -70 mV in order to determine the minimal current intensity required to elicit a spike in each cell. This current was then injected 20 times and we averaged the trials for each cell from which we calculated the first derivative of the V_m and constructed planar phase plots to extract AP threshold values.

Synaptic events were recorded in voltage clamp mode for at least 2-3 minutes. EPSC (spontaneous and miniatures) were isolated by clamping the cells at -70 mV, using an intracellular solution containing $[Cl^-]$ yielding a E_{Cl^-} ~ -69 mV. In some experiments, we applied the glutamate receptor antagonist DNQX at the end of the recording and we could not detect any residual response (not shown). GABA_AR-mediated currents were pharmacologically isolated by applying 10 μ M of DNQX while recorded neurons at -70 mV, using an intracellular solution with a $[Cl^-]$ yielding a calculated E_{Cl^-} of ~ -16 mV.

For paired recordings, unitary synaptic responses were elicited in voltage-clamp mode by brief somatic depolarizing steps evoking action currents in presynaptic cells. We used a high-chloride intracellular solution ($E_{Cl^-} \sim -16$ mV), which allowed us measuring glutamatergic (PN-PV) and GABAergic synaptic responses (PV-PN, PV-PV and autapses) simultaneously. Neurons

were held at -80 mV and a train of 5 presynaptic spikes at 50 Hz was applied to infer short-term plasticity of synaptic responses.

Optical stimulation: ChR2 activation was obtained by brief (0.3 – 1.0 ms) light flashes on cortical slices, using a blue LED ($\lambda = 470$ nm; Thorlab) collimated and coupled to the epifluorescence path of an Olympus BX51 microscope mounting a 60 X water immersion objective (1.0 NA). Light intensity was controlled by the analogue output of an A/D card (Digidata 1440A) via a power supply (Thorlabs, LEDD1), and calibrated with a photodiode and a power meter. Light power ranged between 0.11 and 0.6 mW, over a spot of 0.28 mm of diameter. Although TC axons innervating cortical L4 were severed from their cell bodies, activation of ChR2-expressing fibers generated robust responses onto postsynaptic neurons (Kloc and Maffei, 2014). Light-evoked responses were recorded in voltage clamp mode in L4 PV cells and PNs. Direct recruitment of cortical neurons was performed in aCSF containing $1 \mu\text{M}$ of TTX, to remove polysynaptic activity, and $100 \mu\text{M}$ of the K^+ -channel antagonist 4-aminopyridine (4-AP), to enhance axonal depolarization. Light-evoked EPSCs were isolated by holding neurons at the reversal potential GABA ($E_{\text{Cl}^-} = -69\text{mV}$), in the presence of $10 \mu\text{M}$ gabazine. Disynaptic inhibition was measured in regular aCSF and IPSCs were isolated by holding neurons at the reversal potential for glutamate-mediated responses (between $+10$ and $+20$ mV, taking into account the liquid junction potential). In order to normalize the responses in function of different level of expression of ChR2 across animals and slices, for each experiment and each cell, we performed optical stimulation at a light intensity inducing detectable responses with reliability around 50 % (half responses and half failures). This light intensity was refereed as *threshold stimulation*. More precisely, to define stimulation parameters, firstly we tested different pulse durations, looking for the shortest value inducing light-evoked EPSCs and IPSCs. We thus set for each experiment the duration of stimulation at 0.3ms (for feed-forward, FFI) and 1ms (for the recording of the direct activation). The stimulus duration was longer in the latter case, due to the presence of TTX and 4-AP. With these constant pulse durations and by varying illumination intensity, the *threshold stimulation* was determined for each cell.

For all experiments, neurons were discarded from the analysis if the access resistance was >30 M Ω . All drugs were obtained from Tocris Cookson (Bristol, UK) or Sigma-Aldrich (St-Louis, USA).

2.7 *In vivo* recordings

All mice were older than 60 days. During surgery and experimentation, body temperature was maintained constant through a heating pad and respiration and heart beat were monitored (heart rate range 420-580 bpm). Oxygen-enriched air was administered through all procedures. All necessary efforts were made to minimize the stress of the animals.

Treatment with Chondroitinase-ABC: Animals were administered with antibiotic (Baytril, 1ml/L, in the drinking water) 1 day before surgical procedure. The day of surgery, mice were anesthetized with i.p. injection of avertin (0.2 ml/10g); skull was exposed and cleaned with ethanol. Protease-free Chondroitinase ABC (ChABC, 40 U/ml, Seikagaku) was diluted in sterile artificial cerebrospinal fluid. Three sites of injection were opened anterior of the visual cortex and 1 μ l of solution per site was slowly delivered at a depth of 500 μ m. The skin was sutured and the mouse was moved to a cage for recovery. Antibiotic administration continued for the following 3 days. In control animals, Penicillinase (40 U/ml, Sigma), a bacterial enzyme lacking endogenous substrate, was administered.

Local field potential (LFP) and visual evoked potentials (VEP): Mice were anesthetized by intraperitoneal injection of urethane (0.8 ml/kg in 0.9% NaCl; Sigma). Additional doses (10% of initial dose) were intraperitoneally administered to maintain the anesthetic level when necessary. The head was fixed in a stereotaxic frame. Body temperature during the experiments was constantly monitored with a rectal probe and maintained at 37°C with a heating blanket. The depth of anesthesia was evaluated by monitoring pinch withdrawal reflex and other physical signs (respiratory and heart rate). A portion of the skull overlying the visual cortex (0.0 mm anteroposterior and 2.9 mm lateral to the lambda suture) was drilled and the dura mater was left intact. A chamber was created with a thin layer of a synthetic resin around the edges of the craniotomy. Cortex was maintained constantly wet with aCSF containing (in mM): 132.8 NaCl, 3.1 KCl, 2 CaCl₂, 1 MgCl₂, 1 K₂HPO₄, 10 HEPES, 4 NaHCO₃, 5 glucose, 1 ascorbic acid, 0.5 myo-inositol, 2 pyruvic acid (pH=7.4). Animals deeply anesthetized under urethane were sacrificed by cervical dislocation without regaining consciousness at the end of the experiment. To record LFPs in the two hemispheres, two glass micropipettes (impedance \sim 2 M Ω , filled with ACSF solution) were positioned into the visual cortex at a depth of 250–300 μ m with a motorized micromanipulator (MPI electronic). A common reference Ag-AgCl electrode was placed on the cortical surface. Electrophysiological signals were amplified 1000-

fold (EXT-02F, NPI), band pass filtered (0.1–1000 Hz), and sampled at 5 kHz with 16 bit precision by a National Instruments (NI-usb6251) AD board controlled by custom-made LabView software. Line frequency 50 Hz noise was removed by means of a linear noise eliminator (Humbug, Quest Scientific). VEPs in response to alternating checkerboards modulated at different contrasts were recorded at the same depth of LFPs. All visual stimuli were computer-generated on a display (mean luminance at maximum contrast, 3 cd/m²) by a MATLAB custom program that exploits the Psychophysics Toolbox. The luminance of the checkerboard was calibrated by means of a photometer (Konica Minolta). The contrast values were calculated with the Michelson's formula: $(I_{\max} - I_{\min}) / (I_{\max} + I_{\min})$. Transient VEPs were recorded in response to the reversal (0.5 Hz) of the checkerboard (spatial frequency 0.04 c/deg). The response to a blank stimulus (0% contrast) was also recorded to estimate noise.

2.8 Immunohistochemistry

Thick slices used for electrophysiology experiments (300-350 μm) were fixed overnight in 4% paraformaldehyde in phosphate buffer (PB, pH 7.4) at 4°C. Slices were then rinsed three times at room temperature (10 min each time) in PBS and pre-incubated 1h at room temperature in a blocking solution of PBS with 0.3% Triton and 10% bovine serum albumin. Slices were then incubated 3.5 hours at room temperature in PBS with 0.3% Triton and Fluorescein Wisteria floribunda Lectin (WFA-FITC) which binds to the N-acetylgalactosamine of PNNs (from Vector Laboratories). Slices were then rinsed three times in PBS (10 min each) at room temperature, coverslipped in mounting medium and stored at 4°C. Immunofluorescence was then observed with an epifluorescence microscope (Nikon AZ100) and images were acquired. This *post-hoc* staining was used to check that PNNs is correctly degraded and slices were discarded if a clear disruption of the extracellular matrix was not evident.

Parvalbumin staining was realized on 40 μm -thick slices as following: after fixing the slices overnight in 4% paraformaldehyde in phosphate buffer (PB, pH 7.4) at 4°C, and rinsing them (10 min each time) in PBS, a pre-incubation in a blocking solution of PBT with 0.2% Triton and 3% bovine serum albumin was done at room temperature for 1h. Slices were incubated overnight (4°C) in the same blocking solution containing the primary rabbit anti-PV antibody (1:1000; Thermo Scientific). Slices were then rinsed three times in PBS (10 min each) at room temperature and incubated with Cy-2-anti-rabbit antibody (1:400; Jackson IR) for 3.5 hours at

room temperature. Slices were then rinsed three times in PBS (10 min each) at room temperature and coverslipped in mounting medium. Immunofluorescence was then observed with a confocal microscope (Olympus FV-1000) and images were acquired.

2.9 Data analysis

Experiments on firing dynamics and unitary paired recordings were analysed with Clampfit (Molecular Devices), Origin (Microcal) and custom-made scripts in Matlab (the Mathworks). Firing frequencies were averaged across three trials. Failures of unitary synaptic responses were included in the analysis.

Spontaneous and miniatures synaptic events were detected using custom written software (Wdetecta, courtesy J. R. Huguenard, Stanford University) based on an algorithm that calculate the derivative of the current trace to find events that cross a certain defined threshold. Amplitude and frequencies of the events were then binned and sorted, using other custom-written routines (courtesy J. R. Huguenard, Stanford University).

AP waveforms were investigated using a phase plot analysis (Bean, 2007) based on a routine developed with Matlab (courtesy J. Simonnet). Several parameters can be extrapolated from the loop (dV/dt plotted in function of V_m) obtained: *i*) AP threshold, measured as the potential at which the slope of the AP exceeds a certain threshold, that we conventionally fixed at $dV/dt > 30\text{mV/ms}$ *ii*) depolarization slope (ascending phase) *iii*) AP peak, which is the maximum potential reached *iv*) repolarization slope (descending phase) *v*) after-hyperpolarization *vi*) AP width, measured at the midpoint of the rising phase.

Passive properties as well as optical stimulation experiments were analyzed with Clampfit. Light-induced EPSCs were averaged across at least 20 trials and failures were removed from the analysis (threshold stimulation).

Finally, the analysis of evoked responses (VEP) and of the γ -spectrum was performed with custom MatLab software that exploits the Chronux toolbox for multitaper spectral analysis.

2.10 Statistical tests

All statistical analysis were performed in Prism (GraphPad Software, Inc.). Normality of the data was systematically assessed (D'Agostino & Pearson omnibus normality test). Normal distributions were statistically compared using paired *t* test two-tailed or One-way ANOVA followed by Bonferroni's Multiple Comparison *post hoc* test for more than two independent groups. When data distributions were not normal or *n* was small (Fig. 3.12H), non-parametric tests were performed (Mann Whitney test and Kruskal-Wallis test followed by Dunn's multiple comparison test for more than two groups, respectively). For the comparison of firing dynamics and short term plasticity, Two-way repeated-measures ANOVAs followed by Bonferroni's multiple comparison test were used. Differences were considered significant if $p < 0.05$ (* $p < 0.05$, ** $p < 0.01$, *** $p < 0.001$, **** $p < 0.0001$). Values are presented as mean \pm SEM of *n* experiments.

Chapter III: RESULTS

3.1 *In vivo* enzymatic removal of PNN in V1 of adult mice

The majority of studies interested in neuronal and circuit alterations in response to PNN removal, used acute, direct ChABC incubation of brain culture slices for a few hours (Dityatev et al., 2007). Whereas this approach is useful to understand the acute effects of PNN removal, it does not reveal possible changes, which occur *in vivo* and which might lead to the re-opening of cortical plasticity. Here, we performed *in vivo* stereotaxic injections of ChABC in one hemisphere of adult (> P70) mice V1 and assessed the effect of PNN removal 48-72h post-injections on visual responses *in vivo*, and on cellular and circuit physiology *in vitro*. It has been previously reported that this interval is sufficient to locally disrupt PNNs and obtain substantial physiological modifications (Pizzorusso, 2002). We compared ChABC injected mice with sham-injected mice (Penicillase or PBS) as controls. Importantly, after each electrophysiological experiment, slices were fixed for *post-hoc* PNN immunohistochemistry, using WFA staining, in order to verify the adequate degradation of the nets and discard recordings originating from tissue in which degradation did not occur. Figure 3.1 illustrates the efficacious disruption of PNNs in the region of interest (visual cortical area V1). In this representative slice, PNN disruption by ChABC is indicated by the absence of WFA staining (in green) in the V1 region (dark portion), and in particular around PV cells. Thus, *in vivo* enzymatic injections provide a good removal of PNN from V1.

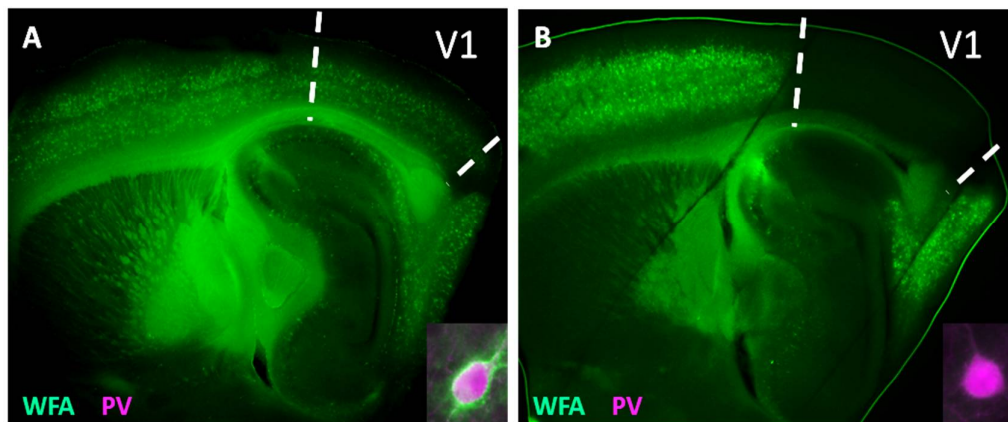


Figure 3.1. *In vivo* enzymatic disruption of PNNs following ChABC injection in V1 of adult mice. (A) Representative micrograph of a sagittal brain slice (thickness: 350 μ m) from a control animal, whose visual cortex was injected with PBS. PNNs are stained with WFA (green) and are present throughout the cortex, including V1 (delimited by dotted lines). The inset shows a magnified micrograph of a cell stained with an anti-PV antibody (magenta), wrapped by PNNs. (B) Same as in A, but from a slice obtained from a ChABC-treated mouse. PNN disruption in V1 is indicated by the absence of WFA staining. The inset illustrates a PV cell devoid of PNNs.

3.2 PNN removal alters the visual gain adaptation curve *in vivo*, and increases the power of visually-evoked oscillations

Gain adaptation of contrast perception is a fundamental computation performed by the primary visual cortex where the gain of signal amplification is gradually reduced as the synaptic input increases, allowing for the extension of the dynamic range of the internal representation of the external scene (Carandini and Heeger, 1994; Anderson et al., 2000; Mitchell and Silver, 2003). Gain adaptation is implemented by the gradual recruitment of inhibitory interneurons by the thalamic inputs and by converging inputs from cortical pyramidal cells. Gain adaptation can be estimated by the transfer function linking the visual stimuli to the evoked potentials: the slope of the transfer function decreases as the stimulus increases, thus extending the dynamic range. We wanted to test whether PNN removal by ChABC digestion results in increased interneuron activity. This would produce a stronger adaptation to the visual scene with a reduction of the slope of the transfer function (Silver, 2010; Atallah et al., 2012). We recorded visually-evoked extracellular potentials (VEPs) in V1 of adult mice. VEPs were recorded in the central part of the primary visual cortex in response to an alternating checkerboard of varying contrast presented to the eye contralateral to the recording site (Fig. 3.2A,B). By increasing the contrast of the checkerboard stimulus, we constructed transfer functions in sham- and ChABC-treated animals (Fig. 3.2C). We found a clear enhancement of adaptation in ChABC-treated animals, consistent with an increased inhibitory activity ($p < 0.05$, Two-way repeated-measures ANOVAs). Interestingly, whereas the spectral power during resting state is unaffected by ChABC treatment, there is a sizable increment of the gamma band power during evoked activity (Fig. 3.2D,E).

Altogether these results suggest that enzymatic disruption of PNNs results in stronger inhibitory interneuron activity during visual stimulations.

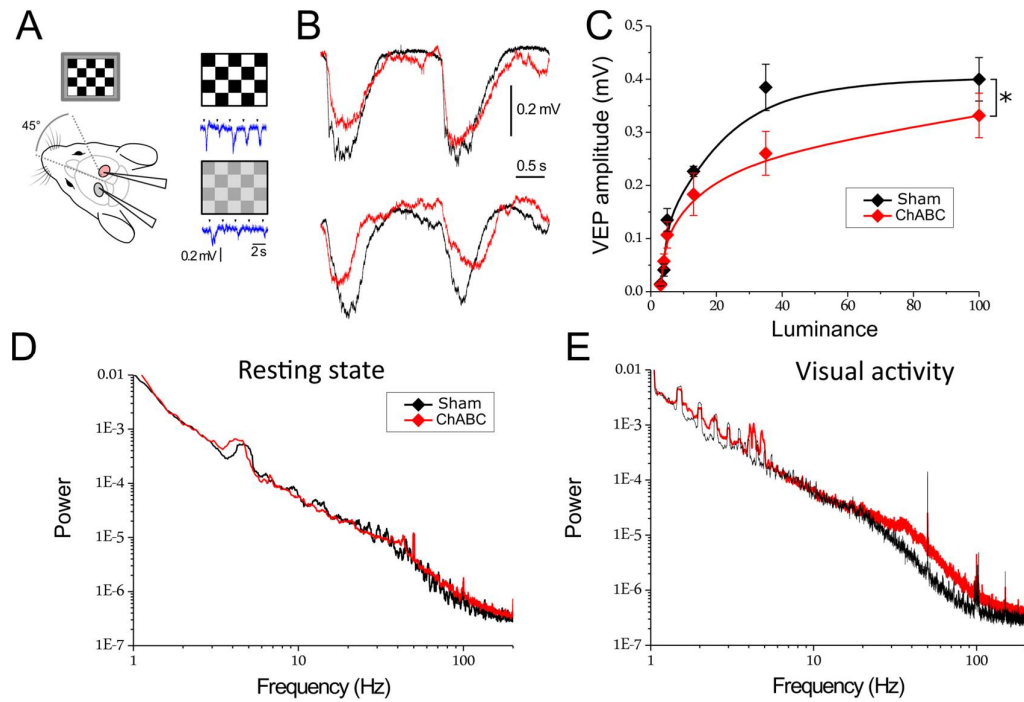


Figure 3.2. *In vivo* recordings of VEP and gamma oscillations after PNN removal in adult mice. (A) Experimental setup. The LFP has been recorded in the injected hemisphere of V1 with either Pennicilase (control) or ChABC. All recordings have been performed 2 days post-injection under urethane anesthesia. The LFP was recorded in resting conditions (the screen was of uniform luminance) or during the presentation of a checkerboard of variable contrast that was inverted every 2 sec. (B) Typical recordings in control (black) and after PNNs degradation (red). (C) Transfer function in control conditions (black) and after PNNs degradation (red). The increment of the VEP responses with stimuli of increasing contrast and luminance lags behind compared to controls, possibly indicating a larger recruitment of inhibitory interneurons curtailing the activity of pyramidal neurons. *: $p < 0.05$ (D) The power spectra recorded in resting state is similar in control and treated mice, indicating no alteration of basal activity. Indeed, slow wave sleep is unaltered in the two groups (data not shown). (E) The power spectra obtained from the recording of visually driven activity indicates a specific increase of activity in the γ -band, consistent with increased recruitment of PV cells.

3.3 Developmental changes of firing dynamics and passive properties of PV cells and PNs. No apparent effect induced by disruption of PNNs

3.3.1 Developmental changes

Perisomatic-targeting PV BCs are known to regulate output spiking of PNs (Freund and Katona, 2007) and drive network oscillations in the γ -frequency band (Klausberger and Somogyi, 2008; Cardin et al., 2009; Sohal et al., 2009; Isaacson and Scanziani, 2011b). The reduced slope of the transfer function of VEPs and the increased light-induced γ -power, upon PNN degradation, suggest that, in the absence of PNNs, the output of inhibitory interneurons is increased. Increased perisomatic inhibitory activity *in vivo* could be explained by one or a combination of the following causes: *i*) increased intrinsic excitability and/ or spiking activity of inhibitory interneurons *ii*) alterations of the glutamatergic (excitatory) or GABAergic (inhibitory) drive onto specific elements of the cortical networks, favoring the recruitment of local GABAergic interneurons. Here we set out to dissect these different possibilities. In particular, we analyzed intrinsic excitability, synaptic and circuit properties of PV cells and PNs in L4 of V1.

We first characterized the intrinsic physiology *i.e* the firing dynamics and the passive properties of PV cells and PNs at different ages, recapitulating the CP and the accumulation of PNNs around PV cells. Indeed, previous studies focused on the maturation profile of PV cells and PNs before (<P20) or during the CP (P25-P32). Here, we compared physiological parameters within a much broader age range, which corresponds to the accumulation of PNNs around PV cells: from pre-CP to adult stages (>P70).

To test whether the maturation of PV cells and PNs is accompanied by changes in their excitability, we analyzed neuronal firing in response to current injections. Both PV cells and PNs were stimulated in current-clamp mode with hyperpolarizing and depolarizing current steps (15 steps of 800 ms) to construct input-output, frequency-current (f-i) curves (Fig. 3.3A,E). In order to avoid changes in firing frequency due to possible developmental variations of membrane resistance (R_m), the amount of the injected current was adjusted in function of R_m in each cell (Table 1; $p > 0.05$, Two-way repeated-measures ANOVAs). Moreover, in each neuron, the pre-step V_m was adjusted to -70mV with constant current injections. This allowed determining whether L4 neurons changed their spiking properties and dynamics during the

developmental window of PNN accumulation around PV cells. Importantly, however, no significant changes were found in passive membrane properties, such as R_m (Fig. 3.3C,G, table 2; $p > 0.05$, Kruskal-Wallis test) and V_{rest} (Fig. 3.3D,H, table 2; $p > 0.05$, Kruskal-Wallis). For each group, the frequency rate of individual cells was averaged across three trials. We found a developmental increase in the input-output relationship for both cell types. Indeed, mean firing rates at older age and in responses to increased current present steeper slopes and higher frequencies values, indicating an age-dependent enhancement of excitability from pre-CP (<P20) to adult (>P70) ages. For PV cells, the excitability of P20 groups and P25-P32 are significantly different from P40-P60 and P70 age groups (Fig. 3.3A, table 2; $p < 0.05$, Two-way repeated-measures ANOVAs). For PNs, the slope of f-I curves increased already after P20 (Fig. 3.3F, table 2; $p < 0.05$, Two-way repeated-measures). These data indicate that PV INs reach “mature” intrinsic excitability around P40-P60, whereas intrinsic excitability of PNs matures more rapidly already at P25-P32.

In conclusion, these data show a robust age-dependent increase of input-output firing relationships in both cell types, with no overall change in their passive electrical properties.

PV	First current (pA)	PN	First current (pA)
< P20	-126.44 ± 12.11	< P20	-50.38 ± 5.43
P25-P32	-100.43 ± 15.32	P25-P32	-60.01 ± 5.11
P40-P60	-101.13 ± 8.34	P40-P60	-55.91 ± 6.90
> P70	-113.01 ± 12.84	> P70	-54.01 ± 8.96

Table 1. First step of injected current normalized in function of the R_m , for PV interneurons and PNs cells. Mean ± SEM.

PV	n	N	R_m (M Ω)	V_{rest} (mV)
< P20	16	9	93.03 ± 9.4	-64.19 ± 1.86
P25-P32	7	4	115.8 ± 14.9	-60.57 ± 3.24
P40-P60	15	7	114 ± 14.8	-67.39 ± 0.81
> P70	15	9	124.2 ± 19.6	-64.37 ± 1.72

PN	n	N	R_m (M Ω)	V_{rest} (mV)
< P20	13	8	231.2 ± 24.3	-67.08 ± 1.3
P25-P32	6	5	192 ± 20.5	-68.17 ± 3.2
P40-P60	8	3	196.4 ± 29	-71.03 ± 1.65
> P70	13	7	228.5 ± 22.9	-71.15 ± 1.9

Table 2. Passive properties of PV and PN cells during development. Mean ± SEM. n=number of cells, N=number of mice. The cells are the same as the ones for the firing dynamics.

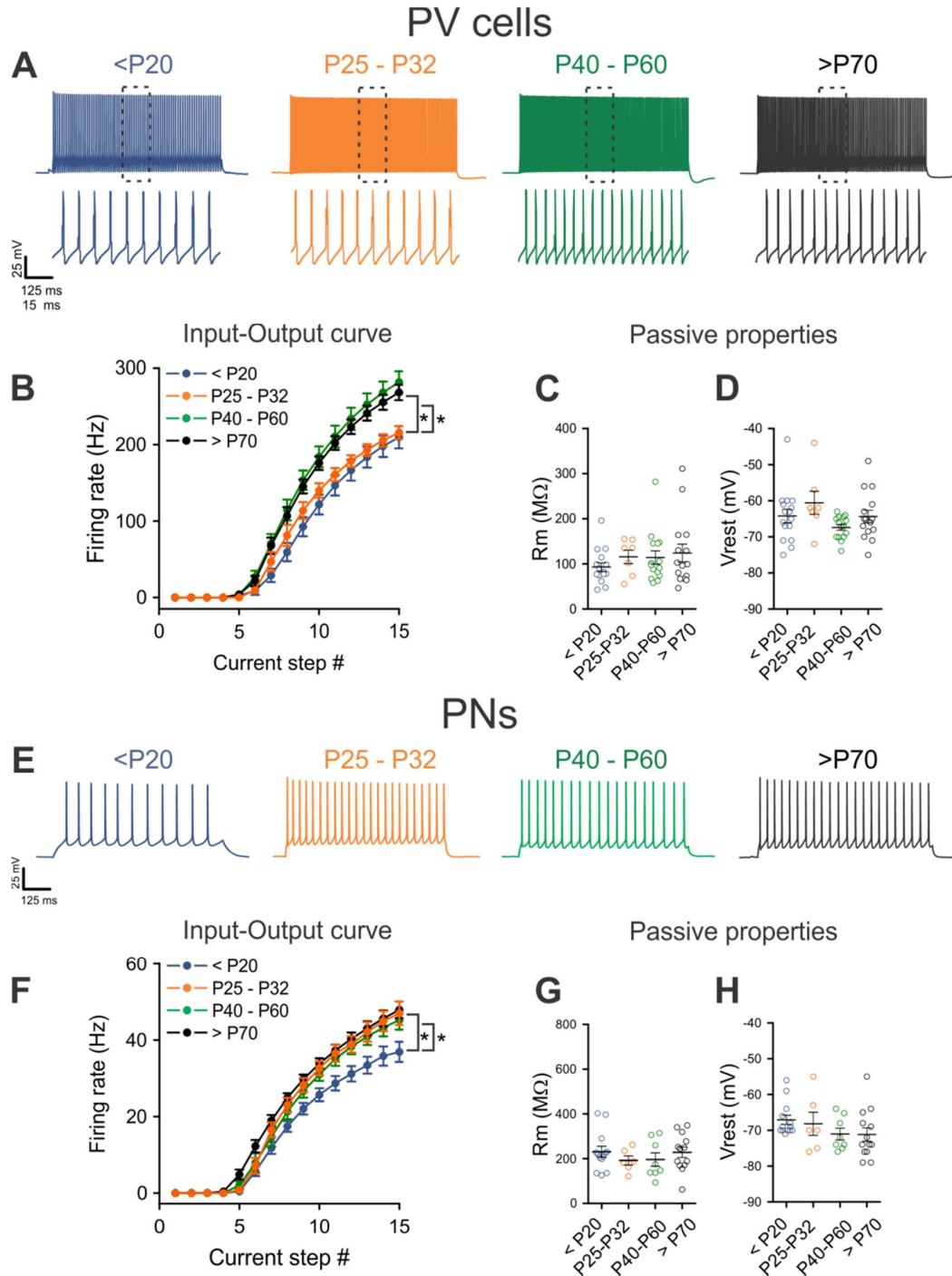


Figure 3.3. Developmental changes in the firing dynamics and passive properties of PV cells and PNs. (A) Representative current-clamp recordings from PV-expressing interneurons, at different post-natal ages. Characteristic fast-spiking patterns in response to depolarizing current injections (insets illustrate firing at a faster timescale corresponding to the dotted region in the upper part). (B) Average spike frequency as a function of the depolarizing stimulus (f-i curves) at all developmental stages. (C-D) Passive properties (Rm and Vrest, C and D, respectively) of PV cells at different developmental stages. (E-H) Same as in B-D but for EGFP-negative PNs, recorded at the same developmental stages. *: $p < 0.05$.

3.3.2 Firing dynamics and passive properties are not altered by PNN removal

The few studies that investigated intrinsic alterations of neuronal excitability following PNN degradation were performed following acute PNN disruption *in vitro*: in hippocampal cultures, direct incubation with ChABC (Dityatev et al., 2007) as well as application of hyaluronidase (Bikbaev et al., 2015) increase neuronal excitability. In the neocortex, it has been shown that incubation of acute slices with ChABC results in decreased excitability of PV cells (Balmer, 2016). Here, we investigated whether PN and PV-cell excitability in adult mice (>P70) were altered following PNN enzymatic disruption *in vivo* by stereotaxic injections of ChABC, 48-72h before the electrophysiological recordings. This protocol was shown to induce the re-opening of cortical plasticity (Pizzorusso, 2002). We constructed f-i curves as described above (section 3.3.1) in PV cells and PNs from animals that were injected with a control (sham) or a ChABC solution. Interestingly, we found that *in vivo* PNN enzymatic disruption in adult V1 did not affect the firing dynamics of PV cells and their glutamatergic PN counterparts in L4 (Fig. 3.4C,D; table 3; $p > 0.05$, Two-way repeated-measures ANOVAs). Number of investigated cells and mice are reported in table 2. In addition, passive properties were not affected by *in vivo* ChABC treatment (Fig. 3.4.E,F; table 4; $p > 0.05$, Mann Whitney test for R_m and Unpaired t test for V_{rest}).

Altogether, our data indicate that *in vivo* PNN removal in adult animals does not affect the intrinsic firing dynamics as well as the passive properties of PV and PNs cells.

PV	First current (pA)	PN	First current (pA)
Sham	-115.27 ± 6.57	Sham	-50.57 ± 3.04
ChABC	-104.68 ± 4.98	ChABC	-49.56 ± 6.64

Table 3. First step of injected current normalized in function of the R_m . Mean ± SEM.

PV	n	N	R_m (M Ω)	V_{rest} (mV)
Sham	26	10	96.2 ± 6.2	-66.31 ± 0.87
ChABC	25	9	96.02 ± 4.5	-65.47 ± 0.92

PN	n	N	R_m (M Ω)	V_{rest} (mV)
Sham	13	7	248.7 ± 39.9	-68.73 ± 1.98
ChABC	9	6	252.5 ± 44.1	-69.04 ± 3.3

Table 4. Passive properties of PV and PN cells in control and ChABC-treated animals. Mean values ± SEM. n=number of cells, N=number of mice. The cells are the same as the ones for the firing dynamics.

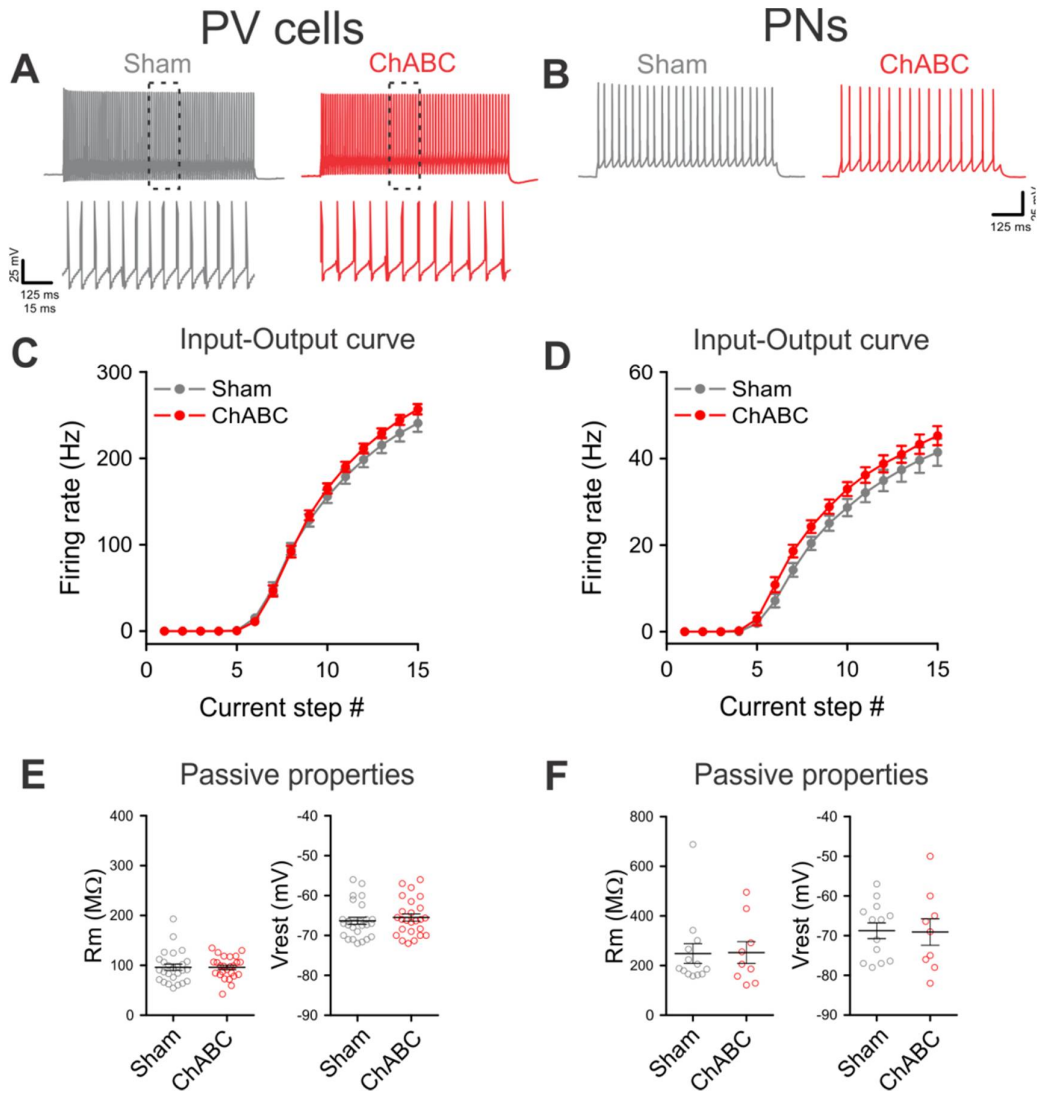


Figure 3.4. Firing dynamics and passive properties are not altered by PNN removal in adult animals. (A) Characteristic firing of PV cells in response to depolarizing current injections, in control condition (sham - grey) and in ChABC-treated animals (red). Insets illustrate firing at a faster timescale corresponding to the dotted region in the upper part. (B) Example firing of PNs in presence (sham - grey) and absence (ChABC - red) of PNNs. (C-D) f-i curves of PV cells (C) and PNs (D). (E-F) Passive properties of PV cells (E) and PNs (F).

3.4 Developmental changes of action potential waveform of both cell types. No apparent effect induced by disruption of PNNs

The results illustrated in figure 3.4 show that despite a developmental change observed in the firing dynamics of both cell types, PNN disruption did not alter the intrinsic excitability of adult L4 neurons. We wondered whether also single AP waveform varies during development and whether it is affected by enzymatic removal of PNNs. A very recent study using a genetic mouse line where the brevican component of PNNs was knocked out showed an increase in the AP half-width and a decrease in AP threshold compared to controls (Favuzzi et al., 2017). We therefore compared the shape of a single AP, elicited by brief (2ms) current injections during development and in mature mice, in the presence and absence of PNNs. Characteristic AP features, such as threshold and peak values were extracted by constructing phase plots (Fig. 3.5A), in which spike derivatives (dV/dt) were plotted against membrane potential values (V_m), whereas AP width at half-maximum amplitude (herein defined as AP width) were computed from actual spikes.

For both PNs and PV cells, the AP threshold in the youngest group (<P20) was significantly less negative than their older counterparts (Fig. 3.5C,G, left part, table 5; $p < 0.05$ for both PV cells and PNs). Moreover, AP width was significantly broader than the other groups (Fig. 3.5D,H, left part, table 5; $*p < 0.05$, $**p < 0.01$, $***p < 0.001$, One way or Kruskal-Wallis test). This is consistent with increased excitability of both cell types during development, as we showed in section 3.3.1. On the other hand, the AP peak value of PV cells as well as PNs did not present significant variations during development (Fig. 3.5E,I, table 5; $p > 0.05$, One-Way ANOVA). For the group P25-P32 of PNs, the number of cells was too low (three) to be included in the analysis.

Importantly, enzymatic degradation of PNNs in adult mice did not affect the three tested parameters in both cell types (Fig. 3.5C-E, G-I, right part, table 5; $p > 0.05$, Unpaired t test or Whitney test).

Altogether, these results and those of figure 3.4 indicate that PNN removal in adult mice does not affect PV-cell and PN intrinsic excitability properties.

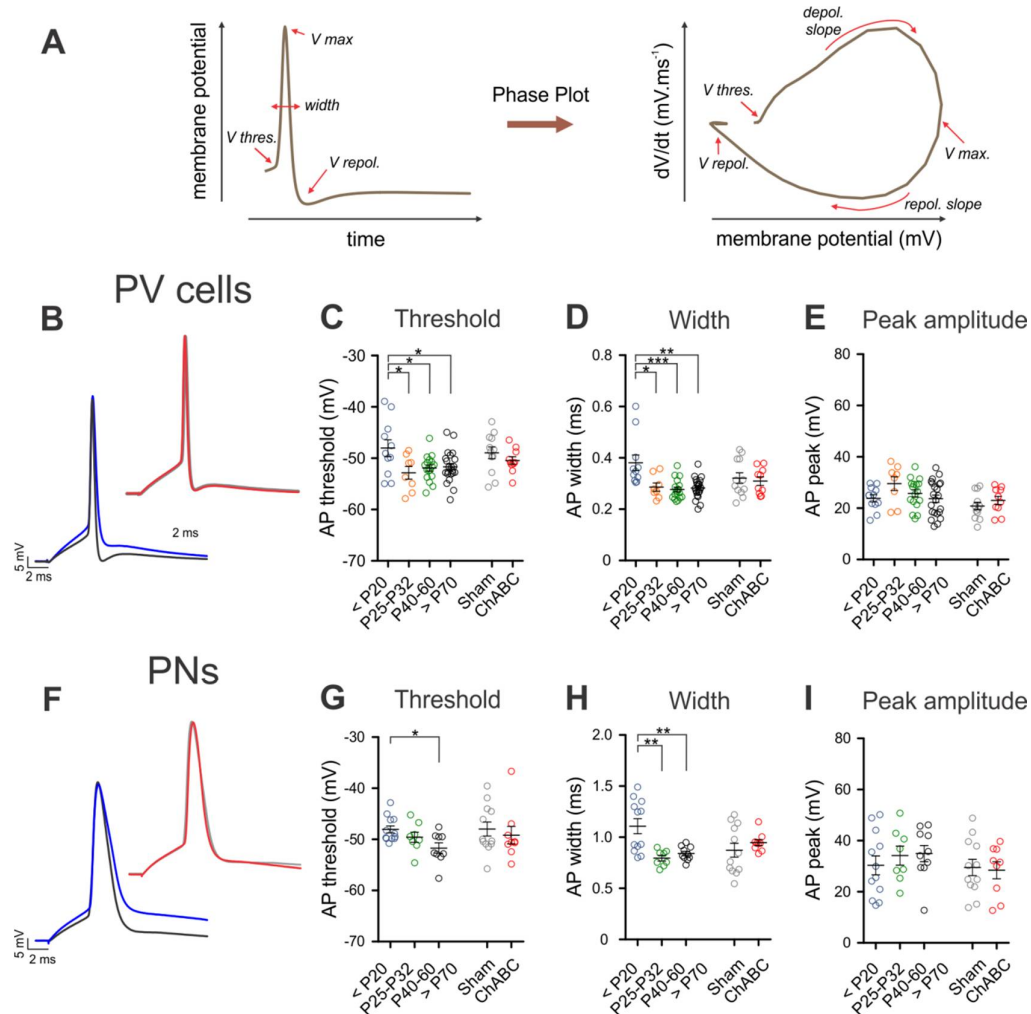


Figure 3.5. Single action potential waveform changes during development but is not affected by PNN degradation in adult mice. (A) Phase plot analysis. Left, example trace of an AP recorded from a PV cell. Several parameters are shown such as AP width (width), AP threshold ($V_{thres.}$), AP peak amplitude (V_{max}) and AP depolarization ($V_{depol.}$) and repolarization ($V_{repol.}$). Right, corresponding phase plot where the first derivative of V_m (dV/dt) is plotted as a function of V_m . Values of AP threshold as well as peak amplitude are extracted from the phase plot, whereas AP width is determined from the actual spike (left). **(B)** Example traces of single APs recorded from PV cells, at P20 (blue), P70 (black), and in sham- (gray) and in ChABC-treated (red) animals. APs accelerate during development but PNN removal does not alter AP shape. **(C-E)** Average AP threshold (C), width (D) and peak (E) in PV cells during development (left part) and after PNN removal (right). **(F-I)** Same as in A-E, but for EGFP-negative PNPs. *: $p < 0.05$, **: $p < 0.01$, ***: $p < 0.001$.

PV	n	N	AP threshold (mV)	AP width (ms)	AP peak (mV)
< P20	11	8	-48.03 ± 1.64	0.3811 ± 0.03	23.86 ± 1.4
P25-P32	8	3	-52.84 ± 1.2	0.2864 ± 0.02	29.59 ± 2.7
P40-P60	17	10	-51.91 ± 0.6	0.2770 ± 0.01	25.77 ± 1.4
> P70	22	11	-51.67 ± 0.6	0.2820 ± 0.009	23.68 ± 1.45
Sham	12	10	-48.95 ± 1.1	0.3211 ± 0.02	20.84 ± 1.5
ChABC	10	9	-50.45 ± 0.75	0.3094 ± 0.017	23.04 ± 1.6

PN	n	N	AP threshold (mV)	AP width (ms)	AP peak (mV)
< P20	12	8	-48.05 ± 0.71	1.108 ± 0.07	30.35 ± 3.7
P40-P60	8	6	-49.58 ± 0.9	0.7955 ± 0.028	34.13 ± 3.7
> P70	9	6	-51.70 ± 1.01	0.8402 ± 0.022	34.94 ± 3.2
Sham	12	10	-47.98 ± 1.4	0.8719 ± 0.07	29.49 ± 3.2
ChABC	9	6	-49.18 ± 1.8	0.9480 ± 0.03	28.40 ± 3.3

Table 5. Action potential (AP) parameters of PV and PN cells during development and after PNN removal. Mean values ± SEM. n=number of cells, N=number of mice.

3.5 Developmental maturation of synaptic transmission onto PV cells and PNs, and alterations induced by PNN digestion

3.5.1 Development of glutamatergic neurotransmission onto L4 neurons and effects of PNN removal

In the next set of experiments, we aimed to determine the developmental profile of synaptic transmission onto both PV cells and PNs, and whether disruption of PNNs resulted in alteration of either glutamatergic or GABAergic neurotransmission in adult mice. We used spontaneous synaptic events as a first indicator of global changes in synaptic connectivity during development and following PNN disruption. In voltage-clamp experiments, we first isolated glutamatergic neurotransmission onto PV cells and PNs by holding neurons at the reversal potential of GABA-mediated responses ($V_h = -70\text{mV}$ using an intracellular solution of K-gluconate 10 mM chloride yielding a $E_{Cl} = -69\text{mV}$) so that only glutamatergic inward currents were recorded. In some experiments, we recorded PNs and PV cells in the continuous presence of the GABA_AR antagonist gabazine (10 μM) and we did not observe changes in the frequency or amplitude of spontaneous excitatory postsynaptic currents (sEPSCs; not shown). Moreover, in some experiments, application of the AMPA- and Kainate-type ionotropic

glutamate receptor antagonist DNOX (10 μ M) completely abolished sEPSCs (not shown), indicating that in these recording conditions, we could isolate glutamate-mediated synaptic responses.

We found that during development, glutamatergic transmission onto PV cells decreases. Indeed, averaged sEPSC amplitude in young (<P20) mice was significantly bigger than older age groups (Fig. 3.6B, left part, table 6; * p <0.05, **** p <0.0001, One way ANOVA). Additionally, sEPSC frequency onto PV cells decreased from P25-P32 (Fig. 3.6C, left part, table 6; p <0.05, Kruskal-Wallis test). In contrast to PV cells, we did not find developmental changes in sEPSC frequency and amplitude onto PNs (Fig. 3.6E,F, left part, table 6; p >0.05, Kruskal-Wallis test).

Remarkably, PNN removal in adult animals led to an increase in both the amplitude and the frequency of sEPSCs onto PV cells (Fig. 3.6B,C, right part, table 6; * p < 0.05 ** p <0.01, Unpaired t test for the ampl. and Mann Whitney test for the freq.) similarly to younger, pre-CP groups (<P20). Importantly, the effect of enzymatically removing PNNs is specific to PV INs, while *in vivo* ChABC treatment left sEPSCs onto PNs unaffected (Fig. 3.6E,F, right part, table 6; p >0.05, Unpaired t test).

Taken together, these data show that PNN removal in adult animals increased excitatory transmission selectively onto PV cells, recapitulating younger, pre-CP states.

PV	n	N	sEPSC ampl. (pA)	sEPSC freq. (Hz)
< P20	16	8	15.79 \pm 0.5	27.85 \pm 1.6
P25-P32	18	7	13.53 \pm 0.4	37.40 \pm 3.9
P40-P60	22	11	11.47 \pm 0.6	36.73 \pm 3.4
> P70	27	7	11.27 \pm 0.41	25.40 \pm 1.9
Sham	29	15	9.806 \pm 0.4	33.50 \pm 3.04
ChABC	24	9	11.88 \pm 0.5	46.80 \pm 4.7

PN	n	N	sEPSC ampl. (pA)	sEPSC freq. (Hz)
< P20	11	5	7.373 \pm 0.4	8.028 \pm 1.4
P25-P32	8	5	9.834 \pm 0.8	6.674 \pm 1.3
P40-P60	18	8	8.279 \pm 0.6	8.662 \pm 1.4
> P70	13	7	9.549 \pm 0.7	5.822 \pm 1.2
Sham	16	13	7.935 \pm 0.35	7.701 \pm 1.2
ChABC	15	11	8.802 \pm 0.7	9.114 \pm 1.3

Table 6. Glutamatergic transmission onto PV and PN cells during development and after PNN removal. sEPSC: spontaneous excitatory postsynaptic currents. Mean values \pm SEM. n=number of cells, N=number of mice.

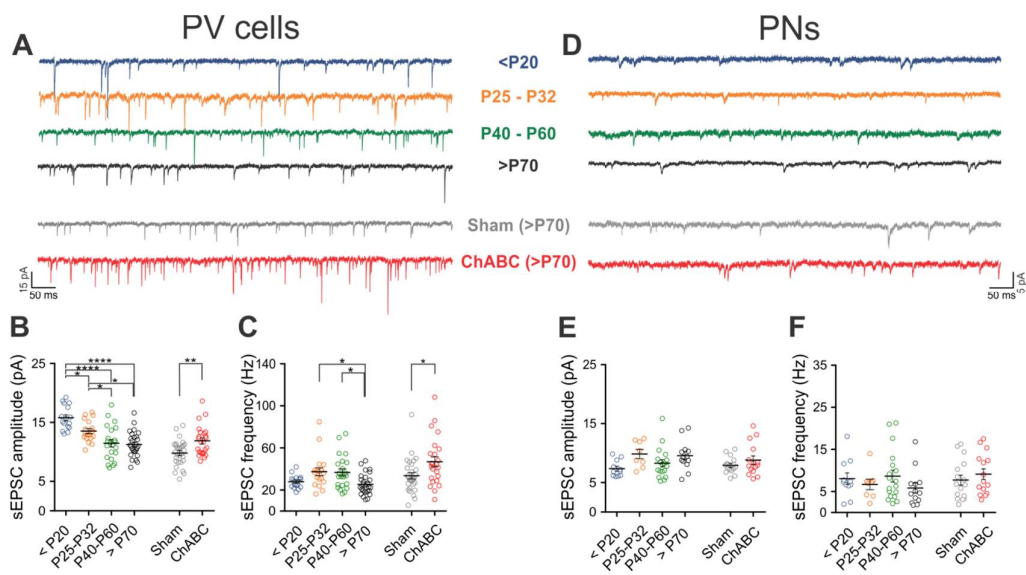


Figure 3.6. Developmental maturation of glutamatergic synaptic transmission onto PV cells and PNs, and its specific enhancement onto PV following PNN digestion. (A) Example voltage-clamp traces of sEPSCs recorded in PV cells during development and after ChABC treatment. **(B-C)** Plots of average sEPSC amplitude (B) and frequency (C) in PV cells. Developmental profile is represented on the left part of the graphs and the effect of PNN removal is shown on the right part (sham/grey and ChABC/red). **(D-F)** Same as in A-C, but on PNs. *: $p < 0.05$, **: $p < 0.01$, ***: $p < 0.001$, ****: $p < 0.0001$.

3.5.2 Development of GABAergic neurotransmission onto L4 neurons and effects of PNN removal

To determine if the balance between excitation and inhibition was altered by PNN removal, we also assessed the spontaneous inhibitory transmission onto both PV cells and PNs. Also these recordings were performed during development and after PNN degradation in adult animals (Fig. 3.7). GABAergic transmission was pharmacologically isolated by applying 10 μM DNQX in the aCSF, and recording spontaneous inhibitory postsynaptic currents (sIPSCs) in voltage clamp at a $V_h = -70$ mV, with an intracellular solution containing 70 mM Cl ($E_{Cl} \sim -16$ mV). Intriguingly, in contrast to glutamatergic neurotransmission that decreased during development in PV cells (Fig. 3.6), sIPSC frequency and amplitude were constant across all age stages in this cell type (Fig. 3.7B,C, left part, table 7; $p > 0.05$, Ampl: One way ANOVA, Freq: Kruskal-Wallis test).

Similarly, no significant differences were found for PN cells (Fig. 3.7E,F, left part, table 7; $p > 0.05$, Kruskal-Wallis test).

Interestingly, ChABC treatment enhanced both sIPSC amplitude and frequency specifically onto PV neurons (Fig. 3.7B,C, right part, table 7; $p < 0.05$, Unpaired t test), as spontaneous inhibitory transmission onto PNs was unaffected (Fig. 3.7E,F, right part, table 7; $p > 0.05$, Mann Whitney test).

Together with the results of section 5.1, our experiments on global spontaneous transmission onto PV cells and PNs revealed that glutamatergic neurotransmission decreases during development selectively onto PV cells, whereas GABAergic transmission remained constant.

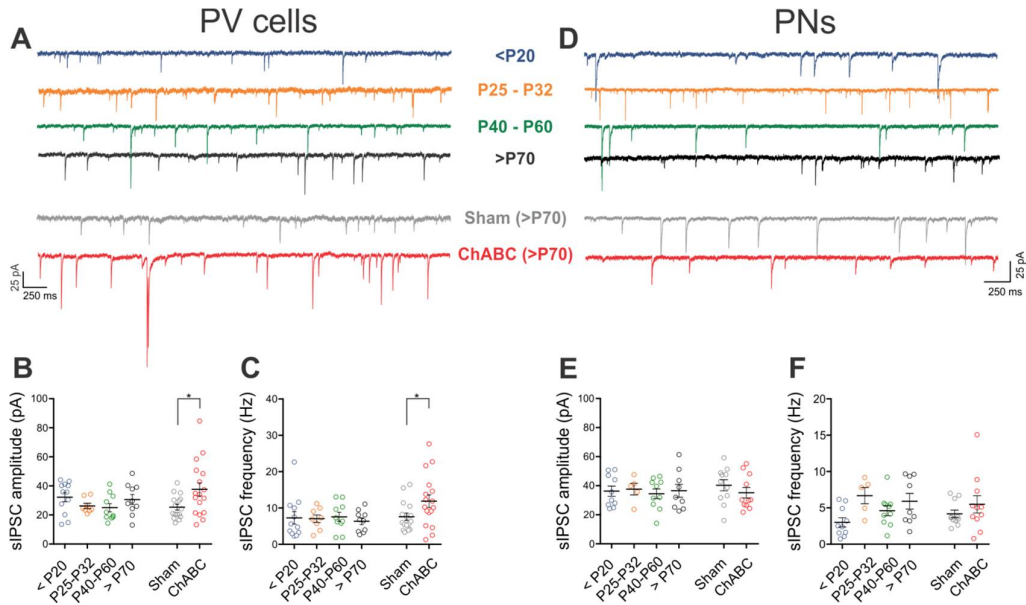


Figure 3.7. Developmental maturation of GABAergic synaptic transmission onto PV cells and PNs, and its specific enhancement onto PV following PNN digestion. (A) Example voltage-clamp traces of sIPSCs recorded in PV cells during development and after ChABC treatment. **(B-C)** Plots of average sIPSC amplitude (B) and frequency (C) in PV cells. Developmental profile is represented on the left part of the graphs and the effect of PNN removal is shown on the right part (sham/grey and ChABC/red). **(D-F)** Same as in A-C, but on PNs. * $p < 0.05$.

PV	n	N	sIPSC ampl. (pA)	sIPSC freq. (Hz)
< P20	12	5	32.24 ± 3.2	7.288 ± 1.7
P25-P32	8	3	26.24 ± 1.8	7.058 ± 1.1
P40-P60	10	7	25.01 ± 2.9	7.555 ± 1.3
> P70	10	5	30.65 ± 3.4	6.346 ± 0.9
Sham	16	7	25.37 ± 2	7.589 ± 1.0
ChABC	17	7	37.60 ± 4.5	11.88 ± 1.7

PN	n	N	sIPSC ampl. (pA)	sIPSC freq. (Hz)
< P20	10	2	36.26 ± 3.5	3.013 ± 0.6
P25-P32	5	2	37.62 ± 3.98	6.677 ± 1.1
P40-P60	10	5	34.47 ± 3.3	4.604 ± 0.69
> P70	9	4	36.50 ± 4.5	5.913 ± 1.07
Sham	11	6	40.33 ± 3.4	4.181 ± 0.51
ChABC	11	8	35.15 ± 3.6	5.490 ± 1.2

Table 7. GABAergic transmission onto PV and PN cells during development and after PNN removal. sIPSC: spontaneous GABAergic events. Mean values ± SEM. n=number of cells, N=number of mice.

3.5.3 Effects of PNN removal on quantal synaptic transmission onto PV cells

Spontaneous neurotransmission includes synaptic events that can depend on stochastic AP firing within the neuronal network and quantal, AP-independent events. To test whether increased glutamatergic and GABAergic neurotransmission onto PV cells following PNN removal (section 3.5.1 and 3.5.2) was due to increased slice excitability or quantal synaptic transmission, we recorded miniature mEPSCs and mIPSC in the presence of 1 μ M TTX (Fig. 3.8, table 8). Even in the absence of AP firing, we found a significant increase in the frequency of the glutamatergic events specifically onto PV cells (Fig. 3.8C, table 8; $p < 0.01$, Unpaired t test), whereas mEPSC amplitude was unaffected (Fig. 3.8B, table 8; $p > 0.05$, Unpaired t test). Remarkably, we found that mIPSCs onto PV cells were not affected by ChABC injection, indicating that increased sIPSCs was due to a network effect, rather than a direct synaptic alteration (Fig. 3.8E,F, table 8; $p > 0.05$, Unpaired t test).

Altogether, the results onto sPSCs and mPSCs indicate that *in vivo* PNN removal in adult mice increased both excitatory and inhibitory spontaneous transmission selectively onto PV cells.

Whereas the increase of excitatory neurotransmission is due to PNN-dependent alterations at the level of the synapse, alterations of GABAergic neurotransmission were due to increased spiking activity of cortical interneurons. Interestingly, it seems that the overall effect of PNN removal on glutamatergic neurotransmission recapitulates younger, pre-CP states.

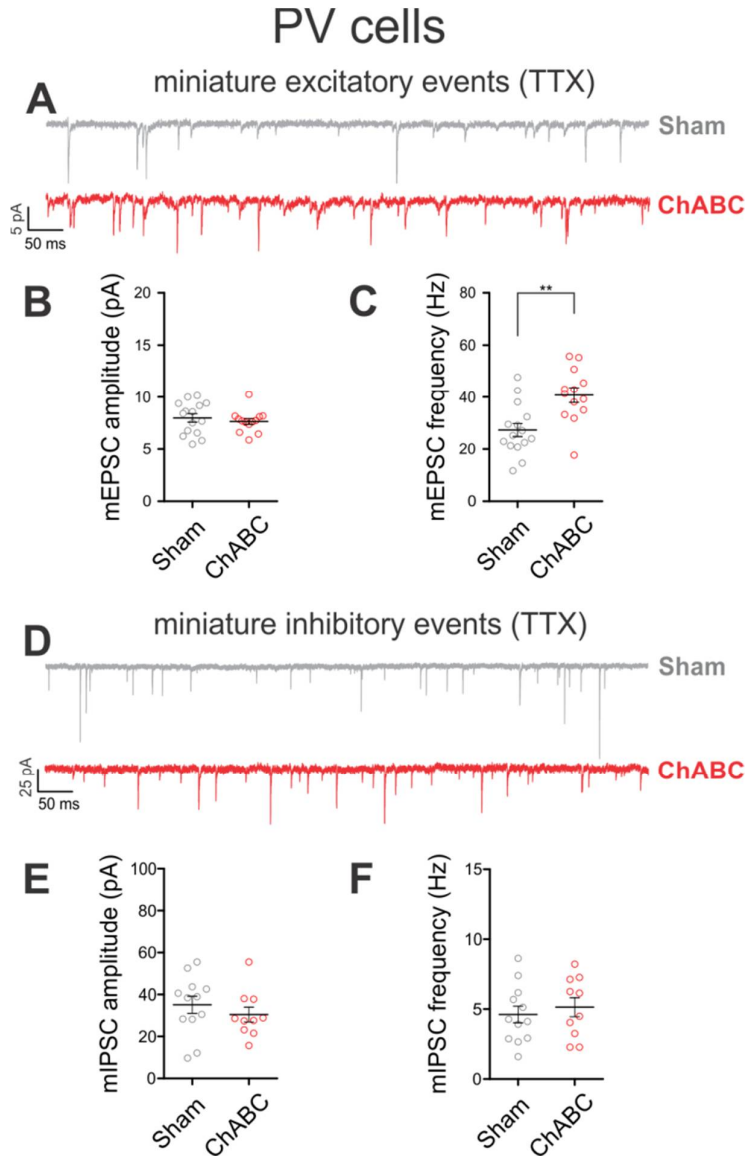


Figure 3.8. PNN removal affects quantal excitatory but not inhibitory synaptic transmission onto PV cells. (A) Example traces of mEPSCs recorded in the continuous presence of TTX in controls animals (sham – grey) and ChABC-treated mice (ChABC – red). **(B-C)** Average mEPSC amplitudes (B) and frequency (C). **(D-F)** Same as in A-C, but for mIPSCs, recorded with a high-chloride intracellular solution, in the presence of TTX and the glutamate receptor antagonist DNQX ** $p < 0.01$.

PV	n	N	mEPSC ampl. (pA)	mEPSC freq. (Hz)
Sham	12	5	7.981 ± 0.4	27.30 ± 2.5
ChABC	8	3	7.647 ± 0.3	40.76 ± 2.9
			mIPSC ampl. (pA)	mIPSC freq. (Hz)
Sham	12	5	35.13 ± 4.1	4.619 ± 0.6
ChABC	10	7	30.44 ± 3.6	5.140 ± 0.7

Table 8. Quantal neurotransmission onto PV after PNN removal. mEPSC: miniatures glutamatergic events recorded in TTX. mIPSC: miniature GABAergic events. Mean values are indicated with ± SEM. n=number of cells, N=number of mice.

3.6 Does monocular deprivation alter the E/I balance after PNN removal?

The morphological and physiological alterations following a sensory deprivation in young animals are well-documented. During the CP, MD leads to strengthening of PV to PN synapses in L4 (Maffei et al., 2006, 2010; Lefort et al., 2013; Nahmani and Turrigiano, 2014) (Lefort et al., 2013) as well as an increase of inhibition in L2/3 (Kannan et al., 2016). Previous works revealing the CP reopening in adult animals after PNN disruption were tested with the ocular dominance plasticity (ODP) paradigm *i.e* the shift in neuronal responses after MD. Therefore, here we wondered whether triggering plasticity in adult mice would enhance the effects on synaptic transmission described above, or perhaps unmask some other effects on intrinsic excitability. In order to answer to this question, during the same surgical sessions of ChABC or sham injections, we performed monocular sensory deprivation by lid suture. We then performed exactly the same experiments in the contralateral binocular portion of V1 (identical protocols and conditions of recordings), but in adult mice monocular deprived where PNN were (or not) disrupted: we monitored the intrinsic excitability, the passive properties, the AP waveform and both glutamatergic and GABAergic neurotransmission.

3.6.1 Firing dynamics, passive properties and AP shape are not altered

To test whether PNN removal associated to MD increased neuronal excitability, we examined firing dynamics of both PV cells and PNs. We found that firing properties were not affected by

MD and PNN removal (Fig. 3.9C,D; table 9; $p > 0.05$, Two-way repeated-measures ANOVAs). In addition, no changes in the passive properties of both cell types were observed between control, monocular deprived (Sham + MD) and ChABC-injected, monocular deprived mice (ChABC + MD) (Fig. 3.9E,F, table 10; $p > 0.05$, Unpaired t test). Accordingly, AP waveforms were not altered neither in PV INs or in PNs (Fig. 3.9G,H, table 11; $p > 0.05$, Unpaired t test).

Importantly, these experiments indicate that triggering plasticity *in vivo* by MD does not induce alterations of excitability and spiking dynamics of PV cells and PNs in L4 of V1.

PV	First current (pA)	PN	First current (pA)
Sham + MD	-75.40 ± 6.65	Sham + MD	-47.423 ± 6.24
ChABC + MD	-88.23 ± 7.99	ChABC + MD	-48.33 ± 6.04

Table 9. First step of injected current normalized in function of the Rm. Mean \pm SEM.

PV	n	N	Rm (M Ω)	Vrest (mV)
Sham + MD	10	5	144.7 ± 13	-63.67 ± 1.7
ChABC + MD	13	8	121.6 ± 13	-61.57 ± 1.4

PN	n	N	Rm (M Ω)	Vrest (mV)
Sham + MD	8	4	261.4 ± 33	-69.5 ± 1.9
ChABC + MD	9	6	253 ± 31	-70.89 ± 0.85

Table 10. Passive properties of PV and PN cells in control and ChABC-treated animals which have been monocular-deprived. Mean values \pm SEM. n=number of cells, N=number of mice, MD=monocular deprivation. The cells are the same as the ones for the firing dynamics.

PV	n	N	AP threshold (mV)	AP width (ms)	AP peak (mV)
Sham + MD	12	10	-51.92 ± 0.9	0.3913 ± 0.011	17.59 ± 1.76
ChABC + MD	10	9	-51.71 ± 0.9	0.3795 ± 0.014	18.58 ± 1.4

PN	n	N	AP threshold (mV)	AP width (ms)	AP peak (mV)
Sham + MD	12	10	-50.56 ± 1.3	1.114 ± 0.08	28.66 ± 3.1
ChABC + MD	10	9	-49.97 ± 1.3	1.033 ± 0.03	23.18 ± 2.3

Table 11. Action potential (AP) parameters of PV and PN cells during development and after PNN removal. Mean values \pm SEM. n=number of cells, N=number of mice.

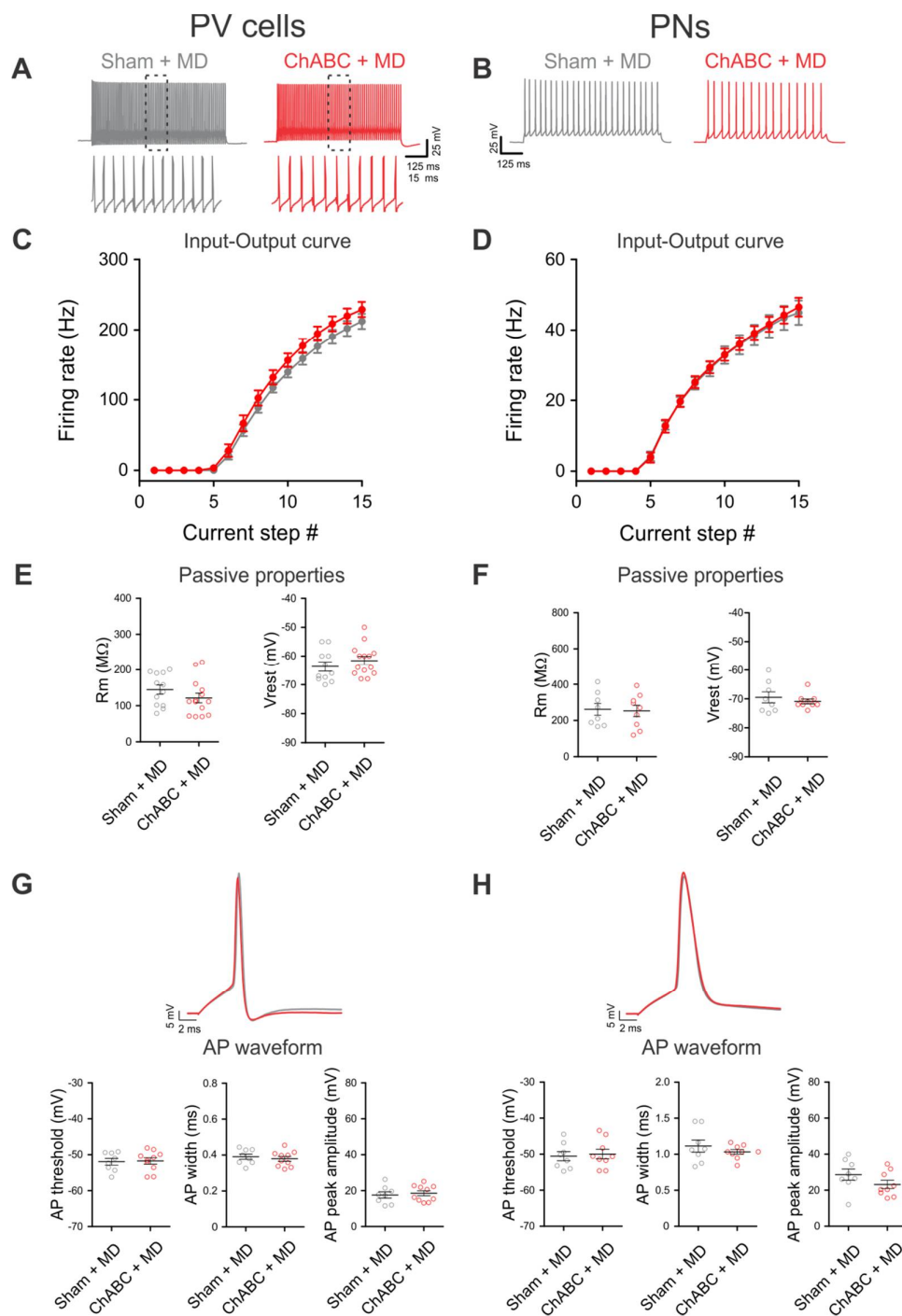


Figure 3.9. PNN removal in adult monocular-deprived mice does not alter the firing dynamics, the intrinsic properties neither the AP waveform. (A-B) Characteristic firing pattern of PV cells and PNs respectively, in response to depolarizing current injections, in control condition (sham/grey) and in ChABC-treated animals (ChABC/red); Inset in A shows the firing behavior of PV cells at a faster time scale. (C-D) Average f-i curves of PV cells and PNs respectively. (E-F) Passive properties of PV neurons (E) and PNs (F). (G-H) Single spike analysis (threshold, width and peak amplitude) of PV-positive neurons (G) and PNs (H). Top, example trace of a spike in control condition (grey) and after ChABC injection (red).

3.6.2 Effects of monocular deprivation on synaptic transmission onto PV cells and PNs following enzymatic PNN removal in adult mice

We have shown that *in vivo* PNN digestion in adult mice is accompanied by increased spontaneous synaptic transmission selectively onto PV cells, with different mechanisms at glutamatergic and GABAergic synapses. Does plasticity induced by MD alter these effects? Similarly to our previous results, we found that both glutamatergic and GABAergic spontaneous synaptic transmission are enhanced specifically onto PV cells in ChABC-treated mice in presence of MD (Fig. 3.10, table 12).

In particular, sEPSC frequency onto PV cells is higher in ChABC- than sham-treated animals (Fig. 3.10C, table 12; $p < 0.001$, Unpaired *t* test) whereas no changes are seen in sEPSC amplitude (Fig. 3.10B, table 12; $p > 0.5$, Unpaired *t* test). The specific effect on sEPSC frequency differs from what we observed without MD, where both sEPSC amplitude and frequency were enhanced (Fig. 3.6B,C). Similarly to what we observed in absence of MD, sEPSCs onto PNs were unaffected (Fig. 3.10H,I, table 12; $p > 0.5$, Unpaired *t* test).

Similarly, the analysis of spontaneous GABAergic transmission, showed that sIPSC frequency increased in monocular deprived animals, in which PNNs were removed (Fig. 3.10F, table 12; $p < 0.5$, Unpaired *t* test) with no changes in the amplitude (Fig. 3.10E, table 12; $p > 0.5$, Unpaired *t* test). This, once again, was slightly different from what we observed in mice that were not monocular deprived, in which both amplitude and frequency were altered (Fig. 3.7B,C). Again, GABAergic events onto PNs were not changed by ChABC treatment, even in the presence of MD (Fig. 3.10K,L, table 12; $p > 0.5$, amplitude: Unpaired *t* test, frequency: Mann Whitney test).

We then compared the changes induced by PNN removal in the presence and absence of monocular deprivation. We tested if induction of cortical plasticity induced a boost of synaptic transmission onto PV cells or PNs. For this purpose, we normalized each value in ChABC groups with respect to the mean value of their corresponding Sham treatment ($\Delta\text{ChABC}/\text{sham}$ and $(\Delta\text{ChABC}+\text{MD})/(\text{sham}+\text{MD})$). This allowed us comparing normalized ChABC values with ChABC + MD ones. We compared changes in sPSC (both glutamatergic and GABAergic) frequency, as this parameter was consistently altered by PNN digestion. No significant effects were observed between groups in the presence or absence of MD ($p > 0.05$; not shown).

Overall, we found that *in vivo* ChABC-mediated disruption of PNNs in the presence of MD increased both glutamatergic and GABAergic spontaneous synaptic transmission onto PV cells selectively. Although we found some differences in the specific effects on sPSC frequency and amplitude, the overall effect is similar in the presence and absence of MD. Remarkably, triggering plasticity *in vivo* by MD does not increase the effect on sPSC frequency induced by PNN removal. mPSCs in monocular deprived animals were recorded in too few neurons to be statistically relevant: this will be implemented in the near future, to confirm the differential synaptic and network effect of PNN removal on glutamatergic and GABAergic transmission, respectively.

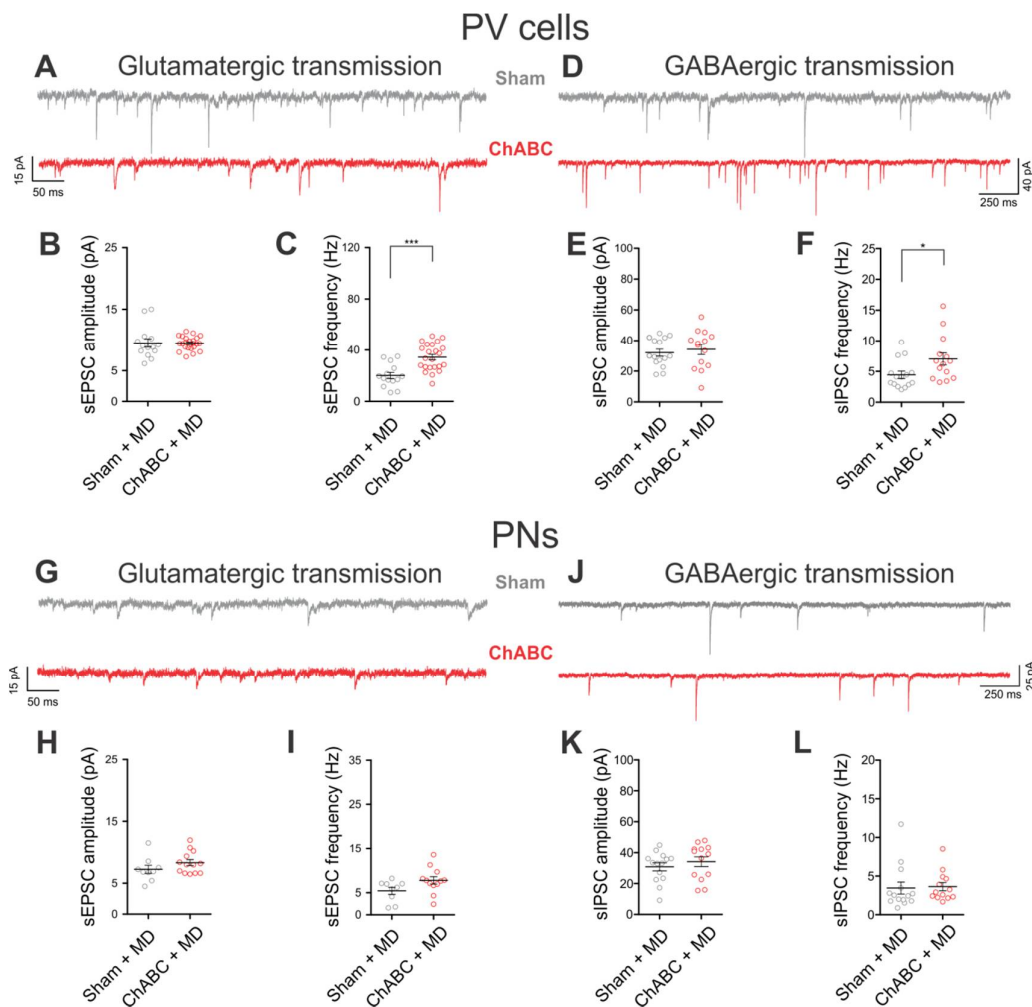


Figure 3.10. Effects of PNN removal in monocular-deprived adult animals on spontaneous transmission of PV and PNs. (A) Representative voltage-clamp traces of sEPSCs onto PV cells in control (sham, grey) and ChABC-treated (red) mice. (B-C) population sEPSC amplitude (B) and frequency (C) in PV cells. (D-F) same as in A-C, but for sIPSCs PV cells, pharmacologically isolated in the presence of DNOX. (G-L) Same as in A-F, but for sEPSCs and sIPSCs onto PNs. * $p < 0.05$, *** $p < 0.001$.

PV	n	N	sEPSC ampl. (pA)	sEPSC freq. (Hz)
Sham + MD	14	6	9.52 ± 0.7	20.15 ± 2.5
ChABC + MD	23	9	9.463 ± 0.2	34.47 ± 2.2
			sIPSC ampl. (pA)	sIPSC freq. (Hz)
Sham + MD	15	5	32.04 ± 2.6	4.444 ± 0.6
ChABC + MD	14	5	34.21 ± 3.4	7.033 ± 0.9

PN	n	N	sEPSC ampl. (pA)	sEPSC freq. (Hz)
Sham + MD	9	6	7.251 ± 0.67	5.43 ± 0.8
ChABC + MD	12	7	8.327 ± 0.50	7.798 ± 0.8
			sIPSC ampl. (pA)	sIPSC freq. (Hz)
Sham + MD	14	4	30.83 ± 2.6	3.455 ± 0.8
ChABC + MD	13	4	34.22 ± 3.2	3.648 ± 0.5

Table 12. sPSC onto PV and PN cells after PNN removal. Mean values ± SEM. n=number of cells, N=number of mice, MD=monocular deprivation.

3.7 PNN removal does not alter unitary GABAergic connections

We have shown that PNN removal in adult mice increases both excitatory and inhibitory spontaneous transmission specifically onto PV cells (Fig. 3.6 and Fig. 3.7). Interestingly, however, whereas glutamatergic transmission onto PV cells seems to be due to synaptic alterations, miniature inhibitory transmission was not altered by PNN removal (Fig. 3.8). Yet, analysis of s- and mPSCs does not provide information whether some specific circuit was specifically affected by PNN removal. We therefore focused on the effects of PNN removal in adult mice, as we wanted to investigate in more detail whether PNN disruption could lead to some circuit-specific effects. Previous studies indicated that sensory deprivation during the CP leads to strengthening of the PV-PN synapses (Maffei et al., 2006, 2010; Lefort et al., 2013; Nahmani and Turrigiano, 2014). Given the lack of effect of PNN removal on mIPSC amplitude and frequency, we hypothesized that unitary PV-PV and PV-PN connections are similar in the presence and absence of PNNs. To test this hypothesis, we performed simultaneous recordings between pairs of PV cells and between PV cells and PNs in L4 of V1 in sham- and ChABC-treated animals, in the presence and absence of MD. In addition, we measured autaptic connections in PV cells, as self-inhibition is a major feature of cortical PV neurons (Tamás et al., 1997; Bacci et al., 2003; Bacci and Huguenard, 2006; Manseau et al., 2010; Deleuze et al., 2014). Neurons were voltage-clamped at -80 mV to reduce stimulus-mediated distortions

typical of autaptic responses, and a train of 5 presynaptic spikes at 50 Hz was applied. We quantified the strength of unitary GABAergic synapses by, measuring the peak of the first unitary uIPSC in the train (averaged across at least 20 repetitions), converted to its corresponding conductance. Moreover, we quantified the short-term plasticity of GABAergic synapses from PV cells by calculating the ratio between the n^{th} and 1^{st} uIPSCs. This measure reflects use-dependent changes of presynaptic GABA release within the stimulus train. We found no significant changes between sham- and ChABC-treated animals in the amplitude of unitary PV-PV connections, both autaptic and synaptic (Fig. 3.11C, table 13; $p > 0.05$, Mann Whitney test). Similarly, short-term plasticity was unaffected by PNN removal (Fig. 3.11E, table 13; $p > 0.05$, Two-way repeated-measures ANOVAs). Importantly, MD did not affect the strength (Fig. 3.11D, table 13; $p > 0.05$, Mann Whitney test) and short-term plasticity (Fig. 3.11F, table 13; $p > 0.05$, Two-way repeated-measures ANOVAs) of uIPSCs between pairs of PV cells (both autaptic and synaptic). Likewise, unitary connections from PV cells to PNs were not affected by PNN removal both in the absence (Fig. 3.11I, table 13; $p > 0.05$, Mann Whitney test) and presence of MD (Fig. 3.11J, table 13; $p > 0.05$, Unpaired t test). Also short-term plasticity was not affected in non-deprived (Fig. 3.11K, table 13; $p > 0.05$, Two-way repeated-measures ANOVAs), as well as in sensory-deprived animals (Fig. 3.11L, table 13; $p > 0.05$, Two-way repeated-measures ANOVAs).

These experiments indicate that GABAergic synapses from PV cells to relevant targets of the L4 microcircuit (themselves and PNs) are unaffected by PNN removal in the presence and absence of monocular deprivation. Our results imply that reopening of cortical plasticity by PNN removal does not rely on synaptic alterations of GABAergic connections from PV cells.

PV-PV syn + aut	n	N	Conductance (nS)
Sham	33	12	5.146 ± 0.82
ChABC	26	16	5.550 ± 0.88
Sham + MD	11	4	3.268 ± 0.52
ChABC + MD	8	5	6.103 ± 1.61

PV-PN	n	N	Conductance (nS)
Sham	10	6	2.527 ± 0.73
ChABC	13	7	3.374 ± 0.97
Sham + MD	8	3	3.945 ± 1.3
ChABC + MD	9	5	5.672 ± 1.4

Table 13. Summary of unitary GABAergic connections from PV cells. Mean values ± SEM. n=number of cells, N=number of mice, MD=monocular deprivation.

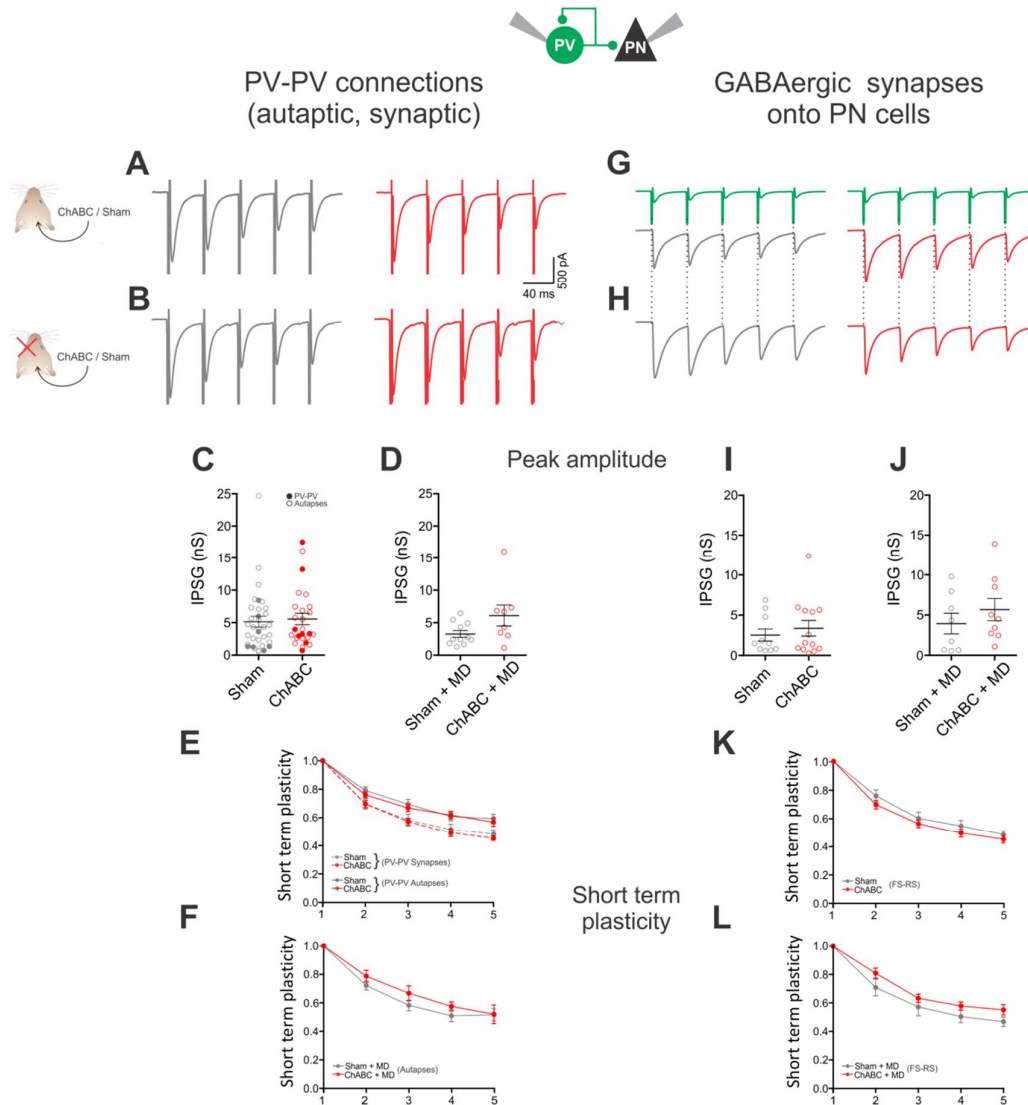


Figure 3.11. Effect of PNN removal on unitary GABAergic PV-PV and PV-PN inhibitory connections. (A-B) Example traces (average of 50 sweeps) of autaptic connections in non-deprived animals (A) and following MD (B) in control (sham, grey) and ChABC-injected (red) mice. (C-D) Peak amplitude conductance of unitary PV-PV synaptic (filled circles) and autaptic (open circles) connections in control (grey) and in ChABC-treated (red) mice in the absence (C) and presence (D) of MD. The analysis was done on the first response in the train (E-F) Same as in (C-D) but for short-term plasticity. Train frequency was 50 Hz. Autaptic responses: filled lines; synaptic responses: dotted lines. (G-L) Same as in A-F, but for PV-PN synapses.

3.8 *In vivo* expression of the light-sensitive channel ChR2 in the dLGN. Double injections

We then wanted to examine whether *in vivo* PNN disruption in adult V1 affected glutamatergic synapses originating from local (intra-cortical) or long-range (thalamo-cortical) excitatory afferents. Indeed, our results on s- and mEPSCs (Fig. 3.6 and fig. 3.8) suggest that PNN removal affects glutamatergic synapses onto PV cells selectively. In our hands, the probability of obtaining connected paired between PNs and PV cells was very low (4.8%; 5 connected out of 104 tested pairs in total). This could be due to a technical reason, *i.e.* mice were old (more than 3 months) and perhaps glutamatergic connections in acute brain slices were degraded more easily than inhibitory connections (probability of connected PV-PN pairs: 44.11%; n = 102; probability of autaptic connections: 67.3%; n = 104). Another possible explanation could be that at this developmental stage, L4 PNs project quasi-exclusively to L2/3 and intralaminar connections are very rare. This possibility was not tested. We therefore focused our attention on the thalamocortical pathway, which is a major glutamatergic input onto both L4 PV cells and PNs.

In order to assess if the effects of PNN removal on glutamatergic synapses can be explained by an alteration of the thalamocortical pathway, we expressed the light-sensitive opsin channelrhodopsin 2 (ChR2) in the visual thalamus of adult mice (Boyden et al., 2005). Stereotaxic injections of adeno-associated viral particles expressing ChR2 in selectively glutamatergic neurons (AAV-CamkII-ChR2-mCherry) were performed in the dLGN 10 to 15 days prior to the electrophysiological recordings. Mice were then subject to a second stereotaxic injection of ChABC (or PBS) 48-72h before the recordings in order to remove (or not) PNNs. In some cases, MD was performed at the time of injection of ChABC or PBS. Figure 3.12 illustrates the double surgery protocols. In an example slice, ChR2 (mCherry, in red) was expressed by dLGN glutamatergic neurons, projecting mCherry-positive fibers to L4 of V1 (Fig. 3.12A). In the same animals, PNNs were removed in V1 as illustrated in figure 3.12B (absence of WFA staining in the injected region). The pattern of fiber innervation (L4 and L6) and the absence of ChR2⁺ somata in the neocortex was a clear indication of the specific thalamic expression of the opsin.

By using this optogenetic approach, we could thus investigate if thalamocortical synapses were affected by PNN removal in adult animals, in the presence and absence of MD. By optically

stimulating TC fibers ChR2⁺ in V1, we first assessed the direct, monosynaptic, excitatory recruitment of PV cells and PNs in L4 and then examined the disynaptic feed-forward inhibitory (FFI) circuit onto both neuronal type (Cruikshank et al., 2010; Kloc and Maffei, 2014).

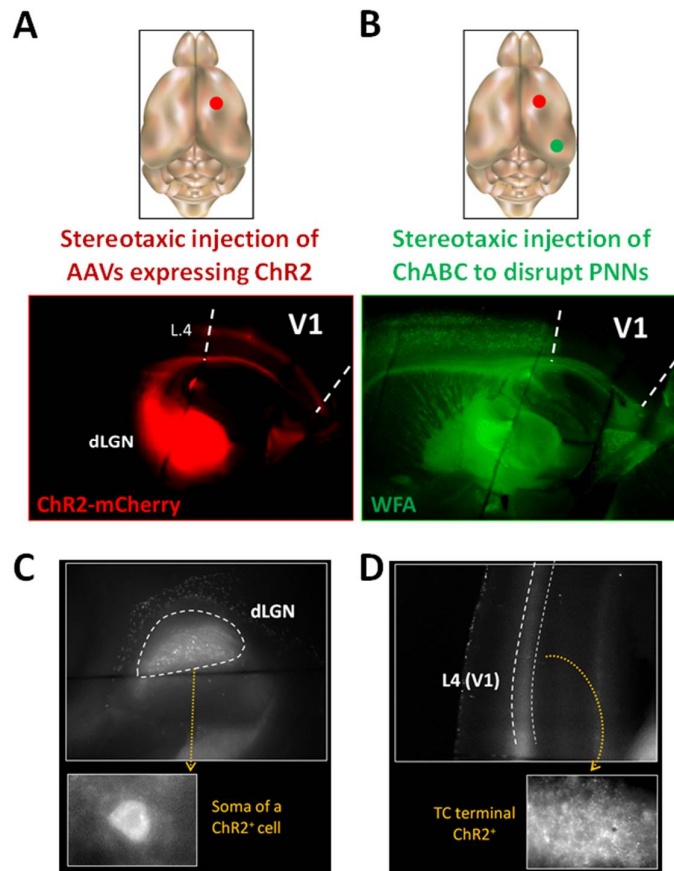


Figure 3.12. Dual surgery to infer the strength of thalamo-cortical connections impinging L4 neurons. (A) Representative micrograph illustrating a parasagittal brain slice obtained from an adult mouse, which was subject to stereotaxic injection of ChR2- and mCherry-carrying AAVs in dLGN. Note the extensive innervation of cortical layers 4 and 6. Top: scheme of the AAV injection (B) The same mouse was injected after 10 days with ChABC in V1. Note the complete depletion of PNNs, as revealed with WFA staining (green). Top: scheme of ChABC injection, 48-72 hours prior to recordings (C-D) Detail of mCherry-positive cell bodies in dLGN (C) and axonal fibers in V1, L4 (D).

In order to infer synaptic measures in the presence of unavoidable non-homogeneities of ChR2⁺ expression between different animals and slices, for each experiment and each cell, we performed photo-stimulation at a light intensity inducing threshold responses with ~50%

reliability. For details on the determination of light power intensities used, see section 2.6 (materials and methods). Importantly we observed that, within the range of light powers that were used, failure rates were not correlated with the absolute light intensity or with the magnitude of the postsynaptic currents. Importantly, threshold light intensity, failure rate and the response latency were not statistically different across groups (data not shown).

3.9 PNN disruption increases thalamocortical glutamatergic synapses specifically onto PV cells

Optogenetic activation of TC fibers can generate uncontrolled multi-synaptic responses onto recorded PV cells and PNs. In order to assess the direct thalamic activation onto PV and PN neurons in L4 we used 1 μM of the Na^+ channel blocker TTX, to remove polysynaptic excitation and 100 μM of the K^+ channel antagonist 4-AP to enhance axonal depolarization (Fig. 3.13) (Petreanu et al., 2009; Mao et al., 2011). By applying TTX, the recruitment of ChR2-negative fibers is eliminated because polysynaptic transmission relies on AP propagation. Light-evoked monosynaptic responses, however, can be triggered directly by ChR2 excitation, if enough ChR2 is expressed in or near the pre-synapse to cause sufficient depolarization. 4-AP, which blocks K^+ channels, increases the depolarization and lowers the threshold of excitation of the axons expressing ChR2. In this configuration, we were sure to optically activate monosynaptic responses to selective activation of thalamocortical, ChR2^+ fibers (Fig. 3.14).

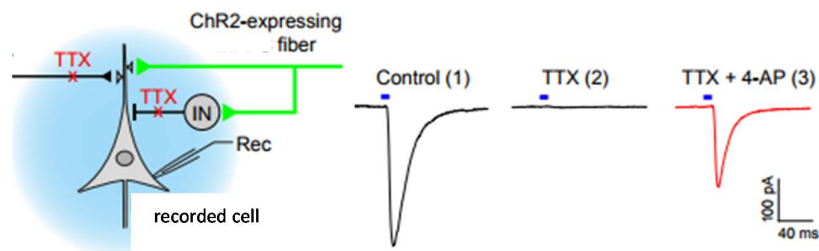


Fig 3.13. Monosynaptic EPSCs in the presence of TTX and 4-AP. Left: experimental design. EPSCs were evoked by photostimulation of ChR2^+ axons (blue lines), and recorded in a principal neuron in voltage-clamp mode. Right: Rescue of optogenetically-induced and TTX-blocked EPSCs by 4-AP (1) TTX completely blocked EPSCs (2). Subsequent application of 4-AP in the presence of TTX partially rescued EPSC (3), indicating monosynaptic nature of connections. Modified from (Cho et al., 2013).

In order to record glutamatergic post-synaptic events, L4 cortical neurons were voltage-clamped at -70 mV, in the presence of TTX and 4AP as well as 10 μ M gabazine to block GABA_A receptors and blue light was shined on L4 of V1 at threshold intensity (0.11 mW to 0.38 mW) for 1ms. This stimulation configuration induced monosynaptic TC release, which was desynchronized and multi-vesicular in nature, making the measure of peak-amplitude responses meaningless. Thus, TC synaptic transmission was quantified as the corresponding charge transfer, measured as the integral of the glutamatergic response over several hundreds of milliseconds following the light stimulus. Interestingly, we found that optically induced EPSCs recorded in PV cells from ChABC-treated animals were significantly larger than in control, sham-injected animals (Fig. 3.14B, table 14; $p < 0.05$, Mann Whitney test). This was also evident in mice that were monocular-deprived (Fig. 3.14F, table 14; $p < 0.01$, Unpaired *t* test). Notably, the effect of PNN removal on direct thalamocortical glutamatergic synapses onto cortical neurons is specific for PV cells, as non-significant changes of light-evoked EPSCs were measured on PNs, in all conditions (Fig. 3.14D,H, table 14; $p > 0.05$, Mann Whitney test).

Taken together, these results indicate that PNN disruption in adult animals increases the specific recruitment of PV cells by thalamocortical fibers.

PV	n	N	Area (pA*ms)
Sham	18	8	156 \pm 22.66
ChABC	16	6	358.9 \pm 85.47
Sham + MD	8	3	91.24 \pm 15.90
ChABC + MD	8	3	169.7 \pm 14.77

PN	n	N	Area (pA*ms)
Sham	8	4	146.1 \pm 19.01
ChABC	8	3	162.7 \pm 22.43
Sham + MD	8	4	95.85 \pm 9.354
ChABC + MD	7	3	131.1 \pm 27.40

Table 14. Thalamocortical glutamatergic responses on PV and PN cells in control conditions and after PNN removal and monocular deprivation. Mean values \pm SEM. n=number of cells, N=number of mice, MD=monocular deprivation. Responses are measured at threshold.

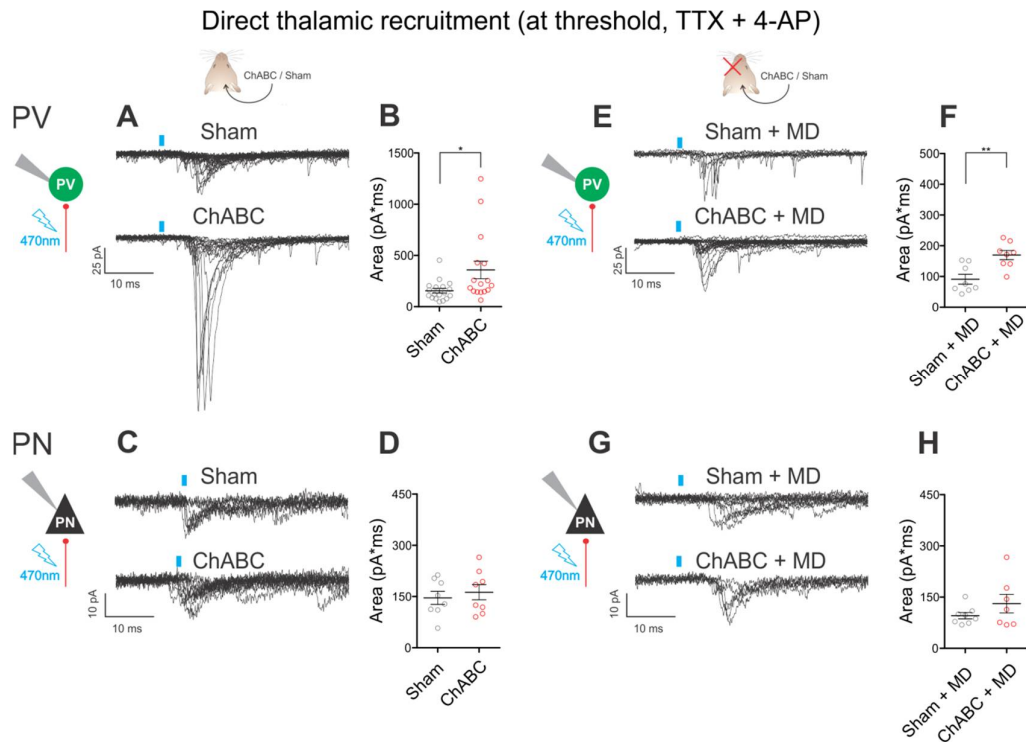


Figure 3.14. Direct thalamic recruitment is enhanced specifically onto PV cells after PNN removal. (A) Representative traces of optically evoked monosynaptic EPSCs recorded onto a PV cell from a control (sham, top) and ChABC-injected (bottom) non-deprived animals. Note the presence of failures in both cases. Recordings were done in the presence of TTX and 4-AP at threshold stimulation (B) Population data of light-evoked EPSCs (excluding failures) in control (sham, grey) and ChABC-treated (red) animals. (C-D) Same as in A-B, but for PNs. (E-H) Same as in A-D, but in sensory-deprived animals. Vertical blue bars correspond to photostimulations. *: $p < 0.05$; **: $p < 0.01$.

3.10 PNN disruption increases thalamocortical feed-forward inhibition onto PV cells

The results outlined above indicate that the recruitment of PV cells by the visual thalamus is enhanced after degradation of PNNs. PV cells are known to be strongly recruited by TC fibers and to provide a powerful disynaptic feed-forward inhibition onto PNs (Gabernet et al., 2005; Sun, 2006). In addition, we have shown that PV cells in L4 are powerfully inter-connected. Therefore, increased recruitment of PV cells in the absence of PNNs should generate enhanced FFI onto both PV cells and PNs. This would provide a compelling explanation of the decreased

slope of the transfer function that we measured *in vivo* (Fig. 3.2). We therefore set out to measure FFI onto PV cells and PNs directly. To do this, we performed experiments with a cesium-based intracellular solution ($E_{Cl} = -63\text{mV}$), and we isolated GABA-mediated inhibitory responses by holding neurons in voltage-clamp at the reversal potential for glutamate-mediated responses (nominally 0 mV, but in reality between +10 and +20 mV, taking into account the liquid junction potential). In these experiments, extracellular aCSF did not include TTX and 4-AP, as we aimed to induce disynaptic inhibitory responses. FFI was stimulated by short (0.3 ms) blue light flashes, and membrane potential was carefully adjusted until the inward glutamatergic response disappeared. Threshold photostimulation power ranged from 0.11 mW to 0.55 mW. In some experiments, we confirmed the disynaptic nature of these GABAergic responses, as they were completely blocked by application antagonists of either GABA_ARs (gabazine) or glutamate (DNQX) receptors (not shown). Threshold responses occurred within a relatively narrow latency (6.15 ± 0.17 ms and 6.04 ± 0.11 ms for PV cells and PNs, respectively), and did not show complex multi-peak waveforms, allowing us to measure the peak current. We found that FFI onto PV cells was strongly enhanced after degradation of PNNs in the absence (Fig. 3.15B,D, table 15; $p < 0.01$, Unpaired *t* test) and presence (Fig. 3.15C,E, table 15; $p < 0.05$, Unpaired *t* test) of monocular deprivation. Regarding PNs, we did not observe a statistically different FFI responses between sham- and ChABC-treated mice both in the absence (Fig. 3.15G,I, table 15; $p > 0.05$, Mann Whitney test) and presence of MD (Fig. 3.15H,J, table 15; $p > 0.05$, Mann Whitney test). This result is somewhat surprising because the increased recruitment of PV cells induced by PNN removal was predictive of a larger FFI also onto PNs.

PV	n	N	Amplitude (pA)
Sham	10	7	208.4 ± 40.7
ChABC	9	7	1095 ± 209
Sham + MD	10	4	257.5 ± 41.2
ChABC + MD	10	5	557.1 ± 121

PN	n	N	Amplitude (pA)
Sham	10	7	148.1 ± 24.03
ChABC	10	5	210.6 ± 45.2
Sham + MD	13	4	203 ± 29.9
ChABC + MD	11	4	390 ± 87.9

Table 15. Thalamocortical feed-forward inhibition on PV and PN cells after PNN removal and monocular deprivation. Mean values \pm SEM. n=number of cells, N=number of mice, MD=monocular deprivation. Responses are measured at threshold stimulation.

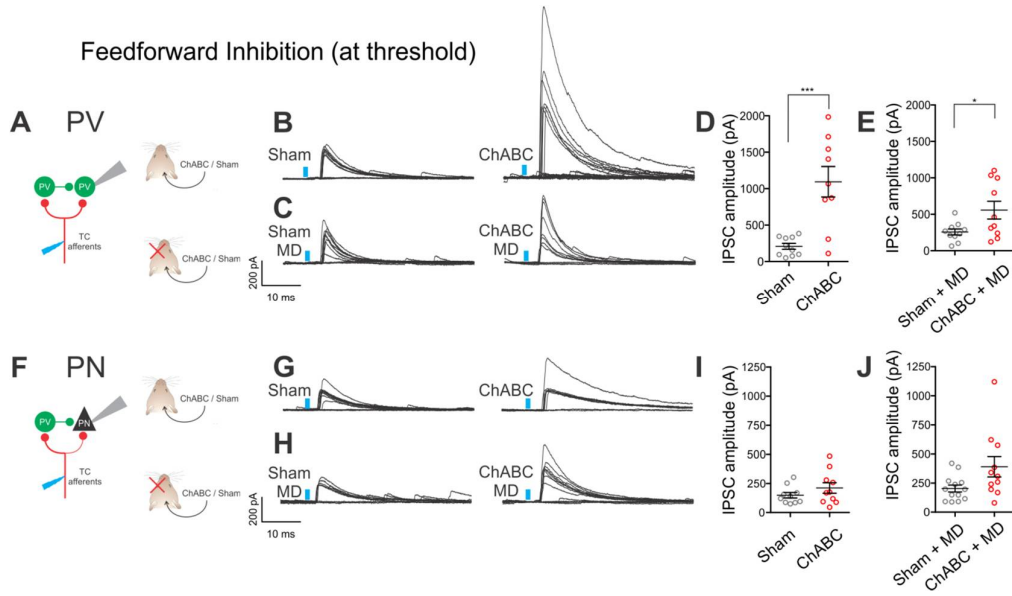


Figure 3.15. Feedforward (disynaptic) inhibition onto PV cells and PNs, following PNN disruption and effect of a sensory deprivation. (A) Scheme of FFI in PV cells induced by light stimulation of TC fibers. **(B)** Example voltage-clamp traces of FFI recorded in PV cells at threshold (note the presence of failures) in control (sham, left) and ChABC-treated (right) non-deprived animals. **(C)** Same as in B but in a monocular-deprived mouse. **(D-E)** Population data of IPSC amplitudes in control (sham, grey) and ChABC-treated (red), in the absence (D) and presence (E) of MD. **(F-J)** Same as in A-E, but for PNs. Neurons were voltage-clamped at the reversal potential for the glutamate-mediated responses, in regular ACSF in order to isolate disynaptic inhibition. Vertical blue bars represents times of photo-stimulations. *: $p < 0.05$; ***: $p < 0.001$.

In conclusion, our optogenetic dissection of the TC pathway revealed that PNN removal increases the recruitment of PV cells by TC fibers leading to a robust increase of FFI onto PV. Although not significantly different, FFI on PNs had a tendency to be larger, especially in monocularly deprived animals ($p = 0.07$). The lack of a clear effect could be due to the fact that we measured FFI on PNs at threshold. Additional experiments will be required to completely rule out a PNN-dependent effect on FFI onto PNs.

Chapter IV: DISCUSSION

In this study, we aimed to understand what are the cellular and synaptic mechanisms underlying the re-opening of cortical plasticity following the degradation of PNNs in the visual cortex of adult mice (Pizzorusso, 2002). Importantly, PNN degradation was shown to be instrumental for making the brain more plastic not only in the visual cortex, but also in other areas of the CNS (Bradbury et al., 2002; Gogolla et al., 2009). Here we focused on the visual cortical area V1, as it has been extensively studied as an established model of experience-dependent plasticity (Levelt and Hübener, 2012). We found that enzymatic disruption of PNNs induced a significant alteration of the visual gain adaptation curve and increased the power of visually evoked γ -activity. This result is consistent with increased activity of inhibitory neurons, and we set out to unravel the cellular and molecular underpinnings of this phenomenon. We therefore studied how PNN enzymatic disruption affects the cellular physiological properties of two major cell types of cortical L4: PV basket cells and excitatory PNs, which are involved in the encoding of sensory information and are subject to plastic changes during the CP (Hensch, 2005b). We analyzed the intrinsic excitability and synaptic properties of PV cells and PNs during a broad range of developmental stages, and following disruption of PNNs in adults. We found that during the transition from a pre-CP stage to a post-CP, both cell types accelerate their firing patterns and AP waveform. In parallel, synaptic transmission (both excitatory and inhibitory) is stable in PNs, but the strength of glutamatergic, but not GABAergic, neurotransmission is decreased selectively onto PV cells during and after the CP. Importantly, PNN degradation does not affect neuronal excitability of both cell types, but increases synaptic transmission onto PV cells selectively. This effect was due to a direct synaptic change at glutamatergic connections, including TC afferents, which induced an indirect, increase of AP-dependent inhibition onto PV cells. Monocular deprivation of adult mice, a protocol known to re-open plasticity in PNN-treated mice (Pizzorusso, 2002), did not produce a further effect. The selective effect of PNN removal on PV cells is consistent with the specific enrichment of this component of the extracellular matrix around this cortical cell types.

Interestingly, we found that PNN disruption affects the input-output relationship in response to increased contrast *in vivo*. The change of the slope of this transformation curve is a measure of gain modulation of visual responses (Mitchell and Silver, 2003; Shu et al., 2003; Carvalho and Buonmano, 2009) and is strongly affected by inhibition. Importantly, a divisive change in the gain is believed to be dependent on synaptic inhibition onto PNs (Pouille et al., 2009; Isaacson and Scanziani, 2011b). Indeed, increased inhibition makes it harder for excitatory PNs to fire in response to increased contrast, thereby significantly decreasing the slope of the

transformation curve. Therefore, PNN degradation in the adult mouse is consistent with increased activity of inhibitory neurons. Given the role of PV cells in modulating cortical gain (Atallah et al., 2012), and the specific enrichment of PNNs around this interneuron subtype, it is highly likely that the divisive shift of the input-output curve by PNN degradation is due to alterations of PV-cell function.

Moreover, we found that the power of rhythmic oscillations was robustly increased in the γ -frequency range, only during visually evoked activity, without any alteration of rhythmic activity during the resting state. This result indicates the crucial involvement of TC activation of cortical circuits. In particular, perisomatic targeting PV basket cells are known to play a crucial role in orchestrating neuronal activity during γ -oscillations (Klausberger and Somogyi, 2008; Cardin et al., 2009; Sohal et al., 2009). Enhanced γ -power by PNN disruption is consistent with increased activity of interconnected PV interneurons (Buzsáki and Wang, 2012).

Our *in vivo* results indicate that PNN removal increased inhibitory activity of GABAergic interneurons. At the cellular and circuit level this could be due to one or a combination of the following factors: *i*) increased INs excitability and firing properties *ii*) alterations of the excitation-to-inhibition ratio onto PNs, yielding a potentiation of GABAergic neurotransmission from perisomatic targeting PV cells *iii*) increased recruitment of PV cells, specifically by TC afferents. These changes should reflect the developmental maturation steps of intrinsic excitability and synaptic connectivity, occurring during the opening and the closure of the CP.

During development, both cell types increase their excitability by reducing spike threshold, fastening AP kinetics and increasing firing rate in response to a sustained depolarization. Interestingly, however, PV cells and PNs followed distinct developmental profiles: PNs became more excitable earlier than PV cells, which increase their excitability in parallel with accumulation of PNNs. Both developmental profiles likely relied on the maturation of ion channels sustaining AP firing, as passive properties were unchanged in both cell types. Overall, it appears that the maturation of PV-cell excitability is more gradual and maintains a juvenile phenotype at a stage when PNs have already reached an adult firing profile. Future experiments will be important to elucidate the functional relevance of this independent developmental profile for the CP of cortical plasticity.

Remarkably, intrinsic passive and firing properties (AP waveform and dynamics) in both cell types were not altered by PNN disruption in adult V1. This is at odds with previous reports

indicating effects of PNNs degradation following ChABC treatment on neuronal excitability. These studies reported either increased (Dityatev et al., 2007) or decreased (Balmer, 2016) neuronal excitability of cultured hippocampal neurons and cortical PV cells, respectively, following PNN degradation. However, these studies analyzed neuronal excitability in response to brief (1-2 hours) acute PNN degradation *in vitro*. This could lead to acute membrane and ion-channel alterations that could reflect altered excitability. Here, we have used an *in vivo* degradation paradigm (lasting 48-72h) that triggers the re-opening of cortical plasticity (Pizzorusso, 2002), structural alterations of dendritic spines (de Vivo et al., 2013) and produced significant alteration of gain modulation and γ -activity *in vivo* (Fig. 3.2). Importantly, in our hands, even inducing plasticity *in vivo* by monocular deprivation did not unmask any alteration of intrinsic excitability. We therefore conclude that PNN disruption opens plasticity via a synaptic or circuit mechanism.

We found that, globally, synaptic transmission onto PNs is unchanged during development. Yet, sEPSCs onto PV cells decrease during the CP, whereas inhibition remains unchanged. This suggests that the E/I ratio in these interneurons changes during development, with a net shift of the E/I balance in favor of GABAergic inhibition onto PV cells. This is consistent with the notion, according to which inhibition is required to open the CP, and boosting inhibition anticipates the opening of the CP (Hensch et al., 1998). Our results indicate that this imbalance of the E/I ratio is specific for PV cells. Therefore, the recruitment of these cells appears to play a fundamental role during the expression of structural plasticity.

Interestingly, when PNNs were removed by ChABC injection in adult mice, we detected a noticeable increase of synaptic transmission, specifically on PV cells. Yet, the mechanisms underlying the increase of glutamatergic and GABAergic transmission are not the same: indeed, mPSC analysis revealed that PNN removal affected glutamatergic synapses directly, as mEPSC frequency (but not amplitude) increased. In contrast, increased GABAergic transmission was abolished in TTX. This suggests that the increase of sIPSCs was due to increased firing of presynaptic interneurons embedded in the local network. PNN removal enhanced sPSC frequency also in deprived animals, again on PV cells only. Future experiments using mPSC analysis will be required to test whether MD affects quantal synaptic transmission.

sIPSCs in somatic recordings of PNs and PV cells mostly originate from perisomatic targeting PV basket cells. We confirmed the lack of inhibitory synaptic alterations at PV-cell synapses in our

paired recordings, in which uIPSCs from PV cells onto both other PV cells and PNs were completely unaffected by PNN removal in the presence and absence of monocular deprivation. The lack of effect of GABAergic synaptic transmission from PV cells indicates that PNN accumulation does not affect GABAergic connections from this cell types and suggests a specific effect on glutamatergic synapses impinging PV cells. In fact, the enhanced recruitment of PV cells, induced by PNN disruption, might explain the divisive effect on the input-output transformation curve that we recorded *in vivo*.

Both interneurons and principal excitatory neurons of cortical L4 are densely innervated by glutamatergic, originating from both local sources and long-range connections (Beierlein et al., 2003; Gabernet et al., 2005; Sun, 2006). We were unable to measure local intracortical glutamatergic synapses from PNs to PV cells. Indeed, we found such a low connectivity yield that it made it impossible to have a statistical meaningful pool. As mentioned above, this could be due to degradation of glutamatergic synapses in our acute slice preparation from old (>P70) animals, or to a physiological preferential targeting of superficial L2/3 neurons by L4 PNs, at this developmental stage. Future experiments using optogenetic approaches will reveal if L4 PNs show intralaminar circuit specificity in adult V1. Importantly, however, a prominent glutamatergic input onto L4 neurons is provided by afferents originating from the dLGN. In addition, the effects on the gain modulation and γ -oscillations that we found *in vivo* require sensory input involving the visual thalamus. Our optogenetic experiments indicate that, indeed, thalamic recruitment of PV cells is selectively enhanced by PNN removal. Also in this case, MD did not boost this effect. We analyzed threshold responses to reduce the risk of misinterpreting our results due to variable expression of ChR2 in different mice. It is important to note that the light intensity to evoke threshold responses was overall similar across different animal groups in different conditions ($p > 0.05$; not shown).

Importantly, we cannot infer whether enhanced TC recruitment of PV cells was due to alterations at pre- or postsynaptic sites. Indeed, to isolate monosynaptic inputs and to prevent unwanted network activation, we performed our experiments in TTX and 4AP, which precluded the analysis of presynaptic parameters. Future experiments using careful thalamocortical minimal electrical stimulations in TC slices will be required to determine if PNN-induced alterations affect more the pre- or postsynaptic compartment.

PV cells in L4 are potentially activated by TC fibers and they are known to produce a strong FFI onto PNs (Sun, 2006; Bagnall et al., 2011). In addition, since PV cells are highly interconnected, TC activation induces disynaptic feed-forward inhibition onto other PV cells of L4. Increased recruitment of PV cells induced by PNN removal had a strong effect on FFI onto PV cells but a smaller, not significant increase of FFI onto PNs. The overall lack of effect of FFI potentiation onto PNs could be because we measured responses at threshold. We have shown that quantal GABAergic transmission was unaffected by PNN removal, therefore the effect on FFI onto PNs will depend on the number of inhibitory interneurons connected to PNs. It is very likely that, had we been able to increase the stimulation to recruit more interneurons, we would have revealed the effect of PNN removal on FFI onto PNs. However, FFI is disynaptic in nature and must be elicited in the absence of TTX and 4-AP. Threshold responses had relatively constant latencies, and IPSC waveforms did not contain multiple peaks. When we stimulated at higher light intensities, we could not prevent multi-synaptic events reflecting unwanted network activation. In these conditions, it was very difficult to estimate the source of inhibitory responses. Alternatively, a powerful FFI in interneurons could prevent the recruitment of multiple inhibitory cells impinging PNs, even during threshold stimulations.

The strong enhancement of FFI on PV cells induced by PNN removal suggests that PV interneurons are potentially interconnected, and alterations of their recruitment will produce a disinhibition of L4, at least at threshold. Accordingly, we found that PV cells form synapses with other PV cells (including themselves) that were significantly stronger than those formed onto PNs. Moreover, PNN disruption induced an increase of sIPSCs only on PV cells (Fig. 3.7). This effect was abolished by TTX, suggesting once again, that the increased recruitment of PV cells can induce spiking activity affecting their synaptic output more on PV cells than glutamatergic PNs.

Importantly, MD did not boost significantly the overall effect of PNN removal in all tested conditions ($p > 0.05$; not shown). This suggests that the enzymatic digestion of the extracellular matrix by ChABC has attained a maximum effect on glutamatergic neurotransmission on PV cells. It will be interesting to test whether reduction of PNN expression by genetic or other means (Carulli et al., 2010; Beurdeley et al., 2012; Favuzzi et al., 2017) might produce more subtle effects that can be modulated by plasticity paradigms. Alternatively, perhaps longer periods of deprivation following PNN disruption by ChABC might also increase the potentiation of PV cell recruitment.

Could selective modulation of glutamatergic synapses onto PV cells be responsible for cortical plasticity during the CP? Plasticity during CP depends on activity of GABAergic interneurons (Hensch, 2005b) and indeed, the level of inhibition increases during the CP (Morales et al., 2002; Huang et al., 2007). Interestingly, GABAergic synapses between PV cells and PNs were shown to increase their strength following MD during the CP (Maffei et al., 2006, 2010; Lefort et al., 2013; Nahmani and Turrigiano, 2014), and disinhibition of PNs was proposed to initiate CP plasticity in L2/3 (Kuhlman et al., 2013). Our results favor the hypothesis of increased inhibition and disinhibition as a secondary effect induced by increased recruitment of PV cells (Fig. 3.16). Moreover, increased glutamatergic synaptic activity onto PV cells recapitulates a more juvenile stage. Yet, it is important to note that the mechanisms underlying cortical plasticity induced by PNN degradation in adult mice differ in some aspects from those triggering the natural onset of the CP during development, due to differences in the overall time course of CP plasticity and the level of maturation of cortical circuits.

In conclusion, we believe that our experiments identified an important, specific mechanism (Fig. 3.16), which might underlie the effects on the gain of the transfer function and on γ -oscillations. Importantly, the specific enhancement of PV-cell recruitment might underlie the re-opening of cortical plasticity, induced by PNN degradation in adult animals. Understanding the mechanisms by which it is possible to re-open cortical plasticity in adult individuals gives us important clues on the physiological function of cortical networks during sensory and cognitive processing. Moreover, our results bear important implications for several psychiatric diseases, such as schizophrenia, in which dysfunctional accumulation of PNNs around cortical PV cells have been hypothesized to be among the pathophysiological mechanisms of this devastating disease (Pantazopoulos and Berretta, 2016).

Figure 3.16 summarizes our interpretation of the cellular and circuit effects, induced by enzymatic digestion of PNNs by ChABC in adult V1.

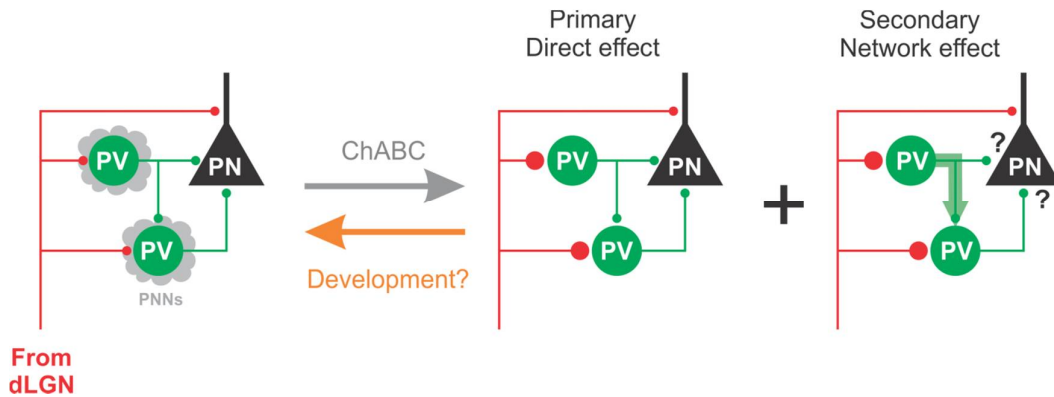


Figure 3.16. Schematic model of the effects induced by PNN removal in L4 of adult V1. In normal adult mice, PV neurons are enwrapped by PNNs (grey). Both PV and PN are contacted by thalamic fibers (red) and form local connections in L4 (green). ChABC injection (grey arrow) disrupts PNNs and induces a specific increase of the recruitment of PV cells by dLGN afferents, schematized by larger red synapses. This primary direct effect leads to a secondary network effect, namely an increase of feed-forward inhibition onto PV cells (and possibly onto PNs also), as represented by the green arrow. Our results on spontaneous transmission suggest that the result of PNN degradation might re-capitulate younger stages (orange arrow).

Future Directions

Our results open a series of questions that will require extensive future investigations. Below I am listing the ones I believe are the most prominent:

1. Is thalamocortical recruitment of PV cells specifically enhanced during the onset of the CP? Could the potentiation of this specific sensory pathway be responsible for the onset of the CP?
2. What is the role of intracortical glutamatergic synapses onto PV cells? Are they also potentiated during the CP and/or PNN removal in the adult?
3. Are there other interneuron subtypes involved in the onset of the CP and in the re-opening of the plasticity induced by PNN degradation in adult mice?
4. Do genetic manipulation reducing the expression of PNNs in adult mice and reopening cortical plasticity rely on a similar mechanism?

5. What are the actual mechanisms underlying the closure of the CP induced by PNNs? Could diminished expression of specific glutamate receptors in PV cells be responsible for setting the rules of plasticity during the onset and offset of the CP in the visual cortex?
6. Is the enhanced recruitment of PV cells by TC fibers a pre- or postsynaptic effect? Could it derive from a combination of pre- and postsynaptic mechanisms?
7. Importantly, not all PV cells express PNNs, even in the adult. Indeed whereas PNNs are widely expressed by PV cells in L4, this is not the case for L2/3 of V1 and for other cortical areas. Could different level of glutamatergic strength co-exist in different PV cells belonging to different cortical layers and/or areas?

Answering these and other outstanding questions will provide a better and more refined understanding of how cortical circuits can be modulated by sensory experience during normal cortical operations and will identify new cellular and molecular players responsible for the development of neurological and psychiatric diseases.

REFERENCES

- A**cuna-Goycolea C, Brenowitz SD, Regehr WG (2008) Active Dendritic Conductances Dynamically Regulate GABA Release from Thalamic Interneurons. *Neuron* 57:420–431.
- Adesnik H, Bruns W, Taniguchi H, Huang ZJ, Scanziani M (2012) A neural circuit for spatial summation in visual cortex. *Nature* 490:226–231.
- Agmon A, Connors BW (1989) Repetitive burst-firing neurons in the deep layers of mouse somatosensory cortex. *Neurosci Lett* 99:137–141.
- Ahmed B, Anderson JC, Douglas RJ, Martin KAC, Nelson JC (1994) Polyneuronal Innervation of Spiny Stellate Neurons in Cat Visual Cortex. *J Neurosci* 14:49–59.
- Ahmed B, Anderson JC, Martin KAC, Nelson JC (1997) Map of the synapses onto layer 4 basket cells of the primary visual cortex of the cat. *J Comp Neurol* 380:230–242.
- Alitto HJ, Usrey WM (2003) Corticothalamic feedback and sensory processing. *Curr Opin Neurobiol* 13:440–445.
- Allene C, Lourenço J, Bacci A (2015) The neuronal identity bias behind neocortical GABAergic plasticity. *Trends Neurosci* 38:524–534.
- Alpár A, Gärtner U, Härtig W, Brückner G (2006) Distribution of pyramidal cells associated with perineuronal nets in the neocortex of rat. *Brain Res* 1120:13–22.
- Amitai Y (2001) Thalamocortical synaptic connections: efficacy, modulation, inhibition and plasticity. *Rev Neurosci* 12:159–173.
- Anderson JS, Carandini M, Ferster D (2000) Orientation tuning of input conductance, excitation, and inhibition in cat primary visual cortex. *J Neurophysiol* 84:909–926.
- Angulo MC (2002) Distinct Local Circuits Between Neocortical Pyramidal Cells and Fast-Spiking Interneurons in Young Adult Rats. *J Neurophysiol* 89:943–953.
- Antonini A, Stryker MP (1996) Plasticity of geniculocortical afferents following brief or prolonged monocular occlusion in the cat. *J Comp Neurol* 369:64–82.
- Ascoli G, Alonso-Nanclares L (2008) Petilla terminology: nomenclature of features of GABAergic interneurons of the cerebral cortex. *Nat Rev Neurosci* 9:557–568.

Atallah B V., Bruns W, Carandini M, Scanziani M (2012) Parvalbumin-Expressing Interneurons Linearly Transform Cortical Responses to Visual Stimuli. *Neuron* 73:159–170.

Bacci A, Huguenard JR (2006) Enhancement of spike-timing precision by autaptic transmission in neocortical inhibitory interneurons. *Neuron* 49:119–130.

Bacci A, Huguenard JR, Prince D a (2003) Functional autaptic neurotransmission in fast-spiking interneurons: a novel form of feedback inhibition in the neocortex. *J Neurosci* 23:859–866.

Bagnall MW, Hull C, Bushong EA, Ellisman MH, Scanziani M (2011) Multiple Clusters of Release Sites Formed by Individual Thalamic Afferents onto Cortical Interneurons Ensure Reliable Transmission. *Neuron* 71:180–194.

Baker M (2013) Neuroscience: Through the eyes of a mouse. *Nature* 502:156–158.

Balmer TS (2016) Perineuronal Nets Enhance the Excitability of Fast-Spiking Neurons. *eNeuro* 3:e0112–16.2016.

Bannister AP (2005) Inter- and intra-laminar connections of pyramidal cells in the neocortex. *Neurosci Res* 53:95–103.

Bardin J (2012) Neurodevelopment: Unlocking the brain. *Nature* 487:24–26.

Bavelier D, Levi DM, Li RW, Dan Y, Hensch TK (2010) Removing Brakes on Adult Brain Plasticity: From Molecular to Behavioral Interventions. *J Neurosci* 30:14964–14971.

Bean BP (2007) The action potential in mammalian central neurons. *Nat Rev Neurosci* 8:451–465.

Beierlein M, Gibson JR, Connors BW (2003) Two dynamically distinct inhibitory networks in layer 4 of the neocortex. *J Neurophysiol* 90:2987–3000.

Bekku Y, Saito M, Moser M, Fuchigami M, Maehara A, Nakayama M, Kusachi S, Ninomiya Y, Oohashi T (2012) Bral2 is indispensable for the proper localization of brevican and the structural integrity of the perineuronal net in the brainstem and cerebellum. *J Comp Neurol* 520:1721–1736.

Bence M, Levelt CN (2005) Structural plasticity in the developing visual system. *Prog Brain Res* 147:125–139.

- Berardi N, Pizzorusso T, Maffei L (2000) Critical periods during sensory development. *Curr Opin Neurobiol* 10:138–145.
- Berardi N, Pizzorusso T, Ratto GM, Maffei L (2003) Molecular basis of plasticity in the visual cortex. *Trends Neurosci* 26:369–378.
- Bernard C, Prochiantz A (2016) Otx2-PNN Interaction to Regulate Cortical Plasticity. *Neural Plast* 2016.
- Beurdeley M, Spatazza J, Lee HHC, Sugiyama S, Bernard C, Di Nardo AA, Hensch TK, Prochiantz A (2012) Otx2 Binding to Perineuronal Nets Persistently Regulates Plasticity in the Mature Visual Cortex. *J Neurosci* 32:9429–9437.
- Bhaumik B, Shah NP (2014) Development and matching of binocular orientation preference in mouse V1. *Front Syst Neurosci* 8:128.
- Bikbaev A, Frischknecht R, Heine M (2015) Brain extracellular matrix retains connectivity in neuronal networks. *Sci Rep* 5:14527.
- Blitz DM, Regehr WG (2005) Timing and specificity of feed-forward inhibition within the LGN. *Neuron* 45:917–928.
- Bochner DN, Sapp RW, Adelson JD, Zhang S, Lee H, Djuricic M, Syken J, Dan Y, Shatz CJ (2014) Blocking PirB up-regulates spines and functional synapses to unlock visual cortical plasticity and facilitate recovery from amblyopia. *Sci Transl Med* 6:258ra140-258ra140.
- Bourassa J, Deschenes M (1995) Corticothalamic projections from the primary visual cortex in rats: a single fiber study using biocytin as an anterograde tracer. *Neuroscience* 66:253–263.
- Boyden ES, Zhang F, Bamberg E, Nagel G, Deisseroth K (2005) Millisecond-timescale, genetically targeted optical control of neural activity. *Nat Neurosci* 8:1263–1268.
- Bradbury EJ, Moon LDF, Popat RJ, King VR, Bennett GS, Patel PN, Fawcett JW, McMahon SB (2002) Chondroitinase ABC promotes functional recovery after spinal cord injury. *Nature* 416:636–640.
- Brakebusch C, Seidenbecher CI, Rauch U, Matthies H, Meyer H, Krug M, Böckers TM, Zhou X, Kreutz R, Montag D, Gundelfinger ED, Asztely F, Bo TM, Kreutz MR, Fa R (2002) Brevican-Deficient Mice Display Impaired Hippocampal CA1 Long-Term Potentiation but Show No Obvious Deficits in Learning and Memory. *Mol Cell Biol* 22:7417–7427.
- Briggs F, Usrey WM (2008) Emerging views of corticothalamic function. *Curr Opin Neurobiol* 18:403–407.

- Bright DP, Aller MI, Brickley SG (2007) Synaptic Release Generates a Tonic GABAA Receptor-Mediated Conductance That Modulates Burst Precision in Thalamic Relay Neurons. *J Neurosci* 27:2560–2569.
- Brown SP, Hestrin S (2009) Intracortical circuits of pyramidal neurons reflect their long-range axonal targets. *Nature* 457:1133–1136.
- Brückner G, Bringmann A, Härtig W, Köppe G, Delpech B, Brauer K (1998) Acute and long-lasting changes in extracellular-matrix chondroitin-sulphate proteoglycans induced by injection of chondroitinase ABC in the adult rat brain. *Exp Brain Res* 121:300–310.
- Brückner G, Grosche J (2001) Perineuronal nets show intrinsic patterns of extracellular matrix differentiation in organotypic slice cultures. *Exp Brain Res* 137:83–93.
- Bukalo O, Schachner M, Dityatev A (2001) Modification of extracellular matrix by enzymatic removal of chondroitin sulfate and by lack of tenascin-R differentially affects several forms of synaptic plasticity in the hippocampus. *Neuroscience* 104:359–369.
- Buzsáki G, Draguhn A (2004) Neuronal oscillations in cortical networks. *Science* 304:1926–1929.
- Buzsáki G, Wang X-J (2012) Mechanisms of Gamma Oscillations. *Annu Rev Neurosci* 35:203–225.
- C**abelli RJ, Shelton DL, Segal RA, Shatz CJ (1997) Blockade of endogenous ligands of TrkB inhibits formation of ocular dominance columns. *Neuron* 19:63–76.
- Cabungcal J-H, Steullet P, Morishita H, Kraftsik R, Cuenod M, Hensch TK, Do KQ (2013) Perineuronal nets protect fast-spiking interneurons against oxidative stress. *Proc Natl Acad Sci* 110:9130–9135.
- Carandini M, Heeger DJ (1994) Summation and division by neurons in primate visual cortex. *Science* 264:1333–1336.
- Carandini M, Shimaoka D, Rossi LF, Sato TK, Benucci A, Knopfel T (2015) Imaging the Awake Visual Cortex with a Genetically Encoded Voltage Indicator. *J Neurosci* 35:53–63.
- Carcieri SM (2003) Classification of Retinal Ganglion Cells: A Statistical Approach. *J Neurophysiol* 90:1704–1713.

- Cardin JA, Carl?n M, Meletis K, Knoblich U, Zhang F, Deisseroth K, Tsai L-H, Moore CI (2009) Driving fast-spiking cells induces gamma rhythm and controls sensory responses. *Nature* 459:663–667.
- Carstens KE, Phillips ML, Pozzo-Miller L, Weinberg RJ, Dudek SM (2016) Perineuronal Nets Suppress Plasticity of Excitatory Synapses on CA2 Pyramidal Neurons. *J Neurosci* 36:6312–6320.
- Carulli D, Pizzorusso T, Kwok JCF, Putignano E, Poli A, Forostyak S, Andrews MR, Deepa SS, Glant TT, Fawcett JW (2010) Animals lacking link protein have attenuated perineuronal nets and persistent plasticity. *Brain* 133:2331–2347.
- Carvalho TP, Buonomano D V. (2009) Differential Effects of Excitatory and Inhibitory Plasticity on Synaptically Driven Neuronal Input-Output Functions. *Neuron* 61:774–785.
- Casagrande V a, Xu X, Sary G (2002) Static and dynamic views of visual cortical organization. *Prog Brain Res* 136:389–408.
- Celio MR, Blumcke I (1994) Perineuronal nets - a specialized form of extracellular matrix in the adult nervous system. *Brain Res Rev* 19:128–145.
- Celio MR, Spreafico R, De Biasi S, Vitellaro-Zuccarello L (1998) Perineuronal nets: Past and present. *Trends Neurosci* 21:510–515.
- Chen M, Lee S, Park SJH, Looger LL, Zhou ZJ (2014) Receptive field properties of bipolar cell axon terminals in direction-selective sublaminae of the mouse retina. *J Neurophysiol* 112:1950–1962.
- Chen T-W, Wardill TJ, Sun Y, Pulver SR, Renninger SL, Baohan A, Schreiter ER, Kerr RA, Orger MB, Jayaraman V, Looger LL, Svoboda K, Kim DS (2013) Ultrasensitive fluorescent proteins for imaging neuronal activity. *Nature* 499:295–300.
- Cho J-H, Deisseroth K, Bolshakov VY (2013) Synaptic Encoding of Fear Extinction in mPFC-amygdala Circuits. *Neuron* 80:1491–1507.
- Chow A, Erisir A, Farb C, Nadal MS, Ozaita A, Lau D, Welker E, Rudy B (1999) K(+) channel expression distinguishes subpopulations of parvalbumin- and somatostatin-containing neocortical interneurons. *J Neurosci* 19:9332–9345.
- Coleman JE, Nahmani M, Gavornik JP, Haslinger R, Heynen AJ, Erisir A, Bear MF (2010) Rapid Structural Remodeling of Thalamocortical Synapses Parallels Experience-Dependent Functional Plasticity in Mouse Primary Visual Cortex. *J Neurosci* 30:9670–9682.

- Connors BW, Gutnick MJ (1990) Intrinsic firing patterns of diverse neocortical neurons. *Trends Neurosci* 13:99–104.
- Cooke SF, Bear MF (2013) How the mechanisms of long-term synaptic potentiation and depression serve experience-dependent plasticity in primary visual cortex. *Philos Trans R Soc B Biol Sci* 369:20130284–20130284.
- Cruikshank SJ, Lewis TJ, Connors BW (2007) Synaptic basis for intense thalamocortical activation of feedforward inhibitory cells in neocortex. *Nat Neurosci* 219:1705–1716.
- Cruikshank SJ, Urabe H, Nurmikko A V., Connors BW (2010) Pathway-Specific Feedforward Circuits between Thalamus and Neocortex Revealed by Selective Optical Stimulation of Axons. *Neuron* 65:230–245.
- D**auth S, Grevesse T, Pantazopoulos H, Campbell PH, Maoz BM, Berretta S, Parker KK (2016) Extracellular matrix protein expression is brain region dependent. *J Comp Neurol* 524:1309–1336.
- Davis MF, Figueroa Velez DX, Guevarra RP, Yang MC, Habeeb M, Carathedathu MC, Gandhi SP (2015) Inhibitory Neuron Transplantation into Adult Visual Cortex Creates a New Critical Period that Rescues Impaired Vision. *Neuron* 86:1055–1066.
- de Vivo L, Landi S, Panniello M, Baroncelli L, Chierzi S, Mariotti L, Spolidoro M, Pizzorusso T, Maffei L, Ratto GM (2013) Extracellular matrix inhibits structural and functional plasticity of dendritic spines in the adult visual cortex. *Nat Commun* 4:1484.
- De Winter F, Kwok JCF, Fawcett JW, Vo TT, Carulli D, Verhaagen J (2016) The Chemorepulsive Protein Semaphorin 3A and Perineuronal Net-Mediated Plasticity. *Neural Plast* 2016.
- Deepa SS, Carulli D, Galtrey C, Rhodes K, Fukuda J, Mikami T, Sugahara K, Fawcett JW (2006) Composition of perineuronal net extracellular matrix in rat brain: A different disaccharide composition for the net-associated proteoglycans. *J Biol Chem* 281:17789–17800.
- DeFelipe J et al. (2013) New insights into the classification and nomenclature of cortical GABAergic interneurons. *Nat Rev Neurosci* 14:202–216.
- DeFelipe J, Fariñas I (1992) The pyramidal neuron of the cerebral cortex: morphological and chemical characteristics of the synaptic inputs. *Prog Neurobiol* 39:563–607.
- Deleuze C, Paziienti A, Bacci A (2014) Autaptic self-inhibition of cortical GABAergic neurons: Synaptic narcissism or useful introspection? *Curr Opin Neurobiol* 26:64–71.

- Di Cristo G, Chattopadhyaya B, Kuhlman SJ, Fu Y, Bélanger M-C, Wu CZ, Rutishauser U, Maffei L, Huang ZJ (2007) Activity-dependent PSA expression regulates inhibitory maturation and onset of critical period plasticity. *Nat Neurosci* 10:1569–1577.
- Dino MR, Harroch S, Hockfield S, Matthews RT (2006) Monoclonal antibody Cat-315 detects a glycoform of receptor protein tyrosine phosphatase beta/phosphacan early in CNS development that localizes to extrasynaptic sites prior to synapse formation. *Neuroscience* 142:1055–1069.
- Dityatev A, Brückner G, Dityateva G, Grosche J, Kleene R, Schachner M (2007) Activity-dependent formation and functions of chondroitin sulfate-rich extracellular matrix of perineuronal nets. *Dev Neurobiol* 67:570–588.
- Dityatev A, Schachner M (2003) Extracellular matrix molecules and synaptic plasticity. *Nat Rev Neurosci* 4:456–468.
- Dityatev A, Schachner M (2006) The extracellular matrix and synapses. *Cell Tissue Res* 326:647–654.
- Dityatev A, Schachner M, Sonderegger P (2010) The dual role of the extracellular matrix in synaptic plasticity and homeostasis. *Nat Rev Neurosci* 11:735–746.
- Djrbal L, Lortat-Jacob H, Kwok J (2017) Chondroitin sulfates and their binding molecules in the central nervous system. *Glycoconj J*:1–14.
- Donato F, Chowdhury A, Lahr M, Caroni P (2015) Early- and Late-Born Parvalbumin Basket Cell Subpopulations Exhibiting Distinct Regulation and Roles in Learning. *Neuron* 85:770–786.
- Donato F, Rompani SB, Caroni P (2013) Parvalbumin-expressing basket-cell network plasticity induced by experience regulates adult learning. *Nature* 504:272–276.
- Douglas RJ, Martin K a C (2004) Neuronal circuits of the neocortex. *Annu Rev Neurosci* 27:419–451.
- Druga R (2009) Neocortical inhibitory system. *Folia Biol (Praha)* 55:201–217.
- Espinosa JS, Stryker MP (2013) Development and Plasticity of the Primary Visual Cortex. *75*:230–249.
- F**ader S, Imaizumi K, Yanagawa Y, Lee C (2016) Wisteria Floribunda Agglutinin-Labeled Perineuronal Nets in the Mouse Inferior Colliculus, Thalamic Reticular Nucleus and Auditory Cortex. *Brain Sci* 6:13.

- Fagiolini M (2004) Specific GABAA Circuits for Visual Cortical Plasticity. *Science* (80-) 303:1681–1683.
- Fagiolini M, Hensch TK (2000) Inhibitory threshold for critical-period activation in primary visual cortex. *Nature* 404:183–186.
- Fagiolini M, Pizzorusso T, Berardi N, Domenici L, Maffei L (1994) Functional postnatal development of the rat primary visual cortex and the role of visual experience: dark rearing and monocular deprivation. *Vision Res* 34:709–720.
- Favuzzi E, Marques-Smith A, Deogracias R, Winterflood CM, Sánchez-Aguilera A, Mantoan L, Maeso P, Fernandes C, Ewers H, Rico B (2017) Activity-Dependent Gating of Parvalbumin Interneuron Function by the Perineuronal Net Protein Brevican. *Neuron*:1–17.
- Feldman ML (1984) Morphology of the neocortical neuron. In: *The Cerebral Cortex*, pp 123–200. Plenum Press, New York.
- Feldmeyer D (2012) Excitatory neuronal connectivity in the barrel cortex. *Front Neuroanat* 6:1–22.
- Fischer QS, Graves A, Evans S, Lickey ME, Pham T a (2007) Monocular deprivation in adult mice alters visual acuity and single-unit activity. *Learn Mem* 14:277–286.
- Frenkel MY, Bear MF (2004) How Monocular Deprivation Shifts Ocular Dominance in Visual Cortex of Young Mice. *Neuron* 44:917–923.
- Freund TF (2003) Interneuron Diversity series: Rhythm and mood in perisomatic inhibition. *Trends Neurosci* 26:489–495.
- Freund TF, Katona I (2007) Perisomatic Inhibition. *Neuron* 56:33–42.
- Frischknecht R, Happel MFK (2016) Impact of the extracellular matrix on plasticity in juvenile and adult brains. *e-Neuroforum* 7:1–6.
- Frischknecht R, Heine M, Perrais D, Seidenbecher CI, Choquet D, Gundelfinger ED (2009) Brain extracellular matrix affects AMPA receptor lateral mobility and short-term synaptic plasticity. *Neuroforum* 15:94–95.
- Fu Y, Yau KW (2007) Phototransduction in mouse rods and cones. *Pflugers Arch Eur J Physiol* 454:805–819.

- G**abernet L, Jadhav SP, Feldman DE, Carandini M, Scanziani M (2005) Somatosensory integration controlled by dynamic thalamocortical feed-forward inhibition. *Neuron* 48:315–327.
- Galarreta M, Hestrin S (2002) Electrical and chemical synapses among parvalbumin fast-spiking GABAergic interneurons in adult mouse neocortex. *Proc Natl Acad Sci* 99:12438–12443.
- Galtrey CM, Fawcett JW (2007) The role of chondroitin sulfate proteoglycans in regeneration and plasticity in the central nervous system. *Brain Res Rev* 54:1–18.
- Galtrey CM, Kwok JCF, Carulli D, Rhodes KE, Fawcett JW (2008) Distribution and synthesis of extracellular matrix proteoglycans, hyaluronan, link proteins and tenascin-R in the rat spinal cord. *Eur J Neurosci* 27:1373–1390.
- Gao R, Penzes P (2015) Common Mechanisms of Excitatory and Inhibitory Imbalance in Schizophrenia and Autism Spectrum Disorders. *Curr Mol Med* 15:146–167.
- Giamanco KA, Morawski M, Matthews RT (2010) Perineuronal net formation and structure in aggrecan knockout mice. *Neuroscience* 170:1314–1327.
- Gogolla N, Caroni P, Luthi A, Herry C (2009) Perineuronal Nets Protect Fear Memories from Erasure. *Science* (80-) 325:1258–1261.
- Gollisch T, Meister M (2010) Eye Smarter than Scientists Believed: Neural Computations in Circuits of the Retina. *Neuron* 65:150–164.
- Gordon JA, Stryker MP (1996) Experience-dependent plasticity of binocular responses in the primary visual cortex of the mouse. *J Neurosci* 16:3274–3286.
- Grieve KL (2005) Binocular visual responses in cells of the rat dLGN. *J Physiol* 566:119–124.
- Gu Y, Huang S, Chang M, Worley P, Kirkwood A, Quinlan E (2013) Obligatory role for the immediate early gene NARP in critical period plasticity. *Neuron* 79:335–346.
- Guillery RW, Sherman SM (2002) Thalamic relay functions and their role in corticocortical communication: Generalizations from the visual system. *Neuron* 33:163–175.
- Gundelfinger ED, Frischknecht R, Choquet D, Heine M (2010) Converting juvenile into adult plasticity: A role for the brain's extracellular matrix. *Eur J Neurosci* 31:2156–2165.
- Gupta A (2000) Organizing Principles for a Diversity of GABAergic Interneurons and Synapses in the Neocortex. *Science* (80-) 287:273–278.

- H**arris KD, Shepherd GMG (2015) The neocortical circuit: themes and variations. *Nat Neurosci* 18:170–181.
- Hausnø A, Ibrahim M, Bartsch U, Letiembre M, Celio MR, Menoud PA (2000) Morphology of perineuronal nets in tenascin-R and parvalbumin single and double knockout mice. *Brain Res* 864:142–145.
- He H-Y, Ray B, Dennis K, Quinlan EM (2007) Experience-dependent recovery of vision following chronic deprivation amblyopia. *Nat Neurosci* 10:1134–1136.
- Heeger DJ (2017) Theory of cortical function. *Proc Natl Acad Sci* 114:1773–1782.
- Hefft S, Jonas P (2005) Asynchronous GABA release generates long-lasting inhibition at a hippocampal interneuron-principal neuron synapse. *Nat Neurosci* 8:1319–1328.
- Heimel JA, Hartman RJ, Hermans JM, Levelt CN (2007) Screening mouse vision with intrinsic signal optical imaging. *Eur J Neurosci* 25:795–804.
- Hengen KB, Lambo ME, Van Hooser SD, Katz DB, Turrigiano GG (2013) Firing Rate Homeostasis in Visual Cortex of Freely Behaving Rodents. *Neuron* 80:335–342.
- Hensch TK (2005a) Critical Period Mechanisms in Developing Visual Cortex. *Curr Top Dev Biol* 69:215–237.
- Hensch TK (2005b) Critical period plasticity in local cortical circuits. *Nat Rev Neurosci* 6:877–888.
- Hensch TK, Fagiolini M (2005) Excitatory-inhibitory balance and critical period plasticity in developing visual cortex. *Prog Brain Res* 147:115–124.
- Hensch TK, Fagiolini M, Mataga N, Stryker MP, Baekkeskov S, Kash SF (1998) Local GABA circuit control of experience-dependent plasticity in developing visual cortex. *Science* 282:1504–1508.
- Hioki H (2015) Compartmental organization of synaptic inputs to parvalbumin-expressing GABAergic neurons in mouse primary somatosensory cortex. *Anat Sci Int* 90:7–21.
- Hofer SB, Mrsic-Flogel TD, Bonhoeffer T, Hübener M (2006a) Prior experience enhances plasticity in adult visual cortex. *Nat Neurosci* 9:127–132.
- Hofer SB, Mrsic-Flogel TD, Bonhoeffer T, Hübener M (2006b) Lifelong learning: ocular dominance plasticity in mouse visual cortex. *Curr Opin Neurobiol* 16:451–459.

- Hofer SB, Mrsic-Flogel TD, Bonhoeffer T, Hübener M (2009) Experience leaves a lasting structural trace in cortical circuits. *Nature* 457:313–317.
- Hoon M, Okawa H, Della Santina L, Wong ROL (2014) Functional architecture of the retina: Development and disease. *Prog Retin Eye Res* 42:44–84.
- Howarth M, Walmsley L, Brown TM (2014) Binocular integration in the mouse lateral geniculate nuclei. *Curr Biol* 24:1241–1247.
- Hu H, Jonas P (2014) A supercritical density of Na⁺ channels ensures fast signaling in GABAergic interneuron axons. *Nat Neurosci* 17:686–693.
- Huang ZJ, Di Cristo G, Ango F (2007) Development of GABA innervation in the cerebral and cerebellar cortices. *Nat Rev Neurosci* 8:673–686.
- Huang ZJ, Kirkwood A, Pizzorusso T, Porciatti V, Morales B, Bear MF, Maffei L, Tonegawa S (1999) BDNF regulates the maturation of inhibition and the critical period of plasticity in mouse visual cortex. *Cell* 98:739–755.
- Hubel DH (1963) The Visual Cortex of the Brain. *Sci Am* 209:54–63.
- Hubel DH (1982) Exploration of the primary visual cortex. *Nature* 299:515–524.
- HUBEL DH, WIESEL TN (1959) Receptive fields of single neurones in the cat's striate cortex. *J Physiol* 148:574–591.
- Hübener M (2003) Mouse visual cortex. *Curr Opin Neurobiol* 13:413–420.
- Hübener M, Bonhoeffer T (2014) Neuronal plasticity: Beyond the critical period. *Cell* 159:727–737.
- Huberman AD, Niell CM (2011) What can mice tell us about how vision works? *Trends Neurosci* 34:464–473.
- Huberman AD, Wei W, Elstrott J, Stafford BK, Feller MB, Barres BA (2009) Genetic Identification of an On-Off Direction- Selective Retinal Ganglion Cell Subtype Reveals a Layer-Specific Subcortical Map of Posterior Motion. *Neuron* 62:327–334.
- Huguenard JR, McCormick DA (2007) Thalamic synchrony and dynamic regulation of global forebrain oscillations. *Trends Neurosci* 30:350–356.
- Hull C, Isaacson JS, Scanziani M (2009) Postsynaptic Mechanisms Govern the Differential Excitation of Cortical Neurons by Thalamic Inputs. *J Neurosci* 29:9127–9136.

Isaacson J, Scanziani M (2011a) How inhibition shapes cortical activity. *Neuron* 72:231–243.

Iwai Y, Fagiolini M, Obata K, Hensch TK (2003) Rapid critical period induction by tonic inhibition in visual cortex. *J Neurosci* 23:6695–6702.

John N, Krügel H, Frischknecht R, Smalla KH, Schultz C, Kreutz MR, Gundelfinger ED, Seidenbecher CI (2006) Brevican-containing perineuronal nets of extracellular matrix in dissociated hippocampal primary cultures. *Mol Cell Neurosci* 31:774–784.

Kamigaki T, Dan Y (2017) Delay activity of specific prefrontal interneuron subtypes modulates memory-guided behavior. *Nat Neurosci* 20:1–12.

Kannan M, Gross GG, Arnold DB, Higley MJ (2016) Visual Deprivation During the Critical Period Enhances Layer 2/3 GABAergic Inhibition in Mouse V1. *J Neurosci* 36:5914–5919.

Kano M, Ohno-Shosaku T, Hashimoto-dani Y, Uchigashima M, Watanabe M (2009) Endocannabinoid-mediated control of synaptic transmission. *Physiol Rev* 89:309–380.

Kawaguchi Y, Katsumaru H, Kosaka T, Heizmann CW, Hama K (1987) Fast spiking cells in rat hippocampus (CA1 region) contain the calcium-binding protein parvalbumin. *Brain Res* 416:369–374.

Kepecs A, Fishell G (2014) Interneuron Cell Types: Fit to form and formed to fit. *Nature* 505:318–326.

Khibnik LA, Cho KKA, Bear MF (2010) Relative contribution of feedforward excitatory connections to expression of ocular dominance plasticity in layer 4 of visual cortex. *Neuron* 66:493–500.

Kitagawa H, Tsutsumi K, Tone Y, Sugahara K (1997) Developmental regulation of the sulfation profile of chondroitin sulfate chains in the chicken embryo brain. *J Biol Chem* 272:31377–31381.

Klausberger T, Roberts JDB, Somogyi P (2002) Cell type- and input-specific differences in the number and subtypes of synaptic GABA(A) receptors in the hippocampus. *J Neurosci* 22:2513–2521.

Klausberger T, Somogyi P (2008) Neuronal Diversity and Temporal Dynamics: The Unity of Hippocampal Circuit Operations. *Science* (80-) 321:53–57.

- Kloc M, Maffei A (2014) Target-Specific Properties of Thalamocortical Synapses onto Layer 4 of Mouse Primary Visual Cortex. *J Neurosci* 34:15455–15465.
- Klueva J, Gundelfinger ED, Frischknecht RR, Heine M (2014) Intracellular Ca^{2+} and not the extracellular matrix determines surface dynamics of AMPA-type glutamate receptors on aspiny neurons. *Philos Trans R Soc Lond B Biol Sci* 369:20130605.
- Ko H, Cossell L, Baragli C, Antolik J, Clopath C, Hofer SB, Mrsic-Flogel TD (2013) The emergence of functional microcircuits in visual cortex. *Nature* 496:96–100.
- Kobayashi Y, Ye Z, Hensch TK (2015) Clock Genes Control Cortical Critical Period Timing. *Neuron* 86:264–275.
- Kubota Y, Shigematsu N, Karube F, Sekigawa A, Kato S, Yamaguchi N, Hirai Y, Morishima M, Kawaguchi Y (2011) Selective coexpression of multiple chemical markers defines discrete populations of neocortical gabaergic neurons. *Cereb Cortex* 21:1803–1817.
- Kuhlman SJ, Olivas ND, Tring E, Ikrar T, Xu X, Trachtenberg JT (2013) A disinhibitory microcircuit initiates critical-period plasticity in the visual cortex. *Nature* 501:543–546.
- Kwok JCF, Carulli D, Fawcett JW (2010) In vitro modeling of perineuronal nets: Hyaluronan synthase and link protein are necessary for their formation and integrity. *J Neurochem* 114:1447–1459.
- Kwok JCF, Dick G, Wang D, Fawcett JW (2011) Extracellular matrix and perineuronal nets in CNS repair. *Dev Neurobiol* 71:1073–1089.
- L**ander C, Kind P, Maleski M, Hockfield S (1997) A family of activity-dependent neuronal cell-surface chondroitin sulfate proteoglycans in cat visual cortex. *J Neurosci* 17:1928–1939.
- Larkum M (2013) A cellular mechanism for cortical associations: an organizing principle for the cerebral cortex. *Trends Neurosci* 36:141–151.
- Latawiec D, Martin KAC, Meskenaite V (2000) Termination of the geniculo-cortical projection in the striate cortex of the monkey: A quantitative immunoelectron microscopic study. *J Comp Neurol* 419:1–14.
- Lee AT, Vogt D, Rubenstein JL, Sohal VS (2014) A class of GABAergic neurons in the prefrontal cortex sends long-range projections to the nucleus accumbens and elicits acute avoidance behavior. *J Neurosci* 34:11519–11525.

- Lee HHC, Bernard C, Ye Z, Acampora D, Simeone A, Prochiantz A, Di Nardo AA, Hensch TK (2017) Genetic Otx2 mis-localization delays critical period plasticity across brain regions. *Mol Psychiatry*:680–688.
- Lee S, Kruglikov I, Huang ZJ, Fishell G, Rudy B (2013) A disinhibitory circuit mediates motor integration in the somatosensory cortex. *Nat Neurosci* 16:1662–1670.
- Lefort S, Gray AC, Turrigiano GG (2013) Long-term inhibitory plasticity in visual cortical layer 4 switches sign at the opening of the critical period. *Proc Natl Acad Sci* 110:E4540–E4547.
- Lensjø KK, Christensen AC, Tennøe S, Fyhn M, Hafting T (2017a) Differential Expression and Cell-Type Specificity of Perineuronal Nets in Hippocampus, Medial Entorhinal Cortex and Visual Cortex Examined in the Rat and Mouse. *eneuro*:ENEURO.0379-16.2017.
- Lensjø KK, Lepperød ME, Dick G, Hafting T, Fyhn M (2017b) Removal of Perineuronal Nets Unlocks Juvenile Plasticity Through Network Mechanisms of Decreased Inhibition and Increased Gamma Activity. *J Neurosci* 37:1269–1283.
- Levelt CN, Heimel JA, Van Versendaal D (2011) The role of GABAergic inhibition in ocular dominance plasticity. *Neural Plast* 2011.
- Levelt CN, Hübener M (2012) Critical-Period Plasticity in the Visual Cortex. *Annu Rev Neurosci* 35:309–330.
- Levy AD, Omar MH, Koleske AJ (2014) Extracellular matrix control of dendritic spine and synapse structure and plasticity in adulthood. *Front Neuroanat* 8:1–18.
- Lien AD, Scanziani M (2013) Tuned thalamic excitation is amplified by visual cortical circuits. *Nat Neurosci* 16:1315–1323.
- Liu H, Gao P-F, Xu H-W, Liu M-M, Yu T, Yao J-P, Yin Z-Q (2013) Perineuronal nets increase inhibitory GABAergic currents during the critical period in rats. *Int J Ophthalmol* 6:120–125.
- M**affei A, Lambo ME, Turrigiano GG (2010) Critical Period for Inhibitory Plasticity in Rodent Binocular V1. *J Neurosci* 30:3304–3309.
- Maffei A, Nataraj K, Nelson SB, Turrigiano GG (2006) Potentiation of cortical inhibition by visual deprivation. *Nature* 443:81–84.

- Maffei A, Nelson SB, Turrigiano GG (2004) Selective reconfiguration of layer 4 visual cortical circuitry by visual deprivation. *Nat Neurosci* 7:1353–1359.
- Majewska A, Sur M (2003) Motility of dendritic spines in visual cortex in vivo: Changes during the critical period and effects of visual deprivation. *Proc Natl Acad Sci USA* 100:16024–16029.
- Major G, Larkum ME, Schiller J (2013) Active Properties of Neocortical Pyramidal Neuron Dendrites. *Annu Rev Neurosci* 36:1–24.
- Manseau F, Marinelli S, Méndez P, Schwaller B, Prince D a, Huguenard JR, Bacci A (2010) Desynchronization of neocortical networks by asynchronous release of GABA at autaptic and synaptic contacts from fast-spiking interneurons. *PLoS Biol* 8.
- Mao T, Kusefoglu D, Hooks B, Huber D, Petreanu L, Svoboda K (2011) Long - Range Neuronal Circuits Underlying the Interaction between Sensory and Motor Cortex. *Neuron* 72:111–123.
- Marín O (2012) Interneuron dysfunction in psychiatric disorders. *Nat Rev Neurosci* 13:107–120.
- Markram H, Toledo-Rodriguez M, Wang Y, Gupta A, Silberberg G, Wu C (2004) Interneurons of the neocortical inhibitory system. *Nat Rev Neurosci* 5:793–807.
- Masland RH (2012) The Neuronal Organization of the Retina. *Neuron* 76:266–280.
- Massey JM (2006) Chondroitinase ABC Digestion of the Perineuronal Net Promotes Functional Collateral Sprouting in the Cuneate Nucleus after Cervical Spinal Cord Injury. *J Neurosci* 26:4406–4414.
- Mataga N, Mizuguchi Y, Hensch TK (2004) Experience-dependent pruning of dendritic spines in visual cortex by tissue plasminogen activator. *Neuron* 44:1031–1041.
- Matthews RT, Kelly GM, Zerillo C a, Gray G, Tiemeyer M, Hockfield S (2002) Aggrecan glycoforms contribute to the molecular heterogeneity of perineuronal nets. *J Neurosci* 22:7536–7547.
- McCormick D a, Connors BW, Lighthall JW, Prince D a (1985) Comparative electrophysiology of pyramidal and sparsely spiny stellate neurons of the neocortex. *J Neurophysiol* 54:782–806.
- McGee AW (2005) Experience-Driven Plasticity of Visual Cortex Limited by Myelin and Nogo Receptor. *Science* (80-) 309:2222–2226.

- McRae PA, Rocco MM, Kelly G, Brumberg JC, Matthews RT (2007) Sensory Deprivation Alters Aggrecan and Perineuronal Net Expression in the Mouse Barrel Cortex. *J Neurosci* 27:5405–5413.
- Méndez P, Bacci A (2011) Assortment of GABAergic plasticity in the cortical interneuron melting pot. *Neural Plast* 2011:976856.
- Mendez P, Pazienti A, Szabo G, Bacci A (2012) Direct Alteration of a Specific Inhibitory Circuit of the Hippocampus by Antidepressants. *J Neurosci* 32:16616–16628.
- Miao Q-L, Ye Q, Zhang X-H (2014) Perineuronal net, CSPG receptor and their regulation of neural plasticity. *Sheng Li Xue Bao* 66:387–397.
- Mikami T, Kitagawa H (2013) Biosynthesis and function of chondroitin sulfate. *Biochim Biophys Acta - Gen Subj* 1830:4719–4733.
- Mitchell SJ, Silver RA (2003) Shunting inhibition modulates neuronal gain during synaptic excitation. *Neuron* 38:433–445.
- Miyata S, Kitagawa H (2016) Chondroitin 6-Sulfation Regulates Perineuronal Net Formation by Controlling the Stability of Aggrecan. *Neural Plast* 2016:7–9.
- Miyata S, Komatsu Y, Yoshimura Y, Taya C, Kitagawa H (2012) Persistent cortical plasticity by upregulation of chondroitin 6-sulfation. *Nat Neurosci* 15:414–422.
- Miyata S, Nishimura Y, Hayashi N, Oohira A (2005) Construction of perineuronal net-like structure by cortical neurons in culture. *Neuroscience* 136:95–104.
- Morales B, Choi S-Y, Kirkwood A (2002) Dark rearing alters the development of GABAergic transmission in visual cortex. *J Neurosci* 22:8084–8090.
- Morawski M, Reinert T, Meyer-Klaucke W, Wagner FE, Tröger W, Reinert A, Jäger C, Brückner G, Arendt T (2015) Ion exchanger in the brain: Quantitative analysis of perineuronally fixed anionic binding sites suggests diffusion barriers with ion sorting properties. *Sci Rep* 5:16471.
- Morikawa S, Ikegaya Y, Narita M, Tamura H (2017) Activation of perineuronal net-expressing excitatory neurons during associative memory encoding and retrieval. *Sci Rep* 7:46024.
- Morishita H, Hensch TK (2008) Critical period revisited: impact on vision. *Curr Opin Neurobiol* 18:101–107.

Morishita H, Miwa JM, Heintz N, Hensch TK (2010) Lynx1, a Cholinergic Brake, Limits Plasticity in Adult Visual Cortex. *Science* (80-) 330:1238–1240.

Mrsic-Flogel TD, Hofer SB, Ohki K, Reid RC, Bonhoeffer T, Hübner M (2007) Homeostatic Regulation of Eye-Specific Responses in Visual Cortex during Ocular Dominance Plasticity. *Neuron* 54:961–972.

Murray Sherman S (2001) Tonic and burst firing: Dual modes of thalamocortical relay. *Trends Neurosci* 24:122–126.

Nabel EM, Morishita H (2013) Regulating critical period plasticity: Insight from the visual system to fear circuitry for therapeutic interventions. *Front Psychiatry* 4:1–8.

Nagel G, Szellas T, Huhn W, Kateriya S, Adeishvili N, Berthold P, Ollig D, Hegemann P, Bamberg E (2003) Channelrhodopsin-2, a directly light-gated cation-selective membrane channel. *Proc Natl Acad Sci* 100:13940–13945.

Nahmani M, Turrigiano GG (2014) Deprivation-Induced Strengthening of Presynaptic and Postsynaptic Inhibitory Transmission in Layer 4 of Visual Cortex during the Critical Period. *J Neurosci* 34:2571–2582.

Nelson SB, Valakh V (2015) Excitatory/Inhibitory Balance and Circuit Homeostasis in Autism Spectrum Disorders. *Neuron* 87:684–698.

Niell CM, Stryker MP (2008) Highly Selective Receptive Fields in Mouse Visual Cortex. *J Neurosci* 28:7520–7536.

Nörenberg A, Hu H, Vida I, Bartos M, Jonas P (2010) Distinct nonuniform cable properties optimize rapid and efficient activation of fast-spiking GABAergic interneurons. *Proc Natl Acad Sci U S A* 107:894–899.

Norton TT, Holdefer RN, Godwin DW (1989) Effects of bicuculline on receptive field center sensitivity of relay cells in the lateral geniculate nucleus. *Brain Res* 488:348–352.

Nowicka D, Soulsby S, Skangiel-Kramska J, Glazewski S (2009) Parvalbumin-containing neurons, perineuronal nets and experience-dependent plasticity in murine barrel cortex. *Eur J Neurosci* 30:2053–2063.

Oray S, Majewska A, Sur M (2004) Dendritic spine dynamics are regulated by monocular deprivation and extracellular matrix degradation. *Neuron* 44:1021–1030.

Orlando C, Ster J, Gerber U, Fawcett JW, Raineteau O (2012) Perisynaptic Chondroitin Sulfate Proteoglycans Restrict Structural Plasticity in an Integrin-Dependent Manner. *J Neurosci* 32:18009–18017.

Palmer L, Murayama M, Larkum M (2012) Inhibitory Regulation of Dendritic Activity in vivo. *Front Neural Circuits* 6:1–10.

Pantazopoulos H, Berretta S (2016) In sickness and in health: Perineuronal nets and synaptic plasticity in psychiatric disorders. *Neural Plast* 2016.

Peters A JE (1984) Classification of cortical neurons. In: *Cellular components of the cerebral cortex* (Springer, ed), pp 107–122.

Petreaunu L, Mao T, Sternson SM, Svoboda K (2009) The subcellular organization of neocortical excitatory connections. *Nature* 457:1142–1145.

Pfeffer CK, Xue M, He M, Huang ZJ, Scanziani M (2013) Inhibition of inhibition in visual cortex: the logic of connections between molecularly distinct interneurons. *Nat Neurosci* 16:1068–1076.

Pham T a., Graham SJ, Suzuki S, Barco A, Kandel ER, Gordon B, Lickey ME (2004) A semi-persistent adult ocular dominance plasticity in visual cortex is stabilized by activated CREB. *Learn Mem* 11:738–747.

Pi H-J, Hangya B, Kvitsiani D, Sanders JI, Huang ZJ, Kepecs A (2013) Cortical interneurons that specialize in disinhibitory control. *Nature* 503:521–524.

Pizzorusso T (2002) Reactivation of Ocular Dominance Plasticity in the Adult Visual Cortex. *Science* (80-) 298:1248–1251.

Pizzorusso T, Medini P, Landi S, Baldini S, Berardi N, Maffei L (2006) Structural and functional recovery from early monocular deprivation in adult rats. *Proc Natl Acad Sci* 103:8517–8522.

Pouille F (2001) Enforcement of Temporal Fidelity in Pyramidal Cells by Somatic Feed-Forward Inhibition. *Science* (80-) 293:1159–1163.

Pouille F, Marin-Burgin A, Adesnik H, Atallah B V., Scanziani M (2009) Input normalization by global feedforward inhibition expands cortical dynamic range. *Nat Neurosci* 12:1577–1585.

- Preston A, Evans AS (2011) Lateral Geniculate Nucleus of Thalamus. In: Encyclopedia of Clinical Neuropsychology, pp 1435–1436. New York, NY: Springer New York.
- Priebe NJ (2016) Mechanisms of Orientation Selectivity in the Primary Visual Cortex. *Annu Rev Vis Sci* 2:85–107.
- Priebe NJ, Ferster D (2012) Mechanisms of Neuronal Computation in Mammalian Visual Cortex. *Neuron* 75:194–208.
- Priebe NJ, McGee AW (2014) Mouse vision as a gateway for understanding how experience shapes neural circuits. *Front Neural Circuits* 8:1–9.
- Prochiantz A, Fuchs J, Di Nardo AA (2014) Postnatal signalling with homeoprotein transcription factors. *Philos Trans R Soc L B Biol Sci* 369.
- Putignano E, Lonetti G, Cancedda L, Ratto G, Costa M, Maffei L, Pizzorusso T (2007) Developmental Downregulation of Histone Posttranslational Modifications Regulates Visual Cortical Plasticity. *Neuron* 53:747–759.
- Q**i G, Feldmeyer D (2016) Dendritic Target Region-Specific Formation of Synapses between Excitatory Layer 4 Neurons and Layer 6 Pyramidal Cells. *Cereb Cortex* 26:1569–1579.
- R**. Douglas, H. Markram and KM (2004) Neocortex. In: The synaptic organization of the brain, G. Shepherd., pp 499–558. Oxford University Press, New York, NY, USA.
- Ramon y Cajal S (1899) *Textura del sistema nervioso del hombre y de los vertebrados*. Oxford Univ Press.
- Reimers S, Hartlage-Rübsamen M, Brückner G, Roßner S (2007) Formation of perineuronal nets in organotypic mouse brain slice cultures is independent of neuronal glutamatergic activity. *Eur J Neurosci* 25:2640–2648.
- Reinhold K, Lien AD, Scanziani M (2015) Distinct recurrent versus afferent dynamics in cortical visual processing. *Nat Neurosci* 18:1789–1797.
- Ringach DL, Mineault PJ, Tring E, Olivas ND, Garcia-Junco-Clemente P, Trachtenberg JT (2016) Spatial clustering of tuning in mouse primary visual cortex. *Nat Commun* 7:12270.

- Rivlin-Etzion M, Zhou K, Wei W, Elstrott J, Nguyen PL, Barres BA, Huberman AD, Feller MB (2011) Transgenic Mice Reveal Unexpected Diversity of On-Off Direction-Selective Retinal Ganglion Cell Subtypes and Brain Structures Involved in Motion Processing. *J Neurosci* 31:8760–8769.
- Rocheffort NL, Konnerth A (2012) Dendritic spines: from structure to in vivo function. *EMBO Rep* 13:699–708.
- Rockland KS (1998) Complex microstructures of sensory cortical connections. *Curr Opin Neurobiol* 8:545–551.
- Romberg C, Yang S, Melani R, Andrews MR, Horner AE, Spillantini MG, Bussey TJ, Fawcett JW, Pizzorusso T, Saksida LM (2013) Depletion of Perineuronal Nets Enhances Recognition Memory and Long-Term Depression in the Perirhinal Cortex. *J Neurosci* 33:7057–7065.
- Roux L, Buzsáki G (2015) Tasks for inhibitory interneurons in intact brain circuits. *Neuropharmacology* 88:10–23.
- Rudy B, McBain CJ (2001) Kv3 channels: Voltage-gated K⁺ channels designed for high-frequency repetitive firing. *Trends Neurosci* 24:517–526.
- S**aalmann Y, Kastner S (2011) Cognitive and Perceptual Functions of the Visual Thalamus. *Neuron* 71:209–223.
- Sale A, Maya Vetencourt JF, Medini P, Cenni MC, Baroncelli L, De Pasquale R, Maffei L (2007) Environmental enrichment in adulthood promotes amblyopia recovery through a reduction of intracortical inhibition. *Nat Neurosci* 10:679–681.
- Sato M, Stryker MP (2008) Distinctive Features of Adult Ocular Dominance Plasticity. *J Neurosci* 28:10278–10286.
- Sawtell NBB, Frenkel MYY, Philpot BDD, Nakazawa K, Tonegawa S, Bear MFF (2003) NMDA receptor-dependent ocular dominance plasticity in adult visual cortex. *Neuron* 38:977–985.
- Scali M, Baroncelli L, Cenni MC, Sale A, Maffei L (2012) A rich environmental experience reactivates visual cortex plasticity in aged rats. *Exp Gerontol* 47:337–341.
- Scheyltjens I, Arckens L (2016) The current status of somatostatin-interneurons in inhibitory control of brain function and plasticity. *Neural Plast* 2016.

- Schlicker K, Boller M, Schmidt M (2004) GABAC receptor mediated inhibition in acutely isolated neurons of the rat dorsal lateral geniculate nucleus. *Brain Res Bull* 63:91–97.
- Schuett S, Bonhoeffer T, Hübener M (2002) Mapping retinotopic structure in mouse visual cortex with optical imaging. *J Neurosci* 22:6549–6559.
- Sedigh-Sarvestani M, Vigeland L, Fernandez-Lamo I, Taylor MM, Palmer LA, Contreras D (2017) Intracellular, In Vivo, Dynamics of Thalamocortical Synapses in Visual Cortex. *J Neurosci* 37:5250–5262.
- Seeger G, Brauer K, Härtig W, Brückner G (1994) Mapping of perineuronal nets in the rat brain stained by colloidal iron hydroxide histochemistry and lectin cytochemistry. *Neuroscience* 58:371–388.
- Seidenbecher CI, Gundelfinger ED, Böckers TM, Trotter J, Kreuz MR (1998) Transcripts for secreted and GPI-anchored brevicin are differentially distributed in rat brain. *Eur J Neurosci* 10:1621–1630.
- Sherman and Guillery (2004) Thalamus. In: *The synaptic organization of the brain*, G. Shepherd., pp 311–359. Oxford University Press, New York, NY, USA.
- Shu Y, Hasenstaub A, Badoual M, Bal T, McCormick D a (2003) Barrages of synaptic activity control the gain and sensitivity of cortical neurons. *J Neurosci* 23:10388–10401.
- Sidorov MS, Kaplan ES, Osterweil EK, Lindemann L, Bear MF (2015) Metabotropic glutamate receptor signaling is required for NMDA receptor-dependent ocular dominance plasticity and LTD in visual cortex. *Proc Natl Acad Sci* 112:12852–12857.
- Silberberg G, Gupta A, Markram H (2002) Stereotypy in neocortical microcircuits. *Trends Neurosci* 25:227–230.
- Silberberg G, Markram H (2007) Disynaptic Inhibition between Neocortical Pyramidal Cells Mediated by Martinotti Cells. *Neuron* 53:735–746.
- Sillito AM, Jones HE (2002) Corticothalamic interactions in the transfer of visual information. *Philos Trans R Soc B Biol Sci* 357:1739–1752.
- Silver RA (2010) Neuronal arithmetic. *Nat Rev Neurosci* 11:474–489.
- Sirotin YB, Das A (2010) Zooming in on mouse vision. *Nat Neurosci* 13:1045–1046.
- Smith SL, Trachtenberg JT (2007) Experience-dependent binocular competition in the visual cortex begins at eye opening. *Nat Neurosci* 10:370–375.

- Sohal VS, Zhang F, Yizhar O, Deisseroth K (2009) Parvalbumin neurons and gamma rhythms enhance cortical circuit performance. *Nature* 459:698–702.
- Sohn J, Okamoto S, Kataoka N, Kaneko T, Nakamura K, Hioki H (2016) Differential Inputs to the Perisomatic and Distal-Dendritic Compartments of VIP-Positive Neurons in Layer 2/3 of the Mouse Barrel Cortex. *Front Neuroanat* 10:1–18.
- Southwell DG, Froemke RC, Alvarez-Buylla A, Stryker MP, Gandhi SP (2010) Cortical Plasticity Induced by Inhibitory Neuron Transplantation. *Science* (80-) 327:1145–1148.
- Spatazza J, Lee HHC, Di Nardo AA, Tibaldi L, Joliot A, Hensch TK, Prochiantz A (2013) Choroid-Plexus-Derived Otx2 Homeoprotein Constrains Adult Cortical Plasticity. *Cell Rep* 3:1815–1823.
- Spruston N (2008) Pyramidal neurons: dendritic structure and synaptic integration. *Nat Rev Neurosci* 9:206–221.
- Stevens CF (2015) Novel neural circuit mechanism for visual edge detection. *Proc Natl Acad Sci* 112:875–880.
- Stosiek C, Garaschuk O, Holthoff K, Konnerth A (2003) In vivo two-photon calcium imaging of neuronal networks. *Proc Natl Acad Sci U S A* 100:7319–7324.
- Stuart GJ, Spruston N (2015) Dendritic integration: 60 years of progress. *Nat Neurosci* 18:1713–1721.
- Sugiyama S, Di Nardo AA, Aizawa S, Matsuo I, Volovitch M, Prochiantz A, Hensch TK (2008) Experience-Dependent Transfer of Otx2 Homeoprotein into the Visual Cortex Activates Postnatal Plasticity. *Cell* 134:508–520.
- Sugiyama S, Prochiantz A, Hensch TK (2009) From brain formation to plasticity: Insights on Otx2 homeoprotein. *Dev Growth Differ* 51:369–377.
- Sun Q-Q (2006) Barrel Cortex Microcircuits: Thalamocortical Feedforward Inhibition in Spiny Stellate Cells Is Mediated by a Small Number of Fast-Spiking Interneurons. *J Neurosci* 26:1219–1230.
- Sun Y, Ikrar T, Davis MF, Holmes TC, Gandhi SP, Xu Correspondence X, Gong N, Zheng X, Luo ZD, Lai C, Mei L, Xu X (2016) Neuregulin-1/ErbB4 Signaling Regulates Visual Cortical Plasticity. *Neuron* 92:160–173.
- Szabadics J, Varga C, Molnar G, Olah S, Barzo P TG (2006) Excitatory Effect of GABAergic Axo-Axonic Cells in Cortical Microcircuits. *Science* (80-) 311:233–235.

- Takesian AE, Hensch TK (2013) Balancing plasticity/stability across brain development. *Prog Brain Res* 207:3–34.
- Tamamaki N, Tomioka R (2010) Long-range GABAergic connections distributed throughout the neocortex and their possible function. *Front Neurosci* 4:1–8.
- Tamás G, Buhl EH, Somogyi P (1997) Massive autaptic self-innervation of GABAergic neurons in cat visual cortex. *J Neurosci* 17:6352–6364.
- Tanahira C, Higo S, Watanabe K, Tomioka R, Ebihara S, Kaneko T, Tamamaki N (2009) Parvalbumin neurons in the forebrain as revealed by parvalbumin-Cre transgenic mice. *Neurosci Res* 63:213–223.
- Tang Y, Stryker MP, Alvarez-Buylla A, Espinosa JS (2014) Cortical plasticity induced by transplantation of embryonic somatostatin or parvalbumin interneurons. *Proc Natl Acad Sci* 111:18339–18344.
- Taniguchi H, He M, Wu P, Kim S, Paik R, Sugino K, Kvitsani D, Fu Y, Lu J, Lin Y, Miyoshi G, Shima Y, Fishell G, Nelson SB, Huang ZJ (2011) A Resource of Cre Driver Lines for Genetic Targeting of GABAergic Neurons in Cerebral Cortex. *Neuron* 71:995–1013.
- Tigges, J., and Tigges M (1985) Subcortical sources of direct projections to visual cortex. In: *Cerebral cortex* (Plenum, ed), pp 351–378.
- Timofeev I, Grenier F, Steriade M (2002) The role of chloride-dependent inhibition and the activity of fast-spiking neurons during cortical spike-wave electrographic seizures. *Neuroscience* 114:1115–1132.
- Tognini P, Pizzorusso T (2012) MicroRNA212/132 family: Molecular transducer of neuronal function and plasticity. *Int J Biochem Cell Biol* 44:6–10.
- Tognini P, Putignano E, Coatti A, Pizzorusso T (2011) Experience-dependent expression of miR-132 regulates ocular dominance plasticity. *Nat Neurosci* 14:1237–1239.
- Torborg CL, Feller MB (2004) Unbiased analysis of bulk axonal segregation patterns. *J Neurosci Methods* 135:17–26.
- Toyoizumi T, Miyamoto H, Yazaki-Sugiyama Y, Atapour N, Hensch TK, Miller KD (2013) A theory of the transition to critical period plasticity: inhibition selectively suppresses spontaneous activity. *Neuron* 80:51–63.

Trachtenberg JT, Chen BE, Knott GW, Feng G, Sanes JR, Welker E, Svoboda K (2002) Long-term in vivo imaging of experience-dependent synaptic plasticity in adult cortex. *Nature* 420:788–794.

Trachtenberg JT, Stryker MP (2001) Rapid anatomical plasticity of horizontal connections in the developing visual cortex. *J Neurosci* 21:3476–3482.

Ueno H, Suemitsu S, Okamoto M, Matsumoto Y, Ishihara T (2017) Sensory experience-dependent formation of perineuronal nets and expression of Cat-315 immunoreactive components in the mouse somatosensory cortex. *Neuroscience* 355:161–174.

Usrey WM, Alitto HJ (2015) Visual Functions of the Thalamus. *Annu Rev Vis Sci* 1:351–371.

Varga V, Losonczy A, Zemelman B V, Borhegyi Z, Nyiri G, Domonkos A, Hangya B, Holderith N, Magee JC, Freund TF (2009) Fast synaptic subcortical control of hippocampal circuits. *Science* (80-) 326:449–453.

Vetencourt JFM, Sale A, Viegi A, Baroncelli L, De Pasquale R, F. O’Leary O, Castren E, Maffei L (2008) The Antidepressant Fluoxetine Restores Plasticity in the Adult Visual Cortex. *Science* (80-) 320:385–388.

Wallace DJ, Kerr JND (2010) Chasing the cell assembly. *Curr Opin Neurobiol* 20:296–305.

Wang B-S, Sarnaik R, Cang J (2010) Critical Period Plasticity Matches Binocular Orientation Preference in the Visual Cortex. *Neuron* 65:246–256.

Wang D, Fawcett J (2012) The perineuronal net and the control of cns plasticity. *Cell Tissue Res* 349:147–160.

Wickersham IR, Lyon DC, Barnard RJO, Mori T, Finke S, Conzelmann K, Young JAT, Callaway EM (2007) Monosynaptic Restriction of Transsynaptic Tracing from Single, Genetically Targeted Neurons. *Neuron* 53:639–647.

Wiesel TN (1982) Postnatal development of the visual cortex and the influence of environment. *Nature* 299:583–591.

Wiesel TN, Hubel DH (1963) Single-Cell Responses in Striate Cortex of Kittens Deprived of Vision in One Eye. *J Neurophysiol* 26:1003–1017.

Worgotter F, Eyding D, Macklis JD, Funke K (2002) The influence of the corticothalamic projection on responses in thalamus and cortex. *Philos Trans R Soc B Biol Sci* 357:1823–1834.

Yamada J, Ohgomori T, Jinno S (2015) Perineuronal nets affect parvalbumin expression in GABAergic neurons of the mouse hippocampus. *Eur J Neurosci* 41:368–378.

Yamaguchi Y (2000) Lecticans: organizers of the brain extracellular matrix. *C Cell Mol Life Sci* 57:276–289.

Yang S, Cox CL (2007) Modulation of Inhibitory Activity by Nitric Oxide in the Thalamus. *J Neurophysiol* 97:3386–3395.

Ye Q, Miao Q long (2013) Experience-dependent development of perineuronal nets and chondroitin sulfate proteoglycan receptors in mouse visual cortex. *Matrix Biol* 32:352–363.

Yoon B-J, Smith GB, Heynen AJ, Neve RL, Bear MF (2009) Essential role for a long-term depression mechanism in ocular dominance plasticity. *Proc Natl Acad Sci* 106:9860–9865.

Yuan M, Meyer T, Benkowitz C, Savanthrapadian S, Ansel-Bollepalli L, Foggetti A, Wulff P, Alcami P, Elgueta C, Bartos M (2017) Somatostatin-positive interneurons in the dentate gyrus of mice provide local-and long-range septal synaptic inhibition. *Elife* 6:1–25.

Yuste R (2015) The discovery of dendritic spines by Cajal. *Front Neuroanat* 9:1–6.

Zariwala HA, Madisen L, Ahrens KF, Bernard A, Lein ES, Jones AR, Zeng H (2011) Visual Tuning Properties of Genetically Identified Layer 2/3 Neuronal Types in the Primary Visual Cortex of Cre-Transgenic Mice. *Front Syst Neurosci* 4:1–16.

Zhao X, Liu M, Cang J (2013) Sublinear binocular integration preserves orientation selectivity in mouse visual cortex. *Nat Commun* 4:1–21.

Zhuang J, Ng L, Williams D, Valley M, Li Y, Garrett M, Waters J (2017) An extended retinotopic map of mouse cortex. *Elife* 6:1–29.

Zimmermann DR, Dours-Zimmermann MT (2008) Extracellular matrix of the central nervous system: From neglect to challenge. *Histochem Cell Biol* 130:635–653.

ABSTRACT

The maturation of sensory processing undergoes a critical period (CP), during which cortical neural circuits are sculpted and changed by experience. The closure of CP is paralleled by the accumulation of extracellular perineuronal nets (PNN) around parvalbumin (PV)-positive, fast-spiking interneurons. These condensed and specialized extracellular matrix composed of chondroitin sulfate proteoglycans, surround cell body and proximal dendrites of PV cells and restrains neuronal plasticity. Indeed, the degradation of PNNs in adult animals was shown to re-open the structural plasticity typical of the CP, but absent during adulthood. Although the mechanisms underlying CP have been studied, the functional aspects linking PNNs to activity-dependent plasticity remain obscure.

By combining electrophysiological and optogenetic approaches, together with *in vivo* degradation of PNN (stereotaxic injection of the Enzyme Ch-ABC) and sensory deprivation, we aimed at defining *i)* the neurophysiological properties of FS interneurons in layer 4 of primary visual cortex (V1) during the establishment of the CP, and *ii)* how these properties are altered by PNN accumulation. PV cells were compared to their glutamatergic counterparts, the regular spiking (RS) spiny-stellate neurons (referred as principal neurons PN).

We found a robust age-dependent increase of input-output firing relationships in both cell types, with no overall change in their passive electrical properties. Importantly, we found that *in vivo* PNN removal in V1 in adult mice did not affect the action potential properties and firing dynamics. Importantly, we found that *in vivo* PNN removal in V1 in adult mice increased both excitatory and inhibitory transmission selectively onto PV cells, leaving their excitability intact, and recapitulating younger, pre-CP states. In addition, triggering plasticity *in vivo* by monocular deprivation (MD) did not boost the increased activity onto PV interneurons. Interestingly, paired recordings in layer 4 of V1 showed no changes of inhibitory unitary connections in the presence and absences of PNNs. In order to understand the circuit mechanisms underlined, we expressed the light-sensitive opsin channelrhodopsin 2 in the visual thalamus. We found that PNN removal increases the recruitment of PV cells by thalamocortical fibers leading to an increase of feedforward inhibition onto PV cells and possibly onto PN. These results are in agreement with V1 recordings *in vivo* of visually evoked potentials in response of increasing contrast. Indeed, PNN disruption caused a reduction of the slope of the contrast sensitivity curve, indicating a higher recruitment of inhibition.

In conclusion, we found that PNN removal in adult visual cortex increases the specific recruitment of PV cells by thalamic fibers. Increased PV cell recruitment results in a neuron-specific alteration of the E/I balance both *in vitro* and *in vivo*. These experiments shed light on the basic mechanisms underlying cortical plasticity, and its reopening through PNN removal.

RESUME

Il existe au cours du développement du cerveau une fenêtre temporelle dite période critique (PC) pendant laquelle les réseaux neuronaux sont sensibles aux stimuli sensoriels externes qui vont sculpter leur organisation. Un des acteurs clé de la consolidation de ces réseaux est le Perineuronal Net (PNN), un type particulier de matrice extracellulaire qui s'accumule au cours de la PC majoritairement autour du corps cellulaire et des dendrites proximales des interneurons fast-spiking, parvalbumin-positifs (PV). La dégradation des PNNs chez l'adulte restaure une plasticité structurale, typique de la PC mais limitée dans le cerveau mature.

A ce jour, les mécanismes fonctionnels, cellulaires et synaptiques responsables de la réouverture de la PC de plasticité impliquant les PNN restent inconnus. Ce projet de recherche vise à déterminer *i)* les propriétés neurophysiologiques des neurones PV dans la couche 4 du cortex visuel primaire de souris au cours du développement et *ii)* de quelle façon ces propriétés sont altérées par l'accumulation des PNNs. Les cellules PV sont systématiquement comparées aux neurones principaux (PN) excitateurs de la couche 4.

Nous avons montré, au cours du développement, une augmentation de l'excitabilité des deux types de neurones, sans modification de leurs propriétés électriques passives. De manière importante, nos résultats indiquent que la dégradation *in vivo* des PNNs augmente à la fois la transmission glutamatergique et GABAergique spécifiquement sur les PV, récapitulant ainsi un état juvénile. De plus, cette augmentation d'activité synaptique n'est pas potentialisée par une déprivation sensorielle monoculaire, utilisée pour induire la plasticité. De façon intéressante, une absence de PNN chez l'adulte n'affecte pas les connections unitaires inhibitrices dans la couche 4. Afin de comprendre les mécanismes impliqués au niveau du circuit, nous avons exprimé l'opsine sensible à la lumière ChR2 dans les neurones glutamatergiques du thalamus visuel projetant sur la couche 4 du cortex. Nous avons ainsi montré que la dégradation des PNNs augmente le recrutement spécifique des PV par les fibres thalamiques, entraînant une augmentation de l'inhibition feed-forward sur les PV et potentiellement sur les PNs. Ces résultats sont en accord avec des expériences réalisées *in vivo*, au cours desquelles nous avons mesuré les potentiels évoqués en réponse à des stimuli visuels (augmentation de contraste). En effet, suite à la dégradation des PNNs, la pente de la courbe (ou gain) de sensibilité au contraste diminue, indiquant une augmentation du recrutement de l'inhibition.

En conclusion, nos données indiquent que la dégradation des PNN dans le cortex visuel adulte augmente spécifiquement le recrutement des interneurons PV par le thalamus, ce qui entraîne des altérations au niveau de la balance E/I à la fois *in vitro* et *in vivo*. Ces résultats apportent une compréhension des mécanismes sous-jacents à la plasticité corticale et sa réouverture suite à la dégradation des PNNs.